# UNIVERSIDAD COMPLUTENSE DE MADRID

FACULTAD DE VETERINARIA
Departamento de Medicina y Cirugía Animal


## TESIS DOCTORAL

# Aplicación de técnicas de diagnóstico por imagen avanzadas en el estudio de la cabeza del caballo

MEMORIA PARA OPTAR AL GRADO DE DOCTOR

PRESENTADA POR

**Gabriel Manso Díaz**

Directores

María Isabel García Real
Olivier Taeymans
Fidel San Román Ascaso

**Madrid, 2015**

UNIVERSIDAD COMPLUTENSE DE MADRID
FACULTAD DE VETERINARIA
Departamento de Medicina y Cirugía Animal

# Aplicación de técnicas de diagnóstico por imagen avanzadas en el estudio de la cabeza del caballo

# TESIS DOCTORAL

**GABRIEL MANSO DÍAZ**
MADRID, 2015

TESIS DOCTORAL

# Aplicación de TÉCNICAS DE DIAGNÓSTICO por IMAGEN AVANZADAS en el estudio de la CABEZA DEL CABALLO

## Application of advanced diagnostic imaging techniques in the study of the equine head

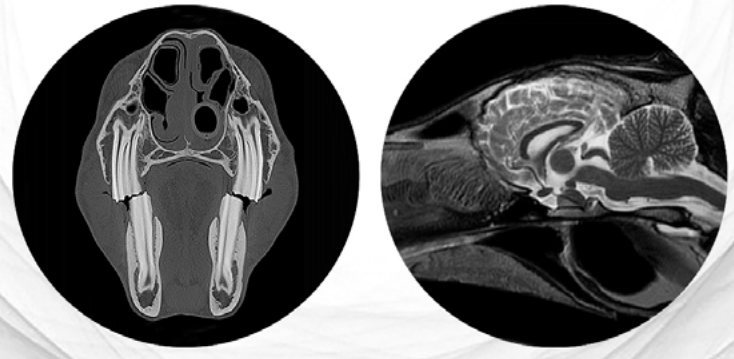

GABRIEL MANSO DÍAZ

Madrid 2015

Departamento de Medicina y Cirugía Animal
Facultad de Veterinaria
Universidad Complutense de Madrid

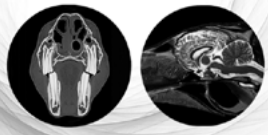

RETURN
TABLE OF CONTENTS

UNIVERSIDAD COMPLUTENSE DE MADRID
FACULTAD DE VETERINARIA
Departamento de Medicina y Cirugía Animal

TESIS DOCTORAL

# Aplicación de técnicas de diagnóstico por imagen avanzadas en el estudio de la cabeza del caballo

MEMORIA PARA OPTAR AL GRADO DE DOCTOR
PRESENTADA POR

**GABRIEL MANSO DÍAZ**

BAJO LA DIRECCIÓN DE LOS DOCTORES

María Isabel García Real  Olivier Taeymans  Fidel San Román Ascaso

MADRID, 2015

Dña. María Isabel García Real, con D.N.I 52125211N, Doctora en Veterinaria, Profesor Contratado Doctor del Departamento de Medicina y Cirugía Animal, en la Facultad de Veterinaria de la Universidad Complutense de Madrid.

D. Olivier Taeymans, con número de pasaporte EI667073, Doctor en Veterinaria, Adjunct Associate Professor del Department of Clinical Sciences, en Cummings School of Veterinary Medicine de Tufts University (EEUU), Honorary Associate Professor en School of Veterinary Medicine and Science de University of Nottingham (Reino Unido) y Head of the Diagnostic Imaging Service from Dick White Referrals (Reino Unido).

D. Fidel San Román Ascaso, con D.N.I 18000514R, Doctor en Veterinaria, Catedrático del Departamento de Medicina y Cirugía Animal, en la Facultad de Veterinaria de la Universidad Complutense de Madrid.

CERTIFICAN:

Que D. Gabriel Manso Díaz, Licenciado en Veterinaria, ha realizado bajo nuestra dirección y supervisión el trabajo titulado: "Aplicación de técnicas de diagnóstico por imagen avanzadas en el estudio de la cabeza del caballo".

Revisado el presente trabajo, se considera que reúne a nuestro juicio la debida calidad y las condiciones de originalidad y rigor metodológico necesarios para su presentación y defensa ante el tribunal correspondiente para optar al título de Doctor Europeo.

En Madrid, a 25 de febrero de 2015,

María Isabel García Real  Olivier Taeymans  Fidel San Román Ascaso

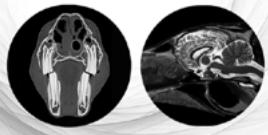



El autor de este trabajo ha disfrutado de una beca predoctoral del programa "Formación de Profesorado Universitario" (F.P.U.) concedida por el Ministerio de Educación, Cultura y Deporte, Gobierno de España. Período Diciembre 2011 – Diciembre 2015 (Referencia AP2010-0498).

Parte de este estudio fue evaluado por el Comité de Experimentación Animal de la Universidad Complutense de Madrid, con un informe favorable que se emitió con fecha de 30 de Marzo de 2012.

"Un ser que tiene sueños es un ente
grande, lo mejor del mundo.
Es la esencia de la vida. Los que no anhelan
ser mejores de lo que son, están
muertos en vida..."

Santiago García-Clairac
El ejército negro

A mi familia,

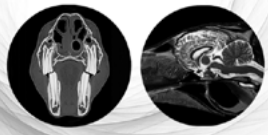



# ACKNOWLEDGEMENTS
# AGRADECIMIENTOS

Son muchas las personas que, de una forma u otra, han participado en este trabajo y, por tanto, a todas ellas les quiero expresar mi más sincero agradecimiento en estas líneas.

En primer lugar me gustaría agradecer a mis padres y hermanas todo su apoyo y comprensión tanto en los momentos buenos como, y principalmente, en los malos. Muchas gracias por estar SIEMPRE a mi lado. Y, por supuesto, no me puedo olvidar de mi querido Copi, que a su modo ha sido el más fiel compañero durante todos estos años.

A mis directores de tesis: Fidel San Román por hacer posible la obtención de la beca que me ha permitido llevar a cabo la tesis, Isabel García por haberme iniciado en el campo del diagnóstico por imagen y Olivier Taeymans. Olivier I cannot express with words how grateful I feel. You have been more than a mentor, a friend, in which I have always found support, guidance and encouragement for undertaking any project. I feel very lucky for having the chance of learning from you. Thank you for being always there, even from the distance.

Muchas gracias a José García-López por estar siempre al otro lado del correo, tus sabios consejos y tu ayuda incondicional en todos los proyectos ha sido fundamental, sabes que te considero un director más de esta tesis.

I would like to express my deepest gratitude to Sue Dyson and Ruth Dennis, who kindly integrated me in their teams at the Animal Health Trust (AHT), and were willing to collaborate in this thesis. Sue, thank you very much for finding always time for our paper, for your wise and useful advices, and for all your efforts for making this possible. I would also like to acknowledge Marianna Biggi, who welcomed me into her office at the AHT, for being always available for answering all my questions and for sharing so many interesting cases with me. I cannot forget Andrew Holloway and Mauro Pivetta, it was a pleasure to work with you.

Many thanks to the Diagnostic Imaging team from Tufts Cummings School of Veterinary Medicine, who has collaborated extensively on this thesis. In particular, I would like to name Dominique Penninck, Mauricio Solano, Amy Sato, Linda Kinney and Kay Hunt. Thank you very much to all of you for opening me the doors of the radiology section and making me feel one more of the team.

I am very thankful to the Diagnostic Imaging team from the Royal Veterinary College, in particular Renate Weller and Jonathon Dixon. Thank you for counting on me in all your projects and giving me the chance of learning and working with you at the hospital, it was such a pleasure.

A Natalia Díez Bru, quien me inició en el campo de la ecografía, siempre ha contado conmigo para todo y ha creído en mi. Muchas gracias por animarme a salir a conocer otros sitios.

A mis compañeras de despacho Paloma Toni y Sonsoles Martín, que han sido un importante apoyo todo este tiempo. Palo, gracias por tus lecciones neurológicas y gastronómicas. Sonso, muchas gracias por esa alegría incombustible que siempre transmites.

A mis compañeros del Área de Grandes Animales del Hospital Clínico Veterinario Complutense (HCVC), por depositar su confianza en mi con sus casos, dándome la oportunidad de seguir mejorando día a día, y muy especialmente a Javier López, Ramón Herrán, Isabel Santiago, Paloma Forés y Marta Varela. Isa, gracias por tantas y tantas anestesias (al final acabará gustándote la resonancia) y, sobre todo, gracias ●●●

# ACKNOWLEDGEMENTS
# AGRADECIMIENTOS

●●● por escucharme y ayudarme. Javier, gracias por contar conmigo, por apoyarme siempre que lo he necesitado y por tus consejos. Paloma, muchas gracias por creer en mi desde el principio. Ramón, nunca podré agradecerte todo lo que me has enseñado en este tiempo.

Al grupo de neurología del HCVC: Paloma Toni, Miriam Portero, Miguel Marín y, por supuesto, la jefa Carmen Pérez. Simplemente, gracias por todo Pin & Pones.

My sincere thanks to Christophe Casteleyn, Paul Simoens and their team from Ghent University, for not only making possible the angiographic anatomic casts but also for significantly improving the original idea. Many thanks to Jimmy Saunders for kindly doing the CT scan of the vascular cast.

A Miguel Bajón, Marta González y Jorge de la Calle, del Hospital Veterinario Sierra de Madrid, que siempre han estado dispuestos a ayudar en cualquier proyecto que les he propuesto.

I would like to thank Sarah Powell (Rossdales and Partners, UK), Henry Tremaine (Bristol University, UK), and Anthony Pease (Michigan University, USA) for their kind contribution to this thesis with some of the pictures included in the figures.

A Brigitte Bidard, con quien he tenido el placer de trabajar en varias ocasiones. Gracias a sus fantásticas ideas y su gran talento ha sido capaz de mejorar esta tesis.

A Gustavo Abuja, quien creyó en mi desde el primer día y no dudó en contar conmigo para su proyecto de bolsa nucal.

Al Servicio de Diagnóstico por Imagen del HCVC, y en especial al personal técnico (Carmen Osorno, Sonia Pavón e Isabel García) con quien tengo el placer de trabajar a diario. No puedo olvidarme de Enrique García por su compañerismo y amistad en estos años.

Un agradecimiento especial a los servicios de Anestesia y Anatomía Patológica del HCVC, y muy especialmente al personal técnico de la sala de necropsias (Ramón Ortiz e Ignacio Herrero), cuya colaboración ha sido fundamental.

Al Departamento de Medicina y Cirugía Animal, y en especial a Laura Andrade por toda su ayuda y paciencia en los trámites y gestiones de la tesis.

Al personal de la hemeroteca de la Facultad de Veterinaria y especialmente a Carmen Muñoz, quien me ha conseguido todos los artículos necesarios por muy difícil de encontrar que fueran.

Al Escuadrón de caballería de la Policía Nacional, y en especial a Gloria Giménez y Silvestre Galera, por ceder parte de los caballos para el estudio anatómico.

Gracias a todos los veterinarios remitentes que han confiado a lo largo de estos años en el HCVC, el Hospital for Large Animals de Tufts University y el Centre for Equine Studies del Animal Health Trust, sin cuyos casos no se podría haber llevado a cabo este trabajo.

Y, finalmente, gracias a todos los caballos que han formado parte de este trabajo, pues su enfermedad ha servido para incrementar nuestros conocimientos y mejorar las técnicas diagnósticas, que espero repercutan de forma beneficiosa en un futuro en muchos otros caballos. ■

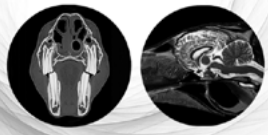



# STRUCTURE OF THE PhD THESIS

The PhD thesis entitled "Aplicación de técnicas de diagnóstico por imagen avanzadas en el estudio de la cabeza del caballo" ("Application of advanced diagnostic imaging techniques in the study of the equine head") is comprised mainly of three peer-reviewed papers:

- **Paper 1: Magnetic resonance imaging characteristics of equine head disorders: 84 cases (2000–2013).** Gabriel Manso-Díaz, Sue J. Dyson, Ruth Dennis, José M. García-López, Marianna Biggi, María Isabel García-Real, Fidel San Román, Olivier Taeymans. Veterinary Radiology & Ultrasound 2014. doi: 10.1111/vru.12210.

- **Paper 2: The role of head computed tomography in equine practice.** Gabriel Manso-Díaz, José M. García-López, Louise Maranda, Olivier Taeymans. Equine Veterinary Education 2015, 27(3):136-145.

- **Paper 3: Time-of-flight magnetic resonance angiography (TOF-MRA) of the normal equine head.** Gabriel Manso-Díaz, María Isabel García-Real, Christophe Casteleyn, Fidel San Román, Olivier Taeymans. Equine Veterinary Journal 2013, 45(2):187-192.

In addition, the research work conducted during the PhD period has derived in the publication of further peer-reviewed papers and has also resulted in several contributions to national and international conferences and meetings:

- **The cranial nuchal bursa: Anatomy, ultrasonography, magnetic resonance imaging and endoscopic approach.** Gustavo Abuja, José M. García-López, Gabriel Manso-Díaz, Tijn J. Spoormakers, Olivier Taeymans. Equine Veterinary Journal 2014, 46(6):745-750.

- **Imaging diagnosis – Nasofrontal suture exostosis in a horse.** Gabriel Manso-Díaz, Olivier Taeymans. Veterinary Radiology & Ultrasound 2012, 53(3):573-575.

- **Magnetic resonance dacryocystography in the horse.** Gabriel Manso-Díaz, José M. García-López, Ramón Herrán Vilella, María Isabel García-Real, Olivier Taeymans. European Veterinary Diagnostic Imaging (EVDI) Meeting. Utrecht (The Netherlands). August 2014. Oral presentation.

- **Comparison of computed tomography and radiography for the diagnosis of equine sinonasal disease.** Gabriel Manso-Díaz, José M. García-López, Louise Maranda, Olivier Taeymans. European Veterinary Diagnostic Imaging (EVDI) Meeting. Utrecht (The Netherlands). August 2014. Poster presentation.

- **Diagnóstico de un quiste en el seno esfenopalatino mediante resonancia magnética.** Gabriel Manso Díaz, Elisa González Alonso Alegre, Alfonso Rodríguez Álvaro, Isabel Santiago Llorente, Jaime Goyoaga Elizalde, Paloma Forés Jackson. XIV Congreso Internacional de Medicina ●●●

y Cirugía Equina. Sevilla (Spain). December 2013. Poster presentation.

- **Magnetic resonance imaging of the equine head.** Gabriel Manso-Díaz, Sue J. Dyson, Ruth Dennis, José M. García-López, María Isabel García-Real, Olivier Taeymans. European Veterinary Diagnostic Imaging (EVDI) Meeting. Cascais (Portugal). August 2013. Oral presentation. Veterinary Radiology & Ultrasound 2014, 55(6):660.

- **Utilidad clínica de la resonancia magnética en el diagnóstico de la patología dentaria equina.** Gabriel Manso Díaz, Javier López San Román, Jaime Goyoaga Elizalde, Isabel Santiago Llorente, María Isabel García Real. XIII Congreso Internacional de Medicina y Cirugía Equina. Sevilla (Spain). November 2012. Oral presentation.

- **Aplicaciones prácticas de la resonancia magnética en caballos.** Gabriel Manso Díaz. I Congreso Solidario de Clínica Equina. Madrid (Spain). April 2012. Lecture. Revista Complutense de Ciencias Veterinarias 2012, 6(2):6-12.

- **Angiografía por resonancia magnética de la cabeza del caballo: descripción y aplicaciones.** Gabriel Manso Díaz, Jaime Goyoaga Elizalde, Javier López San Román. XII Congreso Internacional de Medicina y Cirugía Equina. Sevilla (Spain). November 2011. Oral presentation.

- **Magnetic resonance angiography of the normal equine head.** Gabriel Manso-Díaz, María Isabel García Real, Christophe Casteleyn, Olivier Taeymans. European Veterinary Diagnostic Imaging (EVDI) Meeting. London (United Kingdom). September 2011. Oral presentation. Veterinary Radiology & Ultrasound 2011, 52(6):691.

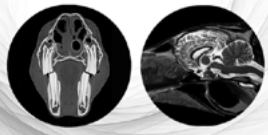



# TABLE OF CONTENTS

TABLE OF CONTENTS

# Aplicación de TÉCNICAS DE DIAGNÓSTICO por IMAGEN AVANZADAS en el estudio de la CABEZA DEL CABALLO

Application of advanced diagnostic imaging techniques in the study of the equine head

## RESUMEN

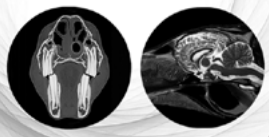



## RESUMEN

La cabeza del caballo es una región muy compleja desde un punto de vista anatómico, y en ella pueden aparecer numerosas patologías de gran importancia clínica. Los signos clínicos asociados dependen en gran medida de las estructuras afectadas, por lo que el diagnóstico de los procesos patológicos que afectan a esta región es a menudo complicado. El abordaje diagnóstico de las enfermedades de la cabeza debe comenzar siempre por una exploración física completa, aunque la información obtenida es con frecuencia limitada y debe ser completada con métodos complementarios, donde las técnicas de diagnóstico por imagen juegan un papel fundamental.

Las técnicas de diagnóstico por imagen empleadas hoy día para el estudio de la cabeza del caballo incluyen la radiología, la ecografía, la gammagrafía, la tomografía computarizada (TC) y la resonancia magnética (RM).

La radiografía es la técnica de imagen más utilizada para el estudio de la cabeza equina en la práctica clínica. Sin embargo, la interpretación radiográfica de esta área puede ser muy difícil como consecuencia de la superposición de numerosas estructuras anatómicas, del enmascaramiento de zonas radiolúcidas por parte del hueso cortical, así como por la complejidad anatómica de la región. Por ello es casi siempre necesaria la obtención de imágenes en numerosas proyecciones, con angulaciones diferentes, para estudiar con mayor precisión distintas zonas de la cabeza. Radiológicamente es posible reconocer las lesiones mediante la identificación de alteraciones o interrupciones del contorno normal de las estructuras, o bien mediante la observación de cambios de tamaño o de opacidad. Estas alteraciones no son siempre fáciles de identificar, lo cual se hace más evidente en zonas anatómicamente complejas. La radiología se suele utilizar como la técnica de imagen inicial para el estudio de alteraciones de los huesos del cráneo y la mandíbula, de la cavidad nasal y senos paranasales, de los dientes y de la faringe.

La ecografía se utiliza para evaluar con gran detalle algunas patologías que se localizan en la cabeza del caballo. La alta calidad de las imágenes ecográficas se basa en el elevado contraste de tejidos blandos y la elevada resolución espacial de esta técnica. Sin embargo, debido a que los ultrasonidos no pueden penetrar el hueso ni el gas, la ecografía no permite evaluar numerosas estructuras de la cabeza de elevado interés clínico. Aunque esta técnica es particularmente útil para el examen del ojo y la órbita, también se puede emplear para evaluar otras estructuras de tejido blando (p.ej. la lengua), los márgenes de las estructuras óseas superficiales y la articulación temporomandibular.

La gammagrafía es una técnica que refleja los procesos fisiológicos activos mediante la detección de rayos γ emitidos por un radioisótopo inyectado por vía endovenosa al paciente. Aunque su uso para evaluar la cabeza del caballo es poco común, se puede utilizar para la detección de patologías dentarias, de los senos paranasales y de los huesos del cráneo.

Las técnicas de diagnóstico por imagen avanzadas, como son la tomografía computarizada y la resonancia magnética, generan imágenes tomográficas, lo que permite la visualización de las estructuras internas de la cabeza sin que se superpongan los tejidos de alrededor. La base física varía enormemente en función de la técnica; las imágenes de TC se obtienen mediante la rotación rápida del conjunto de un generador de rayos X y una matriz de detectores alrededor del paciente, mientras que las imágenes de RM son el resultado de la excitación de los tejidos magnetizados por ondas de radiofrecuencia. Generalmente el paciente es examinado bajo anestesia general, sin embargo recientemente se ha desarrollado una técnica de TC que permite el estudio de la cabeza con el caballo en estación. Mediante la aplicación de un medio de contraste intravenoso es posible incrementar la detección de estructuras patológicas; en TC se utiliza un contraste yodado, mientras que en RM se emplea gadolinio. En general, la TC permite valorar con mayor detalle las estructuras óseas, mientras que la RM es superior para los tejidos blandos gracias a la obtención de diferentes secuencias, lo que permite una caracterización precisa de los diferentes tejidos o lesiones.

## RESUMEN

●●● Ante el dilema que surge en la práctica clínica en la elección de la técnica de imagen (TC o RM) más indicada para el estudio de la cabeza, se plantean los siguientes objetivos:

- Estudiar la utilidad diagnóstica de la resonancia magnética de alto y bajo campo en las patologías de la cabeza del caballo.

- Estudiar la utilidad diagnóstica de la tomografía computarizada en las patologías de la cabeza del caballo.

- Comparar la utilidad diagnóstica de la resonancia magnética y la tomografía computarizada con las técnicas de diagnóstico por imagen convencionales.

- Desarrollar y optimizar un protocolo de angiografía por resonancia magnética para el estudio de la cabeza del caballo utilizando equipos de alto y bajo campo.

- Llevar a cabo una descripción anatómica completa del sistema vascular normal de la cabeza del caballo mediante angiografía por resonancia magnética.

Con el fin de abordar los objetivos propuestos se llevaron a cabo tres estudios independientes.

El primer estudio consistió en la descripción de las lesiones por resonancia magnética identificadas en una amplia población de caballos con patologías de la cabeza. Se llevó a cabo un estudio retrospectivo en un periodo de 13 años, usando equipos tanto de alto como de bajo campo. Un total de 84 caballos cumplieron los criterios de inclusión, incluyendo alteraciones neurológicas (n = 65), sinonasales (n = 14) y de los tejidos blandos (n = 5). La resonancia magnética mostró con gran precisión la anatomía de la cabeza y además permitió la identificación de la lesión primaria y los cambios asociados en cada caso. Hubo una buena correlación entre los hallazgos de resonancia magnética y los resultados intraoperatorios o post-mortem. Asimismo, gracias a esta técnica fue posible la localización, la determinación del tamaño y relación con las estructuras circundantes de cada lesión. La resonancia magnética fue particularmente útil para el diagnóstico de alteraciones del sistema nervioso central y de los tejidos blandos, así como para la identificación de masas ocupantes de espacio de la cavidad nasal y senos paranasales. Mediante el uso de la RM también fue posible evaluar los dientes, especialmente la cavidad pulpar y el espacio periodontal.

En el segundo artículo, se llevó a cabo un estudio retrospectivo en el que se describieron los hallazgos por tomografía computarizada en un grupo grande de caballos con patologías de la cabeza. En este estudio se incluyeron caballos examinados en un periodo de 8 años. Un total de 59 caballos cumplieron los criterios de inclusión, incluyendo alteraciones dentales, nasales y de los senos paranasales (n = 42), óseas y/o articulares (n = 11) y de los tejidos blandos (n = 6). Además se llevó a cabo una comparación de los hallazgos por TC y radiográficos en los casos de patología dental, nasal, sinusal y ósea. La tomografía computarizada mostró una sensibilidad (100%) y especificidad (96,7%) superiores a las de la radiografía en el diagnóstico de alteraciones dentales. En comparación con la TC, la radiología presentó una baja sensibilidad para la detección de afectación de los senos paranasales, siendo especialmente baja en los senos conchal ventral (43,5%) y esfenopalatino (16,7%). La TC además permitió la identificación de un mayor número de fragmentos óseos y líneas de fracturas en los huesos maxilar, lagrimal, esfenoides, temporal y cigomático, que no fueron identificados en las radiografías. Mediante el uso de esta técnica también fue posible la evaluación detallada de las articulaciones temporohioidea y temporomandibular. La TC permitió llevar a cabo una evaluación completa de la cabeza del caballo, aportando información adicional sobre múltiples proyecciones radiográficas.

En el tercer estudio se describió un nuevo método para evaluar la vascularización de la cabeza del caballo con RM, mediante el uso de una técnica angiográfica sin contraste por resonancia magnética conocida como time-of-flight (TOF-MRA). Para llevar a cabo este estudio se utilizaron 5 caballos sanos, de los cuales 4 fueron examinados con un equipo de RM de bajo campo, mientras ●●●

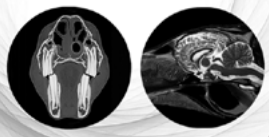



## RESUMEN

●●● que el quinto se exploró en un equipo de alto campo. Las imágenes de obtenidas se compararon con reconstrucciones de TC de un molde vascular, que fue utilizado como referencia anatómica. Esta técnica angiográfica proporcionó una buena visualización de los principales vasos sanguíneos intra- y extracraneales con un diámetro superior a los 2 mm, tanto con el equipo de RM de bajo campo como con el de alto campo. Además, fue posible la evaluación de la morfología, simetría y tamaño de los vasos sanguíneos. La visibilidad de las arterias fue superior a la de las venas, las cuales presentaron una intensidad de señal inferior. En general, la técnica de angiografía por resonancia magnética de alto campo proporcionó una mejor visualización de las arterias, presentando una resolución superior de las pequeñas ramas arteriales.

Las conclusiones generales de este trabajo son las siguientes:

**1.** Tanto la resonancia magnética de alto campo como la de bajo campo son técnicas de diagnóstico por imagen adecuadas para la valoración en detalle de la cabeza del caballo.

**2.** La resonancia magnética es la técnica de elección para el estudio del sistema nervioso central, tanto del encéfalo como de los nervios craneales, y de los tejidos blandos extracraneales, como son la órbita, los linfonódulos, los vasos sanguíneos, los músculos y las glándulas salivares.

**3.** La resonancia magnética es una técnica apta para el estudio de la cavidad nasal y los senos paranasales en el caballo. Gracias al gran contraste de tejidos blandos que ofrece esta técnica es posible una buena diferenciación entre los diferentes tipos de tejidos, lo cual resulta particularmente útil para diferenciar el origen de masas ocupantes de espacio en la cavidad nasal y senos paranasales. Sin embargo, el uso de la resonancia magnética en casos de patología dental se limita a lesiones que afectan a la cavidad pulpar, el espacio periodontal, la lámina dura y la médula ósea del hueso alveolar.

**4.** La técnica de angiografía por resonancia magnética es un excelente método para evaluar los vasos sanguíneos de la cabeza equina y se puede aplicar en resonancia magnética tanto de alto como de bajo campo. Esta secuencia permite visualizar los principales vasos sanguíneos intra- y extracraneales con un grosor superior a 2 mm de diámetro aproximadamente. La visualización del sistema arterial es superior a la del sistema venoso.

**5.** La secuencia time-of-flight se puede incorporar como parte del protocolo rutinario de resonancia magnética en caballos con masas de tejidos blandos o alteraciones vasculares, sin que implique un aumento excesivo del tiempo de estudio.

**6.** La tomografía computarizada es otra técnica de diagnóstico por imagen apta para la valoración en detalle de la cabeza del caballo, pero presenta diferentes indicaciones a las de la resonancia magnética. Ambas técnicas son, por tanto, complementarias entre sí. Sin embargo, cuando se dispone de ambas es preciso tener en cuenta la sospecha clínica a la hora de decidir qué técnica es la más adecuada.

**7.** La tomografía computarizada es la técnica de elección para el estudio de los huesos del cráneo, la mandíbula, la articulación temporomandibular, la articulación temporohioidea y los dientes. Esta técnica es adecuada para el estudio de la cavidad nasal y los senos paranasales, siendo especialmente útil en la identificación de lesiones sutiles que afectan a las paredes de la cavidad nasal y los senos. La tomografía computarizada es innegablemente superior a la radiología en la identificación de alteración de la cavidad nasal, de los senos paranasales y de los dientes. Por tanto, cuando se dispone de esta técnica la radiología queda postergada a un segundo plano en el diagnóstico de lesiones de esta región.

**8.** La tomografía computarizada puede identificar lesiones del sistema nervioso central a nivel intraventricular y extraaxial, sin embargo, su utilidad en casos de lesiones intraaxiales es muy limitada. Esta técnica también puede utilizarse para la identificación de alteraciones de los tejidos blandos extracraneales, aunque con menor detalle que la resonancia magnética. ■

# Aplicación de TÉCNICAS DE DIAGNÓSTICO por IMAGEN AVANZADAS en el estudio de la CABEZA DEL CABALLO

Application of advanced diagnostic imaging techniques in the study of the equine head

## SUMMARY

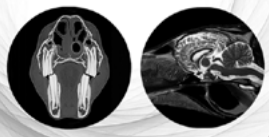



## SUMMARY

The equine head is a highly complex anatomic area and many different disorders of potentially major clinical importance can settle in this area with clinical signs varying largely on the affected structur es, making the diagnosis of this region often challenging. The diagnostic approach of head diseases must start with a thorough physical examination. However, the information obtained from physical examination is commonly limited, and often needs to be complemented by ancillary diagnostic tests with diagnostic imaging techniques playing a crucial role.

Diagnostic imaging modalities used for studying this area include radiography, ultrasonography, scintigraphy, computed tomography (CT) and magnetic resonance imaging (MRI).

Radiography is the most commonly used imaging modality for studying the equine head in practice. Radiographic interpretation of this area is challenging because of superimposition of numerous anatomical structures, dense cortical bone masking more lucent areas, as well as the relatively complex anatomy of this region, making obtention of numerous projections (at various different angles) of each area mandatory. Disease processes are detected radiographically by identifying disrupted or altered contours, or changes in size, or radiopacity. These alterations are not always easy to see in complex anatomical areas. Main indications of radiography as a first line imaging modality are suspected pathology of the skull and mandible, nasal cavity, paranasal sinuses, teeth and pharynx.

Ultrasonography is another imaging modality used for assessing certain conditions affecting the equine head with high detail. High soft tissue contrast and spatial resolution of medical ultrasound technology being at the source of these high quality images. Sound beams however cannot penetrate through the osseous structures of the skull or gas within the airways; precluding assessment of numerous head structures of interest. Although this technique is particularly useful for the examination of the eye and orbit, it can also be used for other soft tissue structures (e.g. tongue), the surface of superficial osseous structures, and the temporomandibular joint.

Scintigraphy is a sensitive technique that reflects active physiological processes by detecting γ-rays emitted from decay of a radionuclide, previously injected in the patient. Although its use in the equine head is uncommon, it can be used for detecting pathology of teeth, paranasal sinuses and the skull.

Advanced diagnostic imaging techniques, such as computed tomography and magnetic resonance imaging, produce images that depict anatomy in a series of two-dimensional cross-sections, allowing visualization of internal structures of the head without being obscured by overlying tissues. The technology is based on different physical mechanisms; CT images are obtained by rapid rotation of an x-ray generator and detector array around the patient, whereas MRI images are the result of the stimulation of magnetized tissues by radiofrequency waves. The patient is commonly imaged under general anesthesia, however recently a CT technique for scanning the equine head in standing position has been developed. Contrast enhancement of pathologic structures can be obtained by injecting an intravenous contrast medium; iodine or gadolinium for CT and MRI, respectively. In general, CT provides better images of bony structures, while MRI is superior in imaging soft tissue by obtaining several sequences, which allows precise characterization of different tissues or lesions.

The question of choosing the best indicated imaging modality between computed tomography and magnetic resonance imaging for studying the equine head in clinical situations derived the following objectives of our study:

- To study the diagnostic usefulness of high-field versus low-field magnetic resonance imaging in horses with head disorders.

- To study the diagnostic usefulness of computed tomography in horses with disorders affecting the head.

- To compare the diagnostic usefulness of magnetic ●●●

## SUMMARY

●●● resonance imaging and computed tomography to conventional diagnostic imaging modalities.

- To develop and optimize a magnetic resonance angiography protocol for the equine head using low-field and high-field magnetic resonance systems.

- To provide a thorough anatomical description of normal magnetic resonance angiography images from healthy horses.

In order to address the proposed objectives we conducted three separate studies.

The first study described MRI characteristics and indications for a large sample of horses with head disorders. Horses imaged over a period of 13 years were included, using either high-field or low-field magnets. Eighty-four horses met the inclusion criteria, having neurological (n = 65), sinonasal (n = 14), and soft tissue (n = 5) disorders. Magnetic resonance imaging accurately depicted the anatomy and allowed identification of the primary lesion and associated changes. There were good correlations between MRI findings and intraoperative or postmortem results with MRI showing exact localization of the lesions, their size, and relation to surrounding structures. This technique was particularly useful for the diagnosis of central nervous system and soft tissue disorders, as well as identification of nasal and paransal sinus occupying lesions. MRI also allowed assessment of dental pulp cavity and periodontal space.

A similar retrospective study was conducted for describing CT characteristics and indications of equine head diseases in the second study. Horses imaged over a period of 8 years were included. Fifty-nine horses met the inclusion criteria, having dental and/or sinonasal (n = 42), osseous and/or articular (n = 11), and soft tissue (n = 6) disorders. Comparison of radiographic and CT findings was performed in cases of dental, sinonasal and osseous disorders. Computed tomography had higher sensitivity (100%) and specificity (96.7%) than radiography in diagnosing dental disease. Compared to CT, radiographic identification of sinus involvement was less sensitive, particularly for ventral conchal and sphenopalatine sinuses and presented an overall sensitivity of 43.5% and 16.7%, respectively. CT allowed identification of a higher number of bone fragments and fractures in the maxillary, lacrimal, sphenoidal, temporal, and zygomatic bones not identified radiographically. Accurate identification of CT changes in the temporomandibular joint and temporohyoid articulation was also possible. CT allowed a thorough evaluation of the equine head, yielding additional information over multiple radiographic views.

In the third study we described a new method for evaluating the equine head vasculature with MRI, by using a non-contrast magnetic resonance angiography (MRA) technique called time-of-flight (TOF-MRA). Five healthy horses were recruited. Four were studied on a low-field magnet and one on a high-field magnet. MRI images were compared to CT images of a vascular corrosion cast, which was used as anatomical reference. MRA protocol provided good visualization of all major intra- and extracranial blood vessels down to a size of approximately 2 mm in diameter on both low- and high-field systems, allowing evaluation of vessel morphology, symmetry and size. The visibility of the arteries was higher than of the veins, which showed lower signal intensity. Overall, MRA obtained with the high-field protocol provided better visualization of the arteries, with superior resolution of small arterial branches.

General conclusions from this work are:

**1.** Both high-field and low-field magnetic resonance imaging systems are suitable imaging techniques for assessing the equine head with high detail, but may be inferior to computed tomography for certain conditions.

**2.** Magnetic resonance imaging can be considered the gold standard for studying the central nervous system, including the brain and cranial nerves, as well as the extracranial soft tissues, including the orbit, lymph nodes, blood vessels, muscles, and salivary glands. ●●●

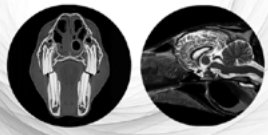



## SUMMARY

●●● **3.** Magnetic resonance imaging is adequate for studying the nasal cavity and paranasal sinuses, and it is particularly useful for differentiating space-occupying lesions, where its high soft tissue contrast resolution allows good differentiation of different tissue types. Diagnostic usefulness of magnetic resonance imaging in cases of dental disease is limited to lesions involving the pulp cavity, the periodontal space, the lamina dura and the bone marrow of the alveolar bone.

**4.** Time-of-flight magnetic resonance angiography is an excellent technique to assess blood vessels of the head and can be performed using both high-field and low-field magnetic resonance imaging systems in equine patients. This rapid sequence provides good visualization of all major intra- and extracranial vessels down to a size of approximately 2 mm in diameter. Visibility of the arterial system is superior than the venous system.

**5.** Time-of-flight magnetic resonance angiography can be incorporated as part of routine imaging protocols in horses affected with soft-tissue space-occupying lesions or vascular abnormalities, without excessive increase in examination time.

**6.** Computed tomography is another suitable imaging technique for assessing the equine head with high detail, but has different indications than magnetic resonance imaging. Both imaging modalities are therefore complementary to each other, and when both modalities are available, preemptive knowledge of the clinically suspected condition is paramount in deciding which modality is most indicated.

**7.** Computed tomography can be considered the gold standard for studying the skull and mandible, the temporomandibular joint, the temporohyoid articulation and the teeth. Computed tomography is adequate for studying the nasal cavity and paranasal sinuses, being particularly useful for identifying subtle nasal and sinusal wall lesions. Computed tomography is undeniably superior to radiology for identifying sinonasal and dental lesions and when available, makes radiology almost obsolete for conditions involving these areas.

**8.** Computed tomography can identify intraventricular and extraaxial brain lesions, however, diagnostic usefulness of computed tomography in cases of intraaxial lesions is limited. Extracranial soft tissue lesions can be identified with computed tomography, but with less detail than with magnetic resonance imaging. ■

# Aplicación de TÉCNICAS DE DIAGNÓSTICO por IMAGEN AVANZADAS en el estudio de la CABEZA DEL CABALLO

Application of advanced diagnostic imaging techniques in the study of the equine head

## LISTS

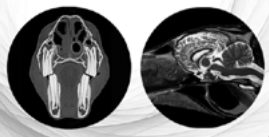



## LIST OF ABREVIATIONS

| | |
|---|---|
| **$^{99m}$TC:** | $^{99m}$Technetium |
| **ADC:** | Apparent diffusion coefficient |
| **B0:** | External magnetic field |
| **B1:** | Radiofrequency pulse |
| **BW:** | Bandwidth |
| **CE-MRA:** | Contrast enhanced magnetic resonance angiography |
| **CSF:** | Cerebrospinal fluid |
| **CT:** | Computed tomography |
| **CTA:** | Computed tomography angiography |
| **DWI:** | Diffusion weighted imaging |
| **FEG:** | Frequency-encoding gradient |
| **FLAIR:** | Fluid attenuated inversion recovery |
| **FOV:** | Field of view |
| **FSE:** | Fast spin echo |
| **GRE:** | Gradient recalled echo |
| **HMPAO:** | Hexamythyl-propyleneamine oxime |
| **HU:** | Hounsfield units |
| **I:** | Iodine |
| **IR:** | Inversion recovery |
| **IRU:** | Increase of radiopharmaceutical uptake |
| **MDCT:** | Multidetector computed tomography |
| **MDP:** | Methylene diphosphonate |
| **MinIP:** | Minimum intensity projection |
| **MIP:** | Maximum intensity projection |
| **MPR:** | Multiplanar reconstruction |
| **MRA:** | Magnetic resonance angiography |
| **MRI:** | Magnetic resonance imaging |
| **Mxy:** | Transverse magnetization |
| **Mz:** | Longitudinal magnetization |
| **NEX / NAD:** | Number of excitations / acquisitions |
| **NPV:** | Negative predictive value |
| **PC-MRA:** | Phase contrast magnetic resonance angiography |
| **PD:** | Proton density |
| **PEG:** | Phase-encoding gradient |
| **PPV:** | Positive predictive value |
| **RF:** | Radiofrequency |
| **ROI:** | Region of interest |
| **SE:** | Spin echo |
| **Se:** | Sensitivity |
| **Sp:** | Specificity |
| **SPGR:** | Spoiled gradient recalled echo |
| **SSG:** | Slice selection gradient |
| **STIR:** | Short tau inversion recovery |
| **T:** | Tesla |
| **T1W:** | T1-weighted |
| **T1WC:** | T1-weighted post contrast |
| **T2W:** | T2-weighted |
| **T2*W:** | T2*-weighted |
| **TE:** | Time of echo |
| **TI:** | Time of inversion |
| **TMJ:** | Temporomandibular joint |
| **TOF-MRA:** | Time of flight magnetic resonance angiography |
| **TR:** | Time of repetition |
| **TSE:** | Turbo spin echo |
| **US:** | Ultrasound |
| **WL:** | Window level |
| **WW:** | Window width |
| **$\mu$:** | Linear attenuation coefficient |
| **$\omega_0$:** | Larmor frequency |

# LIST OF TABLES

## Introduction:



## Paper 1:



## Paper 2:



## Paper 3:

# LIST OF FIGURES

## Introduction:



## Paper 1:

# LIST OF FIGURES

## Paper 2:



## Paper 3:

# Aplicación de TÉCNICAS DE DIAGNÓSTICO por IMAGEN AVANZADAS en el estudio de la CABEZA DEL CABALLO

Application of advanced diagnostic imaging techniques in the study of the equine head

# 1

# INTRODUCTION

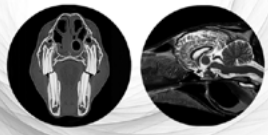



## INTRODUCTION

The equine head is a highly complex anatomic area, as it contains part of the respiratory, digestive and nervous systems as well as the organs of vision and audition (König and Liebich, 2010). Therefore, many different disorders of potentially major clinical importance can settle in this area with clinical signs varying largely on the affected structures, making the diagnosis of these conditions often challenging. The diagnostic approach of head diseases must start with a thorough physical examination (MacDonald, 1993). However, the information obtained from physical examination is commonly limited, and often needs to be complemented by ancillary diagnostic tests with diagnostic imaging techniques playing a crucial role (Mair *et al.*, 2013; Tucker and Farrell, 2001).

Diagnostic imaging modalities used for studying this area include radiography, ultrasonography, scintigraphy and advanced cross sectional techniques, such as computed tomography (CT) and magnetic resonance imaging (MRI). Indications for each modality depend on the affected area as well as the clinically suspected condition (MacDonald, 1993).

INTRODUCTION

## 1.1. Conventional imaging techniques of the equine head

### 1.1.1. Radiography

Traditionally, radiography has been the imaging technique of choice to assess the equine head. The first reports describing its use for this region are from the 1970s (Cook, 1970; 1973). Acquiring high quality diagnostic radiographs of the equine skull can be a challenging task. Complicated by insufficient output of portable x-ray generators commonly used in general practice, and the occasional necessity of general anesthesia for certain cases; its use was initially more restricted to referral centers (Wyn-Jones, 1985b). However, thanks to continuous development of new radiographic systems (e.g. intensifying screens) and more recently the introduction of digital radiology in veterinary medicine, this imaging modality has now become a common diagnostic tool in general practice (Baratt, 2013; Barrett and Easley, 2013).

Radiographs of the skull are usually obtained in the standing sedated horse, using a rope halter and a headstand to stabilize the head (Barrett and Easley, 2013). Because this area is large and anatomically complex, large cassettes (35 cm x 43 cm) should be used in order to maintain spatial relationships when evaluating the radiograph. Radiographic technique will vary depending on the area of interest due to large differences in x-ray attenuation between the different tissues in this region (e.g. enamel is in stark contrast to air within the sinuses) (Park, 1993). Several projections have been described for assessing the different parts of this region; the most common views being the lateral and dorsoventral. However, additional specific views have been described for more specific areas (Table 1) (Ebling *et al.*, 2009; Feichtenhofer *et al.*, 2012; Gibbs and Lane, 1987; Lane *et al.*, 1987a; Park, 1993; Ramzan *et al.*, 2008; Townsend *et al.*, 2009; Wyn-Jones, 1985a; 1985b). Radiographic interpretation of the equine head can be challenging because of superimposition of numerous anatomical structures, dense cortical bone masking more lucent areas, as well as the relatively complex anatomy of this region (Wyn-Jones, 1985b). Detailed indications and description for separate areas of the equine head are given in the following headings.

In order to increase the diagnostic yield of some radiographic examinations of the head, injection of contrast medium within different structures can be performed. The contrast medium consists of a radiopaque substance that fills the injected structure; with the most commonly used being an iodinated non-ionic agent. Contrast radiography is a valuable technique in the investigation of several conditions; its most common form consisting in the injection of the contrast agent into a draining tract (fistulography) for obtaining additional information on the course of a sinus tract, accurately delineating the direction and the boundaries of the lesion (May and Wyn-Jones, 1987). Contrast medium can also been injected into de nasolacrimal duct (dacryocystography), the mandibular and parotid salivary glands and their draining ducts (sialography), the paranasal sinuses (sinusography), or blood vessels (angiography) (Behrens *et al.*, 1991; Colles and Cook, 1983; Cook, 1973; Dehghani *et al.*, 2005; C. A. Latimer *et al.*, 1984; Macdonald *et al.*, 1999). ■

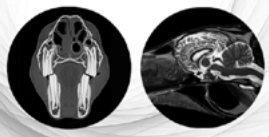



## INTRODUCTION

| EXAMINATION AREA | RADIOGRAPHIC VIEW | STRUCTURES EVALUATED |
|---|---|---|
| Premaxilla (incisor bone) and rostral mandible | Lateral (L) | Incisive bone and rostral mandible |
| | Dorsoventral (DV) | Incisive bone and rostral mandible |
| | Intraoral dorsoventral (DV) | Maxillary incisors and incisive bone |
| | Intraoral ventrodorsal (VD) | Mandibular incisors and rostral mandible |
| Mandible (body) | Lateral (L) | Mandible (body) |
| | Ventro 45º lateral-dorsolateral oblique (V45L-DLO) | Mandible (body) and mandibular cheek teeth |
| | Open-mouth dorso 10º lateral-ventrolateral oblique (D10L-VLO) | Mandibular cheek teeth erupted crowns |
| | Intraoral | Mandibular cheek teeth |
| Nasal cavity and paranasal sinuses | Lateral (L) | Nasal cavity and paranasal sinuses |
| | Dorsoventral (DV) | Nasal cavity, paranasal sinuses and zygomatic arch |
| | Dorso 30º lateral-ventrolateral oblique (D30L-VLO) | Maxillary cheek teeth, paranasal sinuses and orbit |
| | Dorso 75º lateral-ventrolateral oblique (D75L-VLO) | Maxillary sinus and orbit |
| | Open-mouth ventro 15º lateral-dorsolateral oblique (V15L-DLO) | Maxillary cheek teeth erupted crowns |
| | Offset mandible dorsoventral (DV) | Maxillary cheek teeth |
| | Intraoral | Maxillary cheek teeth |
| Caudal skull | Lateral (L) | Cranial vault, temporomandibular joint, tympanohyoid articulation and vertical mandibular rami |
| | Ventrodorsal (VD) | Cranial vault, petrous temporal bone, stylohyoid bone, vertical mandibular rami, paracondylar rocesses, occipital condyles and zygomatic arch |
| | Dorso 30º lateral-ventrolateral oblique (D30L-VLO) | Petrous temporal bone, osseous tympanic bulla and temporohyoid articulation |
| | Rostro 45º ventro 30º lateral-caudodorsolateral oblique (R45V30L-CdDLO) | Temporomandibular joint |
| Pharynx | Lateral (L) | Pharynx, larynx, guttural pouches and soft palate |

**Table 1.** Radiographic projections for evaluation of the equine head. Modified from Park (1993), Barrett *et al.* (2013), and Baratt (2014). The nomenclature follows the recommendations from Smallwood *et al.* (1985).

### 1.1.1.1 Premaxilla (incisor bone) and rostral mandible

The premaxilla and rostral mandible can be evaluated radiographically by obtaining lateral, dorsoventral, intraoral dorsoventral and/or ventrodorsal projections. The main indication of the latter is avoiding overlapping of the rostral mandible or the premaxilla, respectively (Baratt, 2013; Park, 1993; Wyn-Jones, 1985b).

Fractures of the rostral mandible are the most common fracture type observed in this area and are typically seen in young horses (Wyn-Jones, 1985a). In contrast, premaxillary fractures are less common. In both cases incisor teeth are usually involved in the fracture. Therefore intraoral views are recommended for visualizing the course of the fracture line, as well as for assessing the potential dental lesions (Park, 1993).

Root infection of the incisor and canine teeth is less common than of the premolars and molars, but do occur. Radiographic changes consist of an increase of opacity of the alveolar bone surrounding the tooth root, which can be clubbed, and widening of the periodontal space may be also noted. These changes are best visualized using a bisecting angle technique with an intraoral view (Barrett and Easley, 2013; Klugh, 2005). Odontoclastic tooth resorption and hypercementosis may also be observed at the incisor and canine roots of aged horses. This can be radiographically recognized as a widening of the periodontal space and marked hypercementosis of the reserve crowns (Staszyk *et al.*, 2008).

Tumors, although uncommon, may occur in this area. Osteomas, odontogenic tumors (such as ameloblastomas or odontomas) and epidermoid cysts being the most commonly reported (Cook, 1970; Pirie and Dixon, 1993).

### 1.1.1.2. Mandible

The body of the mandible runs from the interalveolar space (diastema) to the vertical ramus, and can be assessed radiographically with a lateral and a ventro 45º lateral-dorsolateral oblique view. Overlapping limits the use of these views for detecting subtle changes, especially around the teeth. Additional projections may therefore be obtained, including open-mouth dorso 10º lateral-ventrolateral oblique view for assessing the erupted (clinical) crowns, and intraoral views (Baratt, 2013; Park, 1993; Wyn-Jones, 1985b).

Fractures of the body of the mandible are most commonly unilateral and have an oblique course, affecting the second premolar and occasionally the third premolar. Tooth root infections may occur if the fracture enters the alveolus (Wyn-Jones, 1985a). Multiple oblique views may be needed for determining the involvement of the teeth, the presence of fragments, the degree of comminution and displacement, the extent of the fracture and any compromise of the neural canals (Park, 1993).

Dental disease commonly affects the mandibular teeth and although there is less overlapping compared to maxillary teeth, oblique radiographs are still essential for accurate diagnosis (Barrett and Easley, 2013). This condition is usually presented as alveolitis or apical abscesses, the first one is identified by a widening of the periodontal space with resorption of the lamina dura, while the latter is characterized by blunting of the tooth root, surrounded by osteolysis and osseous sclerosis of the alveolar bone (Gibbs and Lane, 1987; Park, 1993). Apical abscesses in the mandible often develop into draining tracts to the outside, which can be recognized radiographically as a lytic tract extending through the ventral mandibular cortex (Park, 1993). In these cases the use of metallic probes placed into the draining tract or the injection of contrast medium can provide additional information for identifying the affected apical portion and providing a landmark for surgery planning (Barakzai, 2011).

### 1.1.1.3. Nasal cavity and paranasal sinuses

Radiographic examination of the maxillary region is the most commonly performed skull radiographs in the horse (Barrett and Easley, 2013; Wyn-Jones, 1985b). Radiology provides a good diagnostic complement to physical examination and endoscopy, however, anatomical complexity and superimposition of surrounding structures ●●●

represent an important limitation in this region (Arencibia *et al.*, 2000; D'Août *et al.*, 2014). Obtaining several radiographic projections in order to assess the different structures present in this region is therefore essential. A standard radiographic examination usually includes a lateral, a dorsoventral and both right and left dorso 30º lateral-ventrolateral oblique views. Specific additional projections are also described, such as dorso 75º lateral-ventrolateral oblique for the paranasal sinuses, or open mouth ventro 15º lateral-dorsolateral oblique, offset mandible dorso-ventral, and intraoral views of the maxillary premolar and molar teeth (Barakzai, 2005a; Baratt, 2013; Lane *et al.*, 1987a; Park, 1993; Wyn-Jones, 1985b).

Many different diseases can affect the maxillary region, with dental disease being the most common, and represents approximately 22% of the horses with sinonasal disease (Tremaine and Dixon, 2001). Radiographic identification of dental pathology may be challenging due to overlapping of surrounding structures and frequent association of dental disease with sinusitis, partially obscuring the teeth with a soft tissue opacity from the sinuses (Gibbs and Lane, 1987; Wyn-Jones, 1985a). This is particularly significant in detecting alveolar bone sclerosis, which is one of the radiographic signs of dental disease and already particularly difficult to accurately define (Barrett and Easley, 2013). It is therefore not surprising that radiographic sensitivity in diagnosing dental disease has been reported to be low (51.5 – 57%). In contrast though, a high specificity (91 – 95%) can be achieved with this modality (Tremaine and Dixon, 2001; Weller *et al.*, 2001). Radiographic features of periapical infection can be diverse, but the most reliable indicators include periapical sclerosis, periapical halo formation and clubbing of the tooth root. All of them show good sensitivity and specificity (Townsend *et al.*, 2011). These signs are however only seen in advanced dental disease (Gibbs and Lane, 1987; Wyn-Jones, 1985a). Conversely, radiographic signs detectable in the early stages of apical infection (e.g. widening of the periodontal space and loss of the lamina dura) are less reliable (Townsend *et al.*, 2011). Loss of the lamina dura was found to have high sensitivity (90%), but very low specificity (34%), so this feature should be interpreted cautiously (Bühler *et al.*, 2014; Townsend *et al.*, 2011). Other radiographic features of periapical infection include cementum deposition around the reserve crown, cementoma formation, reserve crown fragmentation, reserve crown lucency, dental dysplasia and dental displacement (Gibbs and Lane, 1987; Townsend *et al.*, 2011; Wyn-Jones, 1985a). Diastemata formation and crown fractures may also be seen in association with periapical infections, being potential causes for this condition (Park, 1993).

Sinusitis consists on an inflammation of the paranasal sinuses, and is commonly associated with presence of fluid within the sinuses (Tremaine and Dixon, 2001). This disease may be caused by primary bacterial or mycotic infection, or can occur secondary to dental disease, facial trauma, sinus cysts, progressive ethmoid hematomas, or sinonasal neoplasia (Gibbs and Lane, 1987; Park, 1993; Tremaine and Dixon, 2001; Wyn-Jones, 1985a). Dental disease is the most common cause of secondary sinusitis (Mason, 1975; Tremaine and Dixon, 2001). Sinusitis can be recognized radiographically by the presence of fluid lines, which represent air-fluid interfaces (Gibbs and Lane, 1987). In cases of more chronic sinusitis, areas of increased soft tissue opacity may be observed within the sinuses as a result of more inspissated fluid. Other radiographic features of sinusitis include a more diffuse increase in soft tissue opacity throughout the paranasal sinuses when these are fully fluid filled, or when generalized mucosal thickening occurs. Cortical bone expansion and sinus septal deviation are less commonly seen (P. M. Dixon *et al.*, 2012; Gibbs and Lane, 1987; Tremaine and Dixon, 2001; Wyn-Jones, 1985a). The caudal and rostral maxillary sinuses are the most commonly affected, although any of the sinus compartments can be affected (P. M. Dixon *et al.*, 2012). Due to further superimposition and their smaller size, assessment of ventral conchal and sphenopalatine pathology is even more challenging, therefore only showing abnormalities when severely affected. As involvement of those sinuses has great diagnostic and prognostic importance, several projections such as offset man-

●●● dible dorsoventral view are needed in order to increase their visibility (Finnegan *et al.*, 2011; Perkins *et al.*, 2009; L. J. Smith and Perkins, 2009).

Fractures secondary to direct trauma are common in the nasal cavity and paranasal sinuses, with depressed fractures being most common (Park, 1993). Radiographic identification of the fracture may be difficult due to overlapping of numerous structures with different opacity, as well as the curved shape of the fracture fragments (Lane *et al.*, 1987a). The x-ray beam therefore needs to be tangential to the bone fragment in order to become visible, and several projections at slightly different angles of obliquity may therefore be required (Park, 1993). Considering their pronounced curvature, this is particularly the case in orbital and zygomatic arch fractures (Barrett and Easley, 2013). Soft tissue opacities within the paranasal sinuses may further obscure the bony fragments. These opacities corresponding to hemorrhage/blood clots and secondary sinusitis in acute and chronic fractures, respectively (Park, 1993).

Masses within the nasal cavity and paranasal sinuses comprise a wide range of different etiologies; the most common ones being sinus cysts, progressive ethmoid hematomas and neoplasms (Gibbs and Lane, 1987; Head and Dixon, 1999; Lane *et al.*, 1987b; Park, 1993; Tremaine, 2013; Tremaine and Dixon, 2001; Woodford and Lane, 2006; Wyn-Jones, 1985a). Sinus cysts are characterized by a well-defined, smoothly marginated, expansile and multiloculated soft tissue opacity within maxillary and conchofrontal sinuses (Lane *et al.*, 1987b; Woodford and Lane, 2006). Secondary radiographic features associated with sinus cysts include nasal septum deviation, dental displacement, cyst wall mineralization, and cortical bone thinning due to expansion (Gibbs and Lane, 1987; Lane *et al.*, 1987b; Tremaine and Dixon, 2001). The dorsoventral view is the most helpful projection for margin delineation of cysts, but concurrent fluid within the sinuses and mucosal thickening may silhouette with, and therefore obscure the cysts (Barrett and Easley, 2013). Progressive ethmoid hematomas are most commonly found in the region of the ethmoid turbinates, but are occasionally also affecting the paranasal sinuses (P. M. Dixon *et al.*, 2012; Gibbs and Lane, 1987; Wyn-Jones, 1985a). This structure generally appears as a well-defined, smoothly marginated soft tissue mass (Gibbs and Lane, 1987; Tremaine and Dixon, 2001). When located in the sinuses, an ethmoid hematoma is indistinguishable from a sinus cyst, and may similarly be obscured by free sinus fluid (Barrett and Easley, 2013). Neoplasms of the nasal cavity and paranasal sinuses are relatively rare in horses (Head and Dixon, 1999). Squamous cell carcinoma is the most commonly reported type of tumor in this location. Other tumors include adenocarcinoma, fibrosarcoma, osteosarcoma, osteoma, myxoma, dental origin tumors, hemangiosarcoma and lymphoma (P. M. Dixon *et al.*, 2012; P. M. Dixon and Head, 1999; Head and Dixon, 1999; Hilbert *et al.*, 1988). Radiographic features will vary depending on the type of tumor from no changes to marked osseous lysis and/or bone proliferation in the more aggressive cases (P. M. Dixon *et al.*, 2012; Park, 1993). The most common radiographic sign consists of increased sinus opacity, occasionally associated with fluid lines, nasal septum deviation, and osseous wall expansion or remodeling (Park, 1993). A merely well-defined soft tissue mass is sometimes visualized radiographically, but concurrent osseous lysis may be missed due to superimposition of other bony structures or obliquity (Barrett and Easley, 2013).

### 1.1.1.4. Caudal skull

Radiographic examination of the cranial vault consists of a lateral and a ventrodorsal view (Park, 1993). An additional dorso 30º lateral-ventrolateral oblique view can be obtained to examine the petrous temporal bone area, the osseous tympanic bulla and the temporohyoid articulation in more detail (Lane *et al.*, 1987a; Park, 1993). Specific views for the temporomandibular joint have also been reported, including a rostro 45º ventro 30º lateral-caudodorsolateral oblique and a caudo 15º dorso 70º medial-rostroventrolateral oblique (Ebling *et al.*, 2009; Ramzan *et al.*, 2008; Townsend *et al.*, 2009). This region is difficult to examine radiographically due to its complex anatomical configuration and the large amount of ●●●

●●● overlapping of surrounding structures (Barrett and Easley, 2013). Radiographic examination of temporomandibular joint requires the use of several projections in order to avoid the superimposition of structures and to expose the curved-shaped articular surface (Weller *et al.*, 1999a). Although tangential projections optimize visualization of the articular surface and joint space, the medial aspect of the joint is still obscured and therefore, radiographic diagnosis of this joint remains very limited.

Fractures of the cranial vault, orbit and the base of the skull are extremely difficult to diagnose using radiography, and numerous tangential views are usually required (Gerding *et al.*, 2014; Gibbs and Lane, 1987; O. Ramirez III *et al.*, 1998; S. Ramirez and Tucker, 2004). Involvement of the surrounding soft tissues (e.g. eye globe and brain) cannot be detected on radiographs (S. Ramirez and Tucker, 2004; Scrivani, 2013).

Radiographic features of temporohyoid osteoarthropathy consist of thickening and fractures of the stylohyoid bone, remodeling of the temporohyoid articulation and sclerosis of the petrous temporal bone (Hilton *et al.*, 2009; Walker *et al.*, 2002). Although these changes are best visualized on a ventrodorsal view, recognition of these changes are extremely difficult using radiography (Barrett and Easley, 2013).

Dentigerous cysts are a distinctive tooth-like tumor that are most frequently found at the base of the ear attached to the temporal bone, but can also be observed in the maxillary region as well (Easley *et al.*, 2010; Gibbs and Lane, 1987; L. C. R. Smith *et al.*, 2012). Its radiographic appearance varies, and can range from being a round radiolucent structure with a striated, vertical radiodense pattern (aka dental buds) to present fully developed dental structures (Easley *et al.*, 2010; Gibbs and Lane, 1987). Dentigerous cysts can consist of more than one dental structure, bilateral at times, and they typically have an associated draining tract (Barrett and Easley, 2013; Easley *et al.*, 2010; Gibbs and Lane, 1987; L. C. R. Smith *et al.*, 2012). Tangential views to the lesion are commonly helpful for making a diagnosis (Park, 1993). Occasionally these cysts develop in the cranium, being intimately associated with the brain, with surgical planning therefore often being incomplete based on radiographs alone (Barrett and Easley, 2013).

### 1.1.1.5. Pharynx

Radiographic examination of the pharyngeal region usually consists of a lateral projection with the head extended to decrease the overlapping of the mandibular rami over the rostral aspect of this region (Gibbs, 2010). Radiography can give complementary information to endoscopy about both intra-luminal and extra-luminal lesions.
In the guttural pouch both active hemorrhage and empyema look similar, from soft tissue opacity with a fluid line to complete obliteration of normal pouch air shadow. However, in chronic cases organization of the blood clot produces soft tissue opacity mottled by irregular and poorly demarcated lucencies; whereas inspissated inflammatory exudates can create chondroids, characterized by multiple smoothly marginated, irregularly shaped mineral opaque masses. Radiography can determine the amount of air accumulation and the degree of distension of the guttural pouch in cases of gutteral tympany. A ventral displacement of the dorsal wall of the pharynx and caudal extension of the guttural pouch beyond the level of the first cervical vertebra are then also observed (Butler *et al.*, 2008; Wyn-Jones, 1985a).

Masses surrounding the pharyngeal area are uncommon. Their origin include the parotid salivary gland, retropharyngeal lymph nodes, or the guttural pouch itself, the latter usually representing squamous cell carcinomas. These lesions can displace or obliterate the guttural pouch and/or the pharynx. Differentiating masses from fluid, and deciding whether the mass is within or adjacent to the guttural pouch using radiography is challenging (Cook, 1973).

Diseases of the soft palate such as persistent dorsal displacement, cleft palate or soft palate cysts can also be diagnosed radiographically (Butler *et al.*, 2008; Haynes *et al.*, 1990; Wong *et al.*, 2011; Wyn-Jones, 1985a). ■

## 1.1.2. Ultrasonography

Ultrasonography is a non-invasive imaging modality with high soft tissue contrast and spatial resolution that can be performed in the standing sedated horse, and has great potential for assessing the anatomy and diseases of the equine head (Plummer and Reese, 2014; Rathmanner and Rijkenhuizen, 2012). However, a number of structures of interest in this region, such as nasal passages, paranasal sinuses, and cranium, are encased within bone and/or gas filled, precluding their ultrasonographic assessment (Plummer and Reese, 2014).

### 1.1.2.1. Eye and adnexa

Ocular ultrasonography is indicated when conventional ophthalmologic examination is not possible. This includes opacities of the cornea, lens, aqueous humor or vitreous humor, or in cases of orbital trauma, severe swelling, masses, and location of ocular foreign bodies (Seco Diaz, 2004).

Ultrasonographic evaluation of the eye globe in cases of ocular trauma allows identification of lesions within the anterior and posterior segments. Main alterations of the anterior segment include fibrin accumulation, hypopyon or hyphema, which often results in an increase of echogenicity associated with aqueous humor (Plummer and Reese, 2014; Schaer, 2007; Seco Diaz, 2004). Lens alterations may also occur, such as capsule rupture or anterior or posterior lenticular luxation or subluxation (Plummer and Reese, 2014; Schaer, 2007). Changes within the posterior segment visualized by ultrasound include vitreal hemorrhage, retinal detachment and tears, choroidal detachment and sclera rupture (Reimer and Latimer, 2011; Schaer, 2007; Scotty *et al.*, 2004a).

Ultrasound is useful to detect and staging cataracts, which are characterized by the presence of echogenic to hypoechogenic areas within the lens (Scotty *et al.*, 2004a). Hypermature cataracts usually show hyperechoic areas causing acoustic shadows consistent with mineralizations within the lens (Seco Diaz, 2004). Ultrasonography is also recommended in cases of cataracts for evaluating the posterior segment in search of concurrent lesions such retinal detachment (Plummer and Reese, 2014).

Periocular masses can have different origin, such as cysts, tumors or abscesses, and ultrasound examination is important in these cases to determine the location, size, shape, and extension of the mass, as well as for defining which structures are affected (Knottenbelt *et al.*, 2007; Seco Diaz, 2004).

Ultrasound also allows examination of the retrobulbar area for confirming the presence of a space occupying lesion, and to determine the location, character, size, and relation of the mass to other structures (Greenberg *et al.*, 2011; Matiasek *et al.*, 2007; Robertson *et al.*, 2002; Scotty *et al.*, 2004b; Seco Diaz, 2004). Ultrasonographic differentiation of the origin of these lesions is challenging; retrobulbar abscesses, hematomas and neoplasms are usually imaged as discrete masses, whereas retrobulbar hemorrhage, cellulitis, or more aggressive tumors are usually more diffuse (S. Ramirez and Tucker, 2004; Seco Diaz, 2004). Ultrasound is limited by the bony margins of the equine orbit, so the orbital space cannot be completely evaluated by ultrasound (S. Ramirez and Tucker, 2004).

Foreign bodies, both intraocular and orbital, can be successfully detected with the use of ultrasound (S. Ramirez and Tucker, 2004; Seco Diaz, 2004).

### 1.1.2.2. Temporomandibular joint

Ultrasonographic evaluation of the temporomandibular joint is limited to the lateral aspect of the condyloid process, and allows examination of the articular surfaces, the articular cartilage, the disc, the intra-articular fat tissue, as well as the joint capsule (Rodríguez *et al.*, 2007; Weller *et al.*, 1999b). Disruption of the smooth periarticular outline of the temporomandibular joint, joint capsule thickening, disruption of the articular disc or abnormal fluid accumulation can be detected using ultrasonography (T. P. Barnett *et al.*, 2014; Weller *et al.*, 1999a).

### 1.1.2.3. Skull

Ultrasound is unable to penetrate bone or dental tissue, however, can highlight the osseous surfaces with high detail (Rathmanner and Rijkenhuizen, 2012). Ultrasound is useful for identifying the origin of swellings or draining tracts that may accompany disease of the maxillary or mandibular arcade due to foreign body, dental disease or formation of a bony sequestrum (Archer, 2014; Puchalski, 2006). Occasionally, a previously undelineated draining tract within a soft tissue swelling can be followed ultrasonographically to its site of origin, especially if the swelling involves the mandible (Puchalski, 2006).

Ultrasonography can also assist with the diagnosis and management of fractures of thin superficial bones of the skull, which may be difficult to visualize radiographically, particularly in mandibular fractures (Archer, 2014; Müller *et al.*, 2011).

### 1.1.2.4. Soft tissues

#### A. Salivary glands

Parotid, mandibular and sublingual salivary glands and their ducts can be evaluated ultrasonographically (Archer, 2014). It is possible to identify obstructive sialolithiasis, foreign bodies, abscess formation, neoplastic infiltration, and generalized inflammation of the gland, as well as distension of the duct (Archer, 2014; Kilcoyne *et al.*, 2015; Rathmanner and Rijkenhuizen, 2012).

#### B. Lymph nodes

Mandibular and retropharyngeal lymph nodes can be examined by ultrasonography, the latter is inconstantly identified in healthy horses, with the medial being easier to visualize than the lateral (De Clercq *et al.*, 2003; Rathmanner and Rijkenhuizen, 2012; Reef, 1998). They consist of small, ovoid structures with a homogeneous soft tissue echogenicity with a discrete more hyperechoic capsule (Archer, 2014). Viral or bacterial infections may result in enlargement of the lymph nodes, with occasional abscess formation. Nasal and paranasal disorders, such as tumors, can also cause lymph node enlargement (De Clercq *et al.*, 2003).

#### C. Tongue

The tongue can be thoroughly evaluated using ultrasonography, using both intra-oral and submandibular approaches (Archer, 2014). Ultrasound may be helpful for identification of foreign bodies, both metallic wires and wood splinters, or abscess formation within the tongue and adjacent structures. Examination is however limited by the body of the mandible (Archer, 2014; Pusterla *et al.*, 2006; Solano and Penninck, 1996).

#### D. Brain

Limited ultrasonographic examination of the brain can be performed in neonates with open fontanels or in any horse with palpable defect in the cranium. It is especially helpful for identifying hydrocephalus (Reef, 1998).

#### E. Other

Overall, ultrasonography is a good diagnostic tool for assessing any soft tissue located in the head that is not covered by bone, and has been reported for also evaluating blood vessels and subcutaneous masses (Bienert-Zeit *et al.*, 2011; Muñoz *et al.*, 2014). ■

## 1.1.3. Scintigraphy

Nuclear scintigraphy is a non-invasive and sensitive technique that reflects active physiological processes, rather than anatomic changes, associated with the organ studied (Driver, 2003). Scintigraphy is based on the detection of γ-rays emitted from the decay of a radionuclide, by a gamma camera (Driver, 2003). The radionuclide is the radioactive component of the radiopharmaceutical, with $^{99m}$ Technetium ($^{99m}$Tc) being currently the most commonly used in equine practice (Archer *et al.*, 2007). The radiopharmaceutical used is dependent on the body component to be targeted. Diphosphonate salts, specifically methylene diphosphonate (MDP), are the most commonly used in equine scintigraphy, as they selectively localize to the bone (Driver, 2003). Other radiopharmaceutical, such as $^{99m}$Tc hexamythyl-propyleneamine oxime (HMPAO)-labeled leucocytes has been described for equine dental scintigraphy, but due to the lack of anatomical detail made identification of diseased teeth impossible (Weller *et al.*, 2001).

A dose of 10 MBq / kg bodyweight $^{99m}$Tc-MDP is administered to the horse via an intravenous catheter. Typically, for sinonasal disorders only bone-phase images are acquired at 2 – 4 hours post injection, as soft tissue phase images do not provide valuable additional information (Archer *et al.*, 2010; Weller *et al.*, 2001).

Heavy sedation, cotton wool ear plugins and blinkers are usually required in order to allow close positioning of the camera to the patient. In addition, a head stand is used to stabilize the patient's head, preventing rotation in the sagittal plane (Archer *et al.*, 2010; Weller *et al.*, 2001). A rope, as opposed to leather and metal, halter should be used to prevent attenuation of the gamma rays (Weller *et al.*, 2001).

Typical scintigraphic views of the equine head include left and right lateral, dorsal and ventral images. Oblique views may be used to assist lesion localization (Archer *et al.*, 2010; Ramzan, 2003). In order to avoid superimposition on dorsal or ventral views, a lead shielding may be placed between the maxillary and mandibular arcades or under the head depending on the view and the diseased area (Ramzan, 2003). The atlantooccipital joint may be imaged by positioning the camera dorsal to the poll and parallel to the floor (Archer *et al.*, 2010).

Scintigraphy can be used for detecting dental, sinonasal, musculoskeletal, and less commonly soft tissue diseases.

### 1.1.3.1. Dental

Scintigraphy has been shown to have high sensitivity (95.5%) and moderate specificity (86.4%) for detecting dental disease in the horse (Weller *et al.*, 2001). Because of the lower specificity, this technique is most useful when combined with other diagnostic techniques such as radiography and oral examination (Boswell *et al.*, 1999; Weller *et al.*, 2001). Periapical dental infection results in a focal and intense increase of radiopharmaceutical uptake (IRU) over the apical region of the affected tooth. If periapical infection is associated with secondary sinusitis, diffuse moderately increase in uptake over the affected sinus is observed surrounding the affected tooth (Weller *et al.*, 2001). Region of interest (ROI) studies comparing the affected region to the contralateral side, specially on the dorsal views, will show marked differences of radiopharmaceutical uptake (Archer *et al.*, 2003). Periodontal disease usually results in a linear pattern of activity over the whole arcade (Archer *et al.*, 2003; Barakzai, 2005b; Weller *et al.*, 2001). Dental diseases due to pulpitis or infundibular necrosis alone do not alter the pattern of uptake (Weller *et al.*, 2001).

### 1.1.3.2. Nasal cavity and paranasal sinuses

Scintigraphy has been reported to have a moderate sensitivity (78.9%) and specificity (91.7%) for detection of paranasal sinus disorders (Barakzai *et al.*, 2006). Primary sinusitis may show variable patterns of uptake, generally associated with diffuse or patchy IRU over the affected sinus (Archer *et al.*, 2003; Barakzai *et al.*, 2006; Weller *et al.*, 2001). However, some cases may exhibit focal areas of moderate to marked IRU. If these focal areas of IRU are superimposed over a cheek

tooth, careful evaluation is essential for avoiding incorrect diagnosis of dental disease (Barakzai *et al.*, 2006; P. M. Dixon *et al.*, 2012).

Sinus cysts usually have a characteristic circular pattern of marked IRU around the cyst margins. Progressive ethmoid hematomas on the other hand have been reported to present non-specific diffuse, moderate IRU that is indistinguishable to sinusitis (Barakzai *et al.*, 2006). Nasal tumors may also be identified using scintigraphy (Archer *et al.*, 2003).

### 1.1.3.3. Musculoskeletal

Sequestra and fractures are commonly associated with moderate to marked IRU (Barakzai *et al.*, 2006; Weller *et al.*, 2001). In contrast, osteotomy sites, such as those caused when creating sinus flaps or trephine holes, appear to be associated with little or no IRU (Archer *et al.*, 2003; Barakzai and Dixon, 2003).

Temporomandibular and temporohyoid diseases may also be detected by using scintigraphy, with marked focal IRU being indicative of a lesion (Archer *et al.*, 2003; Frame *et al.*, 2010; Weller *et al.*, 1999a).

### 1.1.3.4. Soft tissues

Soft tissue phase can also be used when evaluating the equine head for identifying the cause of swellings or for testing the function of the salivary glands (Archer *et al.*, 2003; Montgomery *et al.*, 2012). ■

# 1.2. Advanced diagnostic imaging techniques of the equine head

## 1.2.1. Computed tomography

Clinical use of computed tomography started in the early 1970s, and since then has been introduced progressively in veterinary medicine, nowadays being a routine diagnostic modality in veterinary practice (Hounsfield, 1973; Whatmough and Lamb, 2006). CT was the first tomographic technique combining computer calculation power with medical imaging and thus starting the era of digital imaging (Ohlerth and Scharf, 2007).

### 1.2.1.1. Basic principles

#### A. Physics

##### X-RAY BEAM ATTENUATION

CT uses the same principles as in conventional radiography. As a collimated x-ray beam penetrates the patient's tissues, fractions of the original beam are absorbed while others pass through. Then the x-ray intensity behind the object is measured to form the image, and this is achieved by the use of x-ray detectors (Bushberg *et al.*, 2002a).

The absorption of x-rays within an object is directly proportional to the linear attenuation coefficient (μ) of the object through which the beam passes, and the thickness of the object as seen in Beer's law.

$$I(x) = I_0 e^{-\mu x}$$

Where I(x) is the intensity of the attenuated x-ray beam, I_0 the intensity of the primary x-ray beam and x the thickness of the material (Geleijns, 2014).

This coefficient μ depends on the composition of the object, the electron density of the object, and the photon energy of the x-ray beam. Therefore high electron density tissues, such as bone, possess a higher linear absorption compared to low electron density tissues, such as fluids or fat.

As the patient is composed by different tissues with different linear attenuation coefficients, the intensity of the attenuated x-ray beam would result from the summation of the individual linear attenuation coefficients of each tissue through which the beam passes.

$$I(d) = I_0 e^{-\sum_{i=1}^{i=n} \mu \Delta x}$$

Where d represents the thickness of the tissue and n the number of different tissues that the x-ray beam passes (Bushberg *et al.*, 2002a; Geleijns, 2014).

##### IMAGE FORMATION

The attenuation data obtained from the different projections are re-calculated using a mathematical process called filtered back projection. This produces a matrix of the average relative x-ray absorptions in each volume element (voxel) of the matrix in the slice of tissue examined (Hathcock and Stickle, 1993). These mean attenuation values in each element of the matrix is transformed into a corresponding matrix of Hounsfield units (HU), where the HU is expressed relative to the linear attenuation coefficient of water at room temperature ($\mu_{water}$) (Geleijns, 2014).

$$HU_{tissue} = \frac{\mu_{tissue} - \mu_{water}}{\mu_{water}} x\ 1000$$

This matrix is displayed as picture elements (pixels) in shades of grey in a two-dimensional digital image matrix. A pixel therefore represents a two-dimensional image of a three-dimensional voxel within the patient, the third dimension (z-axis) being the slice thickness of the examined cross-section of the patient (Ohlerth and Scharf, 2007).

##### IMAGE DISPLAY

Water has an attenuation value of 0 HU with only a small amount of the x-ray intensity being attenuated. The HU of other tissues are displayed as a value relative to the attenuation of water, and vary little with change of the x-ray energy (Brink *et al.*, 1994; Bushberg *et al.*, 2002a).

The Hounsfield scale ranges from –1000 HU to +3095 HU, representing the lowest HU as dark (hypoattenuating) and the highest HU as bright (hyperattenuating). However, because human eye only differentiate a limited number of levels

of grey, HU are grouped for creating windows with different width (WW) and level (WL). The WW refers to the range of HU that is represented by the grey scale (ranged from white to black), the window level (WL) defines the central grey color and should be set at the level of the tissue of interest. Optimal visualization of the tissues of interest in the image can only be achieved by selecting the most appropriate WW and WL. Consequently different settings of WW and WL are used to visualized soft tissue, lung tissue or bone (Tidwell and Jones, 1999).

**Figure 1.** Transverse CT images of the equine head at the level of the third premolar (A and B) and the orbit (C and D) displayed using bone (A and C) and soft tissue (B and D) windows.


## B. CT imaging systems

### AXIAL SCANNERS

Over time different generations of scanners have been developed. The first generation scanners of CT used two x-ray detectors, and they measured the transmission of x-rays through the patient for two different slices. These scanners employed a rotate/translate system and a pencil-shaped x-ray beam. Starting at a particular angle, the x-ray tube and detector system translate linearly across the field of view (FOV), acquiring 160 parallel rays, once completed their translation the whole system was rotated slightly to the next position, and then another translation was used to cover the field of view again. This procedure

●●● was repeated at 1-degree intervals until covering the 360 degrees (180 projections), resulting in the complete CT data set. In total this procedure took a scan time of 3 – 5 min for only one slice (Bushberg *et al.*, 2002a; Ohlerth and Scharf, 2007).

In the second generation scanners, the next improvement to the CT scanner was the incorporation of a linear array of detectors and the use of a narrow fan-shaped x-ray beam. Together they translated and then rotated through 360 degrees but needed fewer angular steps to produce the image, thus reducing the scan time to 18 seconds per slice (Bushberg *et al.*, 2002a; Geleijns, 2014).

The third generation scanners used a rotate/rotate conformation, referring to the rotation of the x-ray tube and the detector array in the same geometrical relation fixed on a frame, called gantry, 360 degrees around the patient. The tube produced a wide fan-shaped x-ray beam that fell on a larger array of many detectors. By elimination of the translational motion, the scan time was reduced being shorter than 5 seconds, however, their main limitation consisted of the ring artifacts (Bushberg *et al.*, 2002a; Ohlerth and Scharf, 2007).

Fourth generation scanners were designed to overcome the problem of ring artifacts, therefore a rotate/stationary system was used. The detectors were removed from the rotating gantry and were placed in a stationary 360-degree ring around the patient, requiring many more detectors. Then, the x-ray tube alone rotated through 360 degrees around the patient (Bushberg *et al.*, 2002a).

The first generations scanners were hindered by the tube's electrical cables, which did not allow one-way rotation around the patient, and by the patient table that did not move during the scan. The examination volume had to be covered by subsequent transverse scans in a "step and shot" mode (Bertolini *et al.*, 2006; Bushberg *et al.*, 2002a).

#### HELICAL SCANNERS

The continuous one-way rotation of the tube-detector system became possible with the invention of the slip-ring techniques, which eliminated the need to rewind the gantry after each rotation and enabled continuous data acquisition during subsequent rotations (helical CT) (Crawford and King, 1990). Therefore, the patient is scanned with a rotating tube-detector system while the table transports the patient through the gantry in the longitudinal (z-axis) direction, which allows a significant reduction of the scan time (Ohlerth and Scharf, 2007). The first helical scanners used one tube-detector array pair (single-slice CT); in contrast, multidetector CT (MDCT) or multichannel CT extends the number of detectors to several rows from 2 up to 640 (Bertolini and Prokop, 2011; Bushberg *et al.*, 2002a; Cao *et al.*, 2014). Then, the simultaneous acquisition of several detector rows results not only in an increase in speed but also in an extension of the scan range that could be covered within a certain time by a factor equal to the number of detector sections (Geleijns, 2014).

In single-slice CT scanners, the slice thickness (z–axis), determined by the collimation of the x-ray beam, is substantially larger than the size of each pixel in the x-y plane. The resulting voxels have therefore an elongated shape (anisotropic voxel). Ideally, voxels should be of equal dimensions in all three spatial axes (x–y–z) so that the spatial resolution is isotropic. In which case, images may be reconstructed in any plane from a stack of transverse slices without losing spatial resolution. Such an isotropic resolution results from thin-section scanning with a section thickness of 1 mm or less (Bertolini and Prokop, 2011). The higher number of detector rows available, the larger scan range with isotropic voxels can be covered (Flohr *et al.*, 2005).

### C. Post-processing techniques

Scanned volumes from MDCT systems can be displayed not only as a sequence of cross-sections but also as a true volume. Different types of reconstructions can be performed after images acquisition, which need of a workstation with special software (Lipson, 2006). ●●●

## INTRODUCTION

### MULTIPLANAR RECONSTRUCTION

Multiplanar reconstructions (MPR) allow reformat into any plane in the space (sagittal, dorsal, oblique or curved). This is achieved by staking the transverse images for obtaining a volume (Kinns *et al.*, 2011; Rubin, 2003). The quality of the MPR is directly related to the original image slice thickness, when voxels are isotropic the quality of a reconstructed image in any plane is virtually identical to the original transverse image (Lipson, 2006).

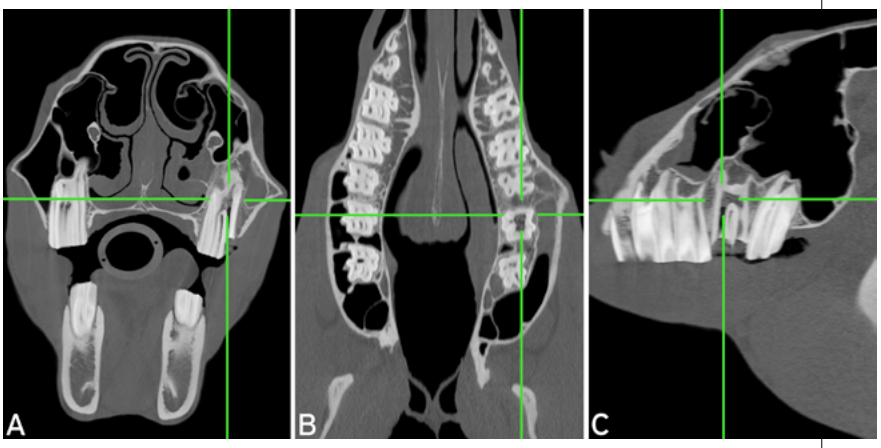


**Figure 2.** Transverse (A), dorsal (B) and sagittal (C) CT images displayed with a bone window using a multiplanar reconstruction showing a lesion within the tooth 210.

### MAXIMUM INTENSITY PROJECTION

Maximum intensity projection (MIP) consists of projecting the voxel with the highest attenuation value on every view throughout the volume onto a 2D image (Bertolini and Prokop, 2011). This method tends to display bone and contrast material–filled structures preferentially, and other lower-attenuation structures are not well visualized. The primary clinical application of MIP is to improve the detection of pulmonary nodules and assess their profusion (Ravenel and McAdams, 2003; Rubin, 2003)

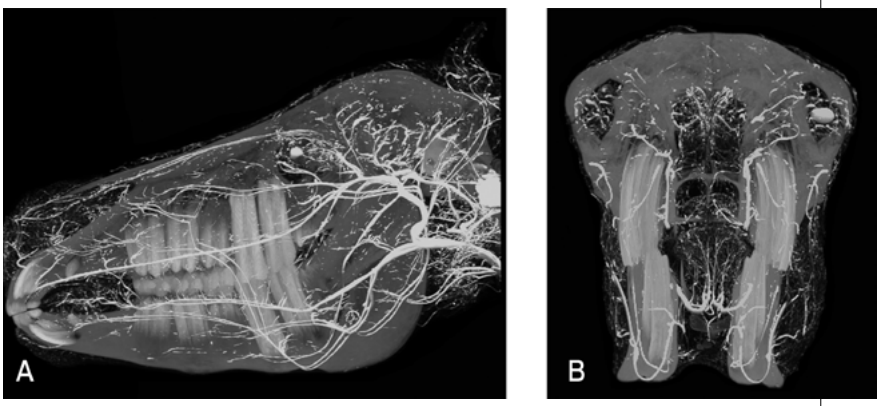


**Figure 3.** Lateral (A) and frontal (B) views of a MIP reconstruction of an equine head CT arteriogram.

### MINIMUM INTENSITY PROJECTION

Minimum intensity projection (MinIP) images are the counter-part of MIP images: instead of projecting the highest attenuation values into the viewing plane, they display the lowest attenuation values. MinIP can be used to generate images of central airways or areas of air trapping within the lung (Lipson, 2006; Rubin, 2003).

**Figure 4.** Dorsal view of a MinIP reconstruction of a canine thorax. Image courtesy of Natalia Díez-Bru (Diagnostic Imaging Service, CMV Delicias, Spain).

## INTRODUCTION

### VOLUME RENDERING

For generating a volume rendering (3D reconstructions) each voxel in the examined volume is used to calculate the final image. This is achieved by assigning each voxel in the examined volume an opacity value (from 0% to 100%, total transparency to total opacity). The resulting images therefore contain more information and are potentially more useful than MIP, which only uses high attenuation value voxels (Lipson, 2006). Volumes can be manipulated in many different ways to demonstrate the desired anatomy. This tool allows appreciation of spatial relationships between structures (Kinns *et al.*, 2011).

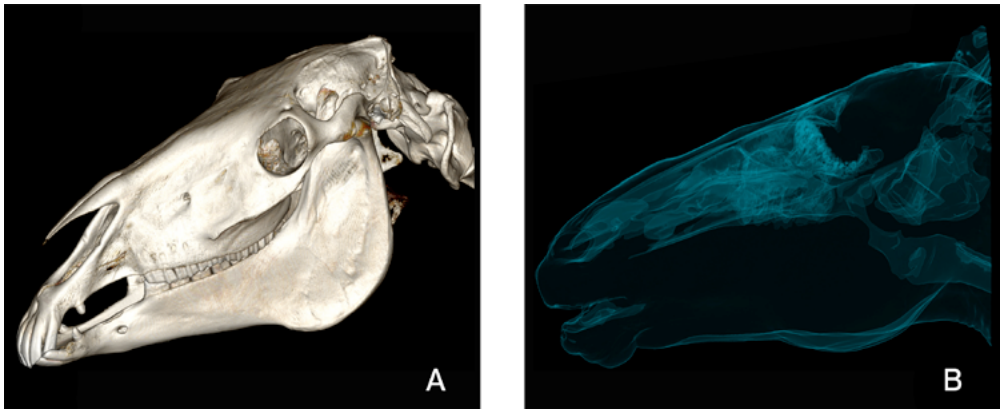


**Figure 5.**
Lateral volume reconstruction of the equine skull (A) and the upper airways (B).

### ENDOLUMINAL VIEW

Endoluminal viewing ("virtual endoscopy") is a perspective volume rendering technique that allows users to visualize the lumen of anatomical or pathological structures (Lipson, 2006). ■

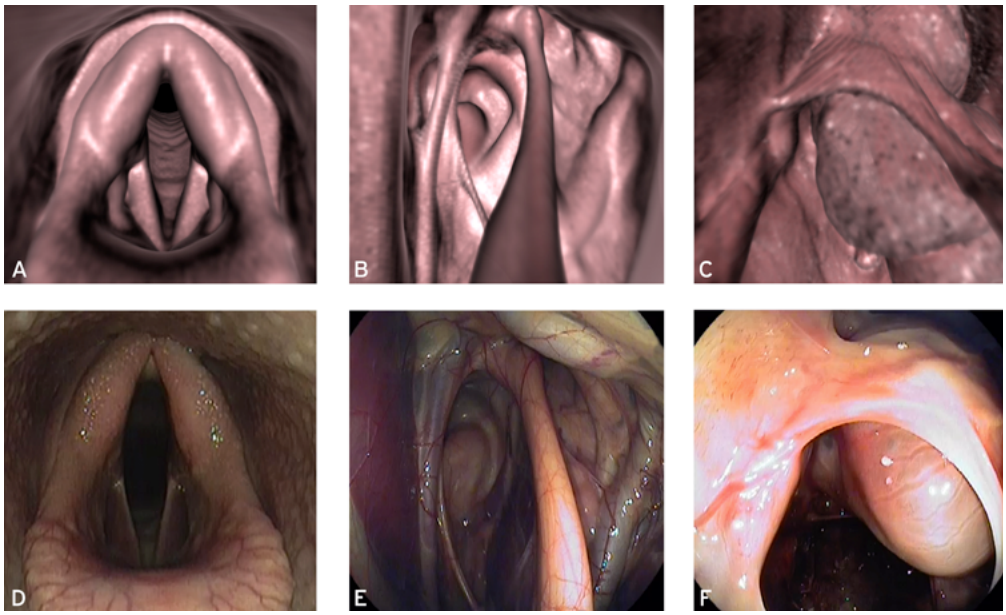


**Figure 6.**
Comparison of CT virtual endoscopy (A, B and C) and real endoscopy (D, E and F) images of the larynx (A and D), left guttural pouch (B and E), and left frontomaxillary aperture (C and F).

## 1.2.1.2. Computed tomography in the equine head

### A. Particularities and patient preparation

CT of the equine head can be performed either with the horse under general anesthesia or with the standing horse under sedation. In either case, CT machine and CT procedure are modified for horses from how it is carried out in human and small animal medicine (Barbee *et al.*, 1987; Dakin *et al.*, 2014; Kinns and Pease, 2009; Porter and Werpy, 2014; Saunders *et al.*, 2011; Solano and Brawer, 2004).

#### CT ON THE ANESTHETIZED HORSE

The sedation and anesthesia of the horse are ideally done in a recovery box located as close as possible to the CT suite and equipped with a hoist to allow the horse to be positioned on the CT table. CT suite has to be spacious for CT table movement and for patient manipulation and positioning, optimal size is approximately 9 m in length, 8 m in width and 5 m in height. A hoist can also be installed into the CT suite, which will facilitate the positioning of the horse. Communication between the recovery box and the CT suite is required for allowing the entrance of the anesthetized horse (Barbee *et al.*, 1987; Saunders *et al.*, 2011).

For CT head studies, horses are commonly placed in dorsal positioning. Instead of the standard table available in the CT machines, a custom-built table specifically designed for horses has to be installed allowing the imaging of patients up to approximately 1000 – 1200 kg (Saunders *et al.*, 2011). Different table models have been designed; ideally the table should be linked to the table drive from the CT machine, allowing helical scanning. If this is not possible, it can be advanced manually by means of a hand crank, but this prevents the use of helical scanning. An alternative technique uses a stationary table and a CT gantry that advances into the table (Barbee *et al.*, 1987; Saunders *et al.*, 2011; Solano and Brawer, 2004). Foam pads for a proper support of the horse, as well as ropes and other containment and positioning materials are mandatory for most equine CT studies (Barbee *et al.*, 1987; Saunders *et al.*, 2011).

#### CT ON THE STANDING HORSE

CT suite characteristics for scanning standing horses are very similar to what has been described for scanning anesthetized horses. However, the CT gantry must be adapted to the level of the horse's head in a standing position, which can be achieved by raising the CT scanner or positioning the horse within a pit (Dakin *et al.*, 2014; Porter and Werpy, 2014; Saunders *et al.*, 2011). Another adaptation is that the CT gantry is reversed to accommodate the equine platform, which is connected to the CT table on which the horse's head rests. The platform is a rectangular ●●●

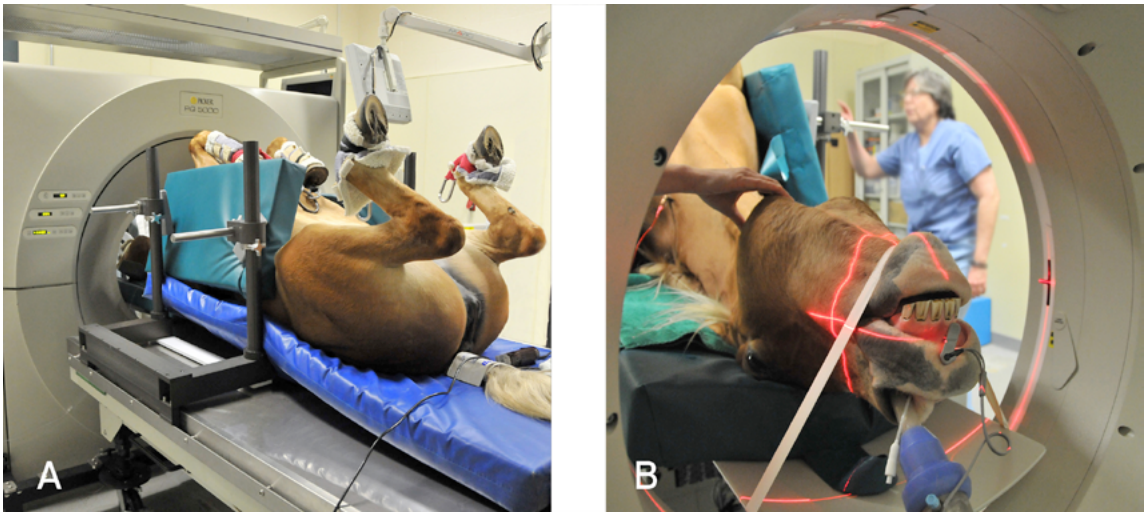


**Figure 7.** Positioning of the horse on the CT table (A) and within the CT gantry (B) for performing a CT scan of the head under general anesthesia. Images courtesy of José M. García-López (Tufts University, USA).

## INTRODUCTION


**Figure 8.** CT systems for scanning the standing horse's head positioning the patient within a pit (A) and raising the CT scanner (B). Pictures C and D show the positioning of the horse within the CT gantry. Images courtesy of Renate Weller (Royal Veterinary College, UK), Henry Tremaine (Bristol University, UK) and Sarah Powell (Rossdales and Partners, UK).

●●● shaped metallic frame with rubber surface that measures approximately 2.6 m in length and 0.9 m in width. Mobile sidebars provide stocks for the horse to stand in. The platform is mounted on air skates, which allow frictionless movement of the platform-horse. Air is supplied via piping and controlled by a pressure gauge; 2 – 3.5 bar is required for a standard adult horse. The compressor is located outside of the CT suite due to the noise generated (Dakin *et al.*, 2014; Saunders *et al.*, 2011).

Stable bandages and over-reach boots are placed on all distal limbs for protection during patient positioning and scanning. Rope halters, cotton wools and blinkers are commonly used; the head can be placed in a cradle as well to restrict its movement. A catheter should be placed in the jugular vein to provide instant intravenous access for repeat sedation. Different sedation protocols can be used along the procedure in order to obtain the ideal plane of sedation, which maximally limits patient motion while limiting the swaying or wobbling motions of a heavily sedated patient. The horse should stand square on all 4 limbs on the platform, with its feet as close to the gantry edge of the platform as possible, and the head should be extended onto the CT table (Dakin *et al.*, 2014; Saunders *et al.*, 2011). A typical CT scan of a single anatomic region takes approximately 20 minutes (Porter and Werpy, 2014). A handler is present in the CT suite during image acquisition to hold the horse, who is positioned at the side of the CT scanner wearing a lead gown and thyroid protector (Dakin *et al.*, 2014; Saunders *et al.*, 2011). An additional person for turning off the airflow to the platform in case of horse movement is required too (Dakin *et al.*, 2014). ●●●

### B. Technical considerations

CT image acquisition of the equine head under general anesthesia is very similar to humans and small animals. However, when acquisition is performed with the horse in standing position, there are some particularities. Firstly, pilot (scout) scans are not conducted due to the rapid table movement and because the head position is liable to change from scan to scan. Therefore, scan length is arbitrarily set up, being approximately 35 and 25 cm for sinonasal and brain studies respectively for a standard adult horse. Because pilot scans are not available, the FOV cannot be adjusted to the head size and, thus, a wide FOV has to be used, resulting in reduction in image resolution. In addition, scan direction is done from caudal to rostral (couch out). Acquisition parameters should be selected to assure the patient comfort, that means a constant and appeased table movement, then scans durations are around 30 seconds for a scan length of 35 cm approximately (Dakin *et al.*, 2014; Porter and Werpy, 2014; Saunders *et al.*, 2011; Solano and Brawer, 2004). Although imaging protocol varies depending on the patient and CT scanners, table 2 summaries the general guidelines for a standard CT of horse's head using a MDCT scanner.

| PARAMETERS | SERIES | |
|---|---|---|
| | Soft tissue | Bone |
| Decubit | Dorsal | |
| Scan margins | Sinonasal and dental: Nostrils - Temporomandibular joint | |
| | Brain: Rostral orbit - Wing of atlas | |
| Voltage (kVp) | 120 | |
| Current (mAs) | 200 - 280 | |
| Tube rotation time (s) | 0.75 - 1 | |
| | | |
| Pitch | 1 - 1.5 | 1 |
| Helical image reconstruction interval | 2.5 | 1.25 |
| Slice thickness (mm) | 5 | 2.5 Dental:1.25 |
| Kernel frequency | Medium | High |
| Window level (HU) | 50 | 400 Dental: 1500 |
| Wind ow width (HU) | 150 | 2000 Dental: 5000 |

**Table 2.** CT imaging protocol for the equine head. Modified from Saunders *et al.* (2011).

### C. Contrast media

The use of contrast medium to evaluate the head using CT is uncommon in horses compared to small animals (Pollard and Puchalski, 2011). Contrast medium can be applied into draining tracts (fistulography), nasolacrimal duct (dacryocystography) or intravascular (Kinns and Pease, 2009; Nykamp *et al.*, 2004; Pollard and Puchalski, 2011). Both intravenous and intraarterial contrast-enhanced CT can be performed in horses, with the intravenous route being the most commonly used (Bergman *et al.*, 2013; Cissell *et al.*, 2012; Dakin *et al.*, 2014; Lacombe *et al.*, 2010; Pollard and Puchalski, 2011; Powell, 2010; Solano and Brawer, 2004). Intravascular contrast-enhanced CT allows delineating the margins of the soft tissue lesions with high detail, and therefore it is recommended when a soft tissue lesion is suspected (Pollard and Puchalski, 2011). In addition, the use of intravascular contrast medium is mandatory in brain studies for increasing the inherent low sensitivity of CT for identifying parenchymal brain lesions (Bergman *et al.*, 2013; Lacombe *et al.*, 2010). However, its main disadvantage consists of the high volume of contrast required for adult horses, increasing substantially the costs of the procedure. This makes that a big variability of contrast doses are used in horses, conversely to small animals where the dose is set as 600 – 800 mg iodine (I) / kg body weight (Pollard and Puchalski, 2011). Generally, the dose for horses has been reduced to half, being approximately 240 – 370 mg I / kg body weight (Dakin *et al.*, 2014; Lacombe *et al.*, 2010). ■

## 1.2.2. Magnetic resonance imaging

Since its introduction into human medicine in the early 1980s, MRI has become established as the gold standard for numerous disorders in people (Bushberg *et al.*, 2002c). MRI was started to be used in equine patients in the late 1990s, and since that time has become a routine technique for investigation musculoskeletal and cranial conditions (Bolas, 2011).

### 1.2.2.1. Basic principles

#### A. Physics

##### NUCLEUS

###### Spins

The nucleus is comprised of neutrons and protons, which give their positive electrical charge. Each proton rotates about its axis (spins), producing a magnetic dipole or magnetic moment. The magnetic moment, represented as a vector indicating magnitude and direction, describes the magnetic field characteristics of the nucleus. In the absence of an external magnetic field, a collection of these magnetic moments (spins) will be oriented randomly in space and cancel each other out (Bushberg *et al.*, 2002c; Song, 2014).

Aside from a few exceptions encountered in research, MRI involves imaging the nucleus of the hydrogen atom, e.g. the proton. Hydrogen is a component of water ($H_2O$) and fat (with many –$CH_2$– chains), both of which are very common in biological tissues (Bolas, 2011).

###### Precession

Under the influence of an external magnetic field, spins are forced to align along the axis of this field ($B_0$) into two energy states: in the same direction (parallel) at a low energy level, and opposite (anti-parallel) at a slightly higher energy level. The magnetic fields of most of these spins cancel out, but a slight excess of these spins, which is proportional to the strength of the magnetic field, will be parallel to $B_0$, producing a net magnetization along that axis. In addition, due to the external field $B_0$ in which they are placed, spins will experience a torque that will cause the spins to wobble about its axis, which is called precession. This movement occurs at an angular frequency, known as Larmor frequency ($\omega_0$), that is proportional to the magnetic field strength $B_0$ and the gyromagnetic ratio ($\gamma$), which is characteristic of each type of nuclei (Bushberg *et al.*, 2002c; D'Anjou, 2012).

$$\omega_0 = \gamma B_0$$

The phenomenon of precession implies that the net magnetization vector (M) of each spinning proton can be broken down into two orthogonal vectorial components:

- Longitudinal magnetization (Mz) that is parallel to $B_0$ (z-axis).
- Transverse magnetization (Mxy) is perpendicular to $B_0$ (xy-plane).

At equilibrium, Mz is maximal and is denoted equilibrium magnetization ($M_0$), with the amplitude determined by the excess number of protons that are in the low-energy state. In contrast, the transverse magnetization is zero, because the vector components of spins that precess out of phase cancel out (D'Anjou, 2012; Song, 2014).

###### Resonance and excitation

Application of a radiofrequency (RF) pulse ($B_1$) synchronized to the Larmor frequency, energy can be transferred trough a process known as resonance. The absorption of this energy by the spins, called excitation, causes a state of imbalance. Thus, the excited protons jump to a higher energy excitation (from parallel to anti-parallel), and the net magnetization vector flips away from the z-axis, toward the xy-plane (Mxy). The transverse magnetization vector growth is caused by spins getting into phase coherence. The angle that the net magnetization vector flips away from the z-axis is called the flip angle, which depends on the strength and duration of the RF pulse. Common angles are 90 and 180-degrees, a 90-degree angle provides the largest possible transverse magnetization. The time required to flip the magnetic moment is linearly related to the displacement angle: for the same $B_0$ field strength, a 90-degree angle takes half the time to produce that a 180-degree angle does. And as such, fast sequences usually use 30-degree and smaller angles to reduce the time needed to generate the transverse magnetization (Bushberg *et al.*, 2002c).

## INTRODUCTION

### Relaxation

As soon as the RF pulse is stopped, spins return to their original state of equilibrium, in a recovery process called relaxation, transmitting their excess energy to the lattice that is detected by the RF coil. Once relaxation begins, two distinct processes occur simultaneously: transverse (T2) and longitudinal (T1) relaxations (Bushberg *et al.*, 2002c; D'Anjou, 2012).

Once the RF pulse stops the in-phase spins gradually lose synchronization and they start interacting with each other, rapidly causing dephasing, and thus eliminating the transverse magnetization (T2 relaxation or decay) (Bushberg *et al.*, 2002c; Song, 2014). T2 relaxation depends on the molecular structure of the sample (degree of mobility of protons), being much longer in fluids and shorter in more solid material. In biological tissues, it ranges from microseconds (in solid bone and tendon) to tens of milliseconds. The sensitivity of T2 relaxation to the local environment, and in particular the increase in T2 relaxation time with increased water content, makes image contrast weighted according to T2 a particularly valuable diagnostic aid (Bolas, 2011; Bushberg *et al.*, 2002c).

In reality, the dephasing process is accelerated further by the fact that the magnetic field is not perfectly uniform in tissues (magnetic inhomogeneities). Indeed, the magnetic field is slightly stronger in some areas because of the presence of metallic objects, air, or calcium or because of the imperfections of the MR system, and weaker in other parts. Such inhomogeneities cause protons to rotate at different speeds once the RF pulse is stopped (e.g. some slower than the average and some faster), leading to very rapid dephasing, shortening T2 relaxation. Thus, instead of decaying according to specific T2 relaxation times, tissue transverse magnetization decays at a very rapid T2* rate (free induction decay or FID). Therefore, T2* depends on the homogeneity of the main magnetic field and susceptibility agents present in the tissues, such as ferromagnetic objects (Bushberg *et al.*, 2002c).

Loss of transverse magnetization occurs relatively quickly, whereas the return to the low-energy state (maximum longitudinal magnetization), also called T1 relaxation, takes a longer time (Bolas, 2011; Bushberg *et al.*, 2002c). Therefore, T1 is significantly longer than T2, and magnetic field strength influences T1 relaxation but has an insignificant impact on T2 relaxation. T1 relaxation is dependent on the physical characteristics of the molecules. Consequently, fluids have a long T1 relaxation time, whereas fat has a short T1 relaxation time. The specific relaxation rates varies among tissues, and the exploitation of these differences is the fundamental source of tissue contrast (D'Anjou, 2012).

## IMAGE FORMATION

### Signal localization

Spatial localization of the signal coming out of tissues is fundamental to MRI. This is performed by intermittently using three orthogonal linear field gradients that generate short-term variations in the magnetic field across the patient (Bushberg *et al.*, 2002c; Leach, 2014). These gradients are obtained by superimposing the magnetic fields of one or more coiled wires placed in the bore of the magnet, precisely adjusted through additional pulses in the imaging sequence (D'Anjou, 2012).

The slice selection gradient (SSG) determines the slice of tissue to be imaged by causing linear variation of magnetic field strength, adjusting the RF pulse frequency to the Larmor frequency of only the protons of that slice. For identifying the voxel origin of each signal in the slice, phase-encoding (PEG) and frequency-encoding gradients (FEG) are used. PEG is turned on after the 90-degree RF pulse, causing each row of protons in the slice to have a different phase. Subsequently, FEG is turned on during the echo to alter the Larmor frequencies for each column within the slice. Therefore, protons, from each voxel creating the matrix of the slice that is being studied, precess at a specific frequency and phase, allowing them to be distinguished (Bolas, 2011; Bushberg *et al.*, 2002c).

Direct transverse, dorsal, sagittal or oblique planes can be obtained in MRI by energizing the

appropriate gradient coils during the image acquisition. The SSG determines the orientation of the slices, where transverse uses z-axis coils, dorsal uses y-axis coils, and sagittal uses x-axis coils for selection of the slice orientation. In addition, oblique plane acquisition depends on a combination of the x-, y-, and z-axis coils energized simultaneously (Bolas, 2011; Leach, 2014).

Slice thickness is determined by the bandwidth (BW) of the RF pulse and the gradient strength across the FOV (Bushberg *et al.*, 2002c).

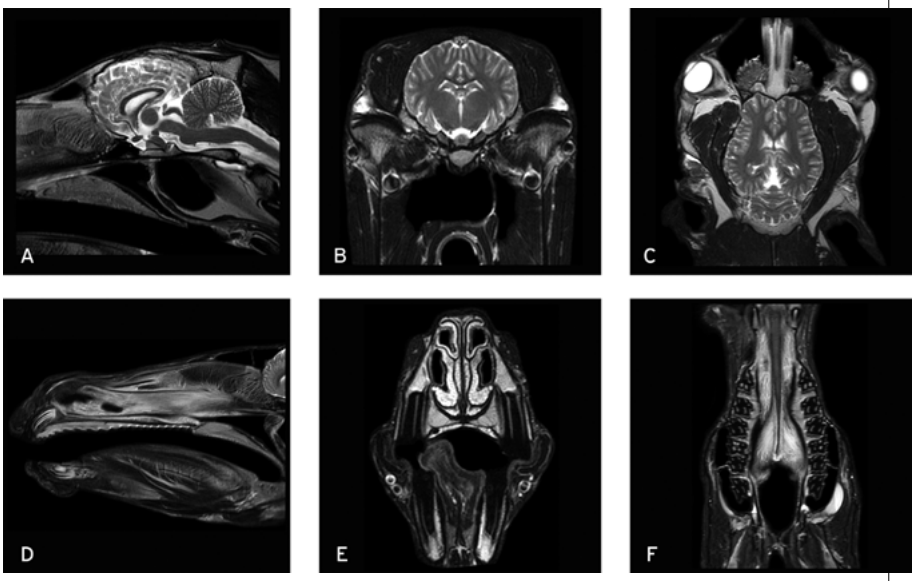


**Figure 9.** Sagittal (A and D), transverse (B and E), and dorsal (C and F) T2W MRI images of the equine head at the level of the brain (A, B and C), and the nasal cavity and paranasal sinuses (D, E and F).

### K-Space and Two-dimensional Fourier transformation

Raw data are initially stored in the k-space matrix determined by the gradients applied during the excitation, which describes a two dimensional matrix of positive and negative spatial values, encoded as complex numbers. Once the matrix is filled, a complex mathematical process called two-dimensional Fourier transformation takes the digital data held in the k-space and converts it into an accurate geometrical representation of tissues within the imaging slice. Therefore, the two-dimensional Fourier transformation converts the data into a visible image (Bushberg *et al.*, 2002b; Leach, 2014).

## PULSE SEQUENCES: SPIN ECHO

Magnetic resonance images are created once signal arising from excited tissues is detected as echoes by receiving coils and processed. Because of the differences in relaxation characteristics among tissues, several technical methods, or sequences, can be used to excite and receive signals using RF and gradient pulses, with variable timing and duration. Therefore, sequences can be divided into two main groups: spin echo (SE) and gradient recalled echo (GRE) sequences (Bushberg *et al.*, 2002c; Song, 2014).

Spin echo describes excitation of the magnetized protons in a sample with a RF pulse and production of the FID, followed by a second RF pulse to produce an echo. At initial 90-degree, the RF pulse produces the maximal transverse magnetization, placing the spins in phase coherence. Then, the signal exponentially decays with T2* relaxation. Subsequently, a 180-degree RF pulse is applied, which inverts the spin system and induce a rephasing of the transverse magnetization. Finally all the spins are dephased and produce a measurable signal (echo). The 180-degree RF pulse has the mission of cancelling the magnetic field inhomogeneities (Bolas, 2011; Bushberg *et al.*, 2002c).

The time between the initial 90-degree RF pulse and the echo production is known as time of echo (TE). The 180-degree RF pulse occurs exactly at TE/2. The time it takes for this sequence to be run one time is called the time to repetition (TR). The time delay after the 180-degree RF pulse and the next 90-degree RF pulse allows recovery of the longitudinal magnetization. However, by the time next 90-degree RF pulse is applied, there usually is not complete longitudinal magnetization re-

covery of the tissues yet. Therefore, the FID generated is less than the first FID, and then tissues become partially saturated. The amount of saturation is dependent on the T1 relaxation time; with short T1 tissues (e.g. fat) having less saturation than long T1 tissues (e.g. fluid) (D'Anjou, 2012; Song, 2014).

### T1 weighting

A T1-weighted (T1W) spin echo sequence potentiates the T1 characteristics of tissues. This is achieved by using short TR (400 – 600 msec) to maximize the difference in longitudinal magnetization, and short TE (5 – 20 msec) to minimize T2 dependency during signal acquisition (Bushberg *et al.*, 2002c). Tissues with short T1, such as fat, will result in high signal intensity, and thus will be seen as bright (hyperintense). In contrast, long T1 tissues, such fluid, will result in low signal intensity, being dark in the images (hypointense) (Bolas, 2011).

### T2 weighting

T2-weighted (T2W) sequences reduce T1 effect with a long TR (2000 – 4000 msec), and potentiate T2 differences with a long TE (80 – 120 msec). Tissues with a long T2 (e.g. fluid) maintain transverse magnetization longer than short T2 tissues, resulting in higher signal intensity at the time of echo (Bushberg *et al.*, 2002c; Song, 2014). Therefore, these tissues will be hyperintense in T2W images (Bolas, 2011).

### Proton density weighting

When both T1 and T2 effects are inhibited by using long TR and short TE, signal intensities mainly depend on different tissue number of magnetizable protons or proton density, called proton density (PD) weighting. Very hydrogenous tissues such as fat show high signal intensity compared with proteinaceous soft tissues (Bushberg *et al.*, 2002c; D'Anjou, 2012).

Manipulations in TR and TE result in varying intensity (or pixel brightness) levels for the same tissue. Although some tissues may appear similar in a given sequence, they may become distinct in another. Standard sequence protocols include multiple sequences to highlight these tissue differences (D'Anjou, 2012). T1W and T2W are the most commonly acquired sequences in MRI studies. Nowadays fast spin echo (FSE) or turbo spin echo (TSE) sequences have replaced conventional spin echo sequences because they allow speed up the acquisition process (Bushberg *et al.*, 2002b; Leach, 2014).

### Inversion recovery sequences

Inversion recovery (IR) sequences can null the signal from specific tissues, which can help confirm the presence of such components in the tissue studied, or improve the conspicuity of nearby tissues with similar signal characteristics. These sequences start with a 180-degree RF pulse (inversion pulse) that inverts the longitudinal magnetization vector of all tissues (from +z to –z). Subsequently, at the end of this pulse, protons begin to relax and tissue magnetization vectors start to regrow longitudinally along $B_0$, going back from –z to +z. During this process, magnetization vectors cross the null point (z = 0) at different times, depending on the T1 relaxation rates of each tissues. A standard spin echo sequence is then applied, using a 90-degree RF pulse, when the tissue aimed to be suppressed crosses the null point. This tissue will not generate a signal at the time of echo. Therefore, the delay between the inversion pulse and the 90-degree RF pulse is known as time of inversion (TI) and depends on the T1 relaxation time of the tissue to be suppressed (D'Anjou, 2012; Song, 2014).

When a short TI (140 – 180 msec) is used, tissues with short T1 relaxation time may be suppressed, such as fat. Short tau inversion recovery (STIR) is a pulse sequence with T2-weighting and short TI that suppresses selectively the fat, it increases the conspicuity of soft tissue lesions, most of which have prolonged T2 (Bushberg *et al.*, 2002c; Leach, 2014).

The use of a longer TI (2000 msec) reduces the signal levels of tissues with long T1 relaxation times, such as cerebrospinal fluid (CSF). Fluid attenuated inversion recovery (FLAIR) sequence helps differentiate brain parenchymal lesions from CSF because suppresses the signal from CSF, and can be T2-weighted or T1-weighted (Bushberg *et al.*, 2002b; Leach, 2014).

### PULSE SEQUENCES: GRADIENT RECALLED ECHO

In the GRE sequences a RF pulse with a small flip angle (e.g. less than 90 degrees) is applied. Instead using a second RF pulse, it uses a magnetic field gradient to induce the formation of an echo. In addition, shorter TR is used, and together with the small flip angle results in a rapid acquisition time. GRE is therefore used for angiography (depicting rapidly moving blood) studies or as localizer images (D'Anjou, 2012; Leach, 2014).

Magnetic field inhomogeneities secondary to magnetic susceptibility differences between tissues (caused by paramagnetic or diamagnetic tissues or contrast agents) are emphasized in GRE sequences. This is due to the dephasing and rephasing occurring in the same direction as the main magnetic field, and do not cancel the inhomogeneity effects, as the 180-degree refocusing RF pulse does in SE sequences. Thus, GRE sequences with long TE are T2*-weighted (T2*W) rather than T2-weighted like SE sequences (Bolas, 2011; Bushberg *et al.*, 2002c). Magnetic susceptibility is exploited for the detection of hemorrhage because the iron contained in the hemoglobin increases the local magnetic field substantially, leading to local signal loss resulting in a signal void. T2*W sequences are therefore sensitive for detecting hemorrhage (D'Anjou, 2012).

### OTHER MAGNETIC RESONANCE SEQUENCES

#### Diffusion sequences

Diffusion weighted images (DWI) are very sensitive to cytotoxic edema in early stages of ischemia. The basis of this sequence consists of the brownian motion of water molecules in tissues.

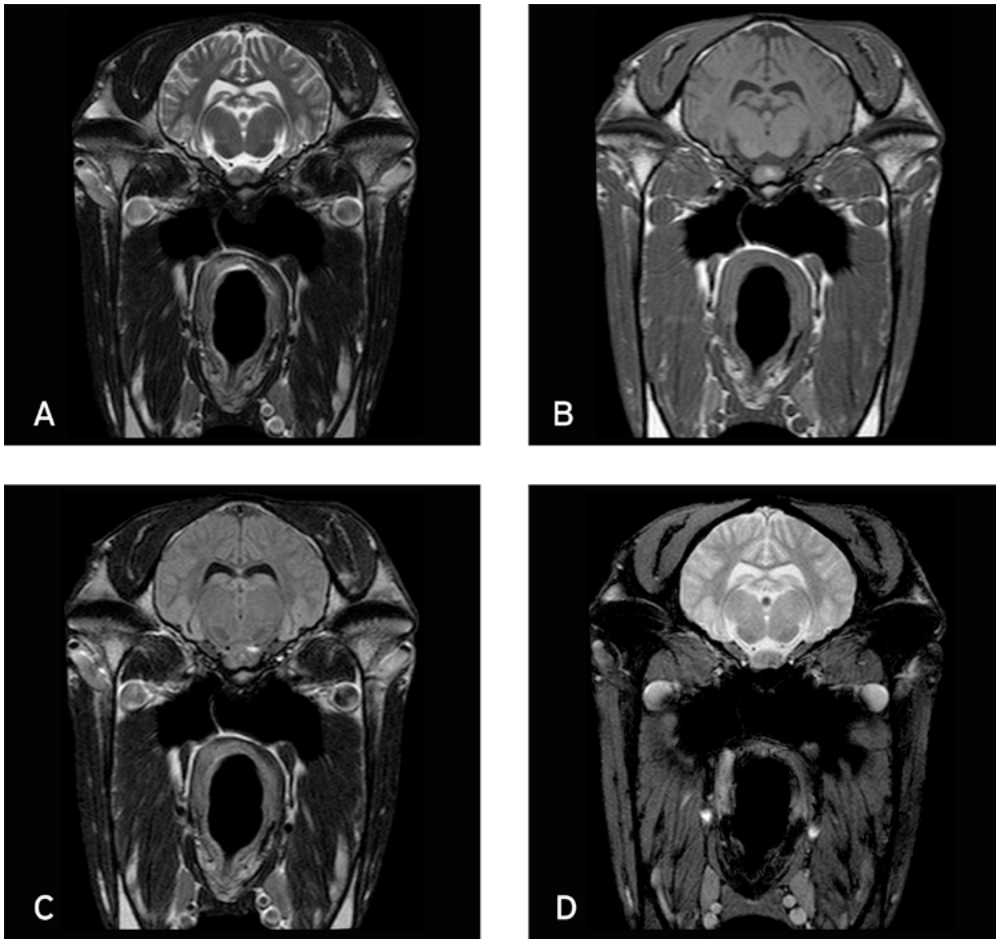


**Figure 10.** Transverse T2W (A), T1W (B), FLAIR (C) and T2*W GRE MRI images of the equine head at the level of the temporomandibular joint.

## INTRODUCTION

DWI determines the water diffusion characteristics by the generation of apparent diffusion coefficient (ADC) maps. Areas of acute stroke show drastic reduction in the diffusion coefficient compared with healthy tissue (Crawley *et al.*, 2003; Sutherland-Smith *et al.*, 2011).

### Perfusion sequences

Perfusion images show measurement of the parameters of cerebral microvascularisation, such as regional blood volume, mean transit time or regional blood flow. It relies on the use of a tracer that may be exogenous (contrast agent) or endogenous (spin labeling). This sequence is a useful tool in assessing stroke, brain tumors and patients with neurodegenerative diseases (Crawley *et al.*, 2003; Pascual *et al.*, 2007).

### Magnetic resonance angiography

Magnetic resonance angiography (MRA) allows visualization of blood vessels and blood flow, and it can be performed according three different techniques: time-of-flight (TOF-MRA), phase contrast (PC-MRA) and contrast enhanced (CE-MRA) (Contreras *et al.*, 2010; Passat *et al.*, 2006). The latter requires the use of contrast medium to highlight the vessels, whereas the other two are flow-dependent. MRI is greatly affected by the movement of protons, and then flow artifacts result in poor-quality images. However, these flow phenomena can also be used to visualize flow spins and therefore to evaluate the blood vessels (Krings *et al.*, 2002).

TOF-MRA relies on the differences in exposure to radiofrequency excitation between in-plane stationary protons from the surrounding tissues and the blood protons flowing into the section. Stationary protons become relatively saturated with repeated excitation pulses, resulting in low signal intensity. Conversely, inflowing blood protons do not experience the excitation pulses, are not saturated, and therefore generate high signal intensity (Krings *et al.*, 2002; Passat *et al.*, 2006). Selective vessel imaging is possible, it is achieved by applying saturation bands proximal or distal to the volume being examined. This sequence is especially sensitive to vessels in which blood flow is perpendicular to the section because the charged protons from this vessel are continually replaced by new completely relaxed spins, which provide a more distinct signal. Acquisitions can be performed by using 2D or 3D methods, depending on the spatial resolution and the extent of the vascular territory to be imaged (Contreras *et al.*, 2010; Passat *et al.*, 2006).

PC-MRA involves the application of bipolar phase-encoding gradient pairs, to encode velocity in the direction of the gradient. As a result, protons moving along the direction of the gradient field undergo a phase shift proportional to their velocity. Conversely, stationary tissue accumulates zero net phase. Subtraction of these flow-sensitive data sets from reference images allows visual representation of vascular flow and, thus, angiographic depiction. Importantly, as the phase shift experienced is proportional to the velocity of moving protons, phase-contrast imaging allows quantitative assessment of flow velocities. As is the case with TOF-MRA, PC-MRA may be applied as either a 2D projectional technique or a 3D technique. However, this latter volumetric technique is a time-consuming process, often requiring more than 20 minutes for image acquisition (Passat *et al.*, 2006).

CE-MRA is based on the presence of a contrast agent in the blood, independent of the flow waveform and flow velocity in the vessels. It does not rely upon the physiologic flow of in-phase protons for signal generation as TOF-MRA and PC-MRA do. The basic pulse sequence for CE-MRA is an ultra-short TR/TE 3D spoiled GRE sequence. The TR is made as short as possible to speed up image acquisition and capture the first pass of contrast, being therefore highly dependent on accurate timing of the contrast bolus. Due to the presence of a contrast medium in blood, the short TR tends to saturate only background tissues. This technique generates images with high spatial resolution, high vascular contrast and short scan times (Krings *et al.*, 2002).

## CONTRAST MEDIA

Contrast media can be injected intravenously for MR imaging to assess the vascular network and tissue perfusion, helping to better

detect, delineate and characterize lesions. Most common contrast agents have a paramagnetic effect, which consists on decreasing the T1 relaxation time of the protons. Thus, tissues accumulating this substance show an increase of signal intensity, called contrast enhancement, on T1W images. Gadolinium-based agents are commonly used in clinical MR examinations (e.g. Omniscan®, Magnevist®, MultiHance® etc.) (Bushberg *et al.*, 2002c; Leach, 2014).

## B. Instrumentation

Magnetic resonance systems are comprised of sophisticated elements, combining electronics, RF generators, coils, and gradients that interact with a computer.

### MAGNETS

The magnet provides the external magnetic field in which the patient is placed. The strength of the MRI signal from the tissues increases with the strength of the magnet, which is measured in units called Tesla (T). Depending on the field strength of the magnet, MRI systems can be grouped in low-field (0.2 – 0.7 T) and high-field (> 1.0 T) magnets (Bushberg *et al.*, 2002b; Leach, 2014). Great care is needed to ensure that no metal objects (e.g. scissors, stethoscopes or gas cylinders) are brought anywhere near the magnet (Bolas, 2011).

Different types of magnets can be used; the main types on offer are permanent, superconducting, and resistive magnets (Bolas, 2011). Permanent magnets are made of a permanently magnetic material such as iron or ceramic. However, the field strength of these systems is limited by the sheer weight of the core (typically over 100 tons), operating therefore typically as low-field systems. Superconducting magnets are electromagnets whose magnetic field is produced by passing a current through superconducting wire loops. These windings are immersed in liquid helium at a temperature of almost absolute zero in order to create superconductivity. Resistive magnets utilize the principles of electromagnetism to generate the magnetic field as with superconducting magnets. A very stable and constant power supply to maintain a homogenous magnetic field and significant (water) cooling of the magnet are required in this system (Jacobs *et al.*, 2007; Leach, 2014).

MRI magnets can have either a closed (superconducting) or an open-bore (permanent or resistive) design. The closed system has a tubular-shape; whereas the open system consists of two flat poles separated by a gap, acquiring a C open on one side (Jacobs *et al.*, 2007).

### FARADAY CAGE

The MRI process is heavily dependent on the use of RF, in order to reduce RF interferences the MRI system is installed inside room that protects it from external RF transmissions. This is achieved by shielding the room with a Faraday cage, which consists in covering the entire scan room including the door with a fine metallic mesh, most commonly of copper (Leach, 2014).

### RADIOFREQUENCY COILS

RF coils are the transmitters of the emitted RF pulses, and also are the receivers of the signal generated. Based on these properties, there are two types of RF coils: transmit and receive (transceiver), and receive-only. The smallest coil that will fit the anatomical area to be studied should always be used to achieve best reception (Leach, 2014). A variety of RF coils configurations can be used. Bird-cage coil provides the best RF homogeneity of all the RF coils and is commonly used as transceiver coil for imaging the head in people. The saddle coil is designed with shaped windings either side of the anatomic area to be studied. This coil type is commonly used for imaging of the extremities in human medicine. Surface coils and phased-array coils are used when high-resolution or small FOV areas are desired. As a receive-only coil, surface and phased array coils have a high signal to noise ratio for adjacent tissues, although the field intensity drops off rapidly at the periphery. The phased array coil is made of several overlapping loops, which extend the imaging FOV in one direction. Surface coils consist of a loop of wire, either circular or rectangular (Bolas, 2011; Jacobs *et al.*, 2007).

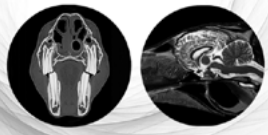



## 1.2.2.2. Magnetic resonance imaging in the equine head

### A. Particularities and patient preparation

Standard equine head MRI examination takes approximately between 40 to 60 minutes, thus general anesthesia is mandatory to keep the horse still (Kraft and Gavin, 2001; Murray, 2011). The sedation and anesthesia of the horse is ideally done in a recovery box located as close as possible to the MRI suite and equipped with a hoist to allow the horse to be positioned on the MRI table. MRI suite has to be spacious enough to allow movement of the MRI table with the horse either in lateral or dorsal recumbency. Communication between the recovery box and the MRI suite is useful avoiding increase in anesthesia time of the patient, however, this can present some issues as any doors and equipment that enters the MRI suite and controlled area must be MRI safe. It is also advisable to separate the MRI shielded doors from the recovery box doors, which can withstand the forces of a horse falling during recovery and thus protect the shielding of the MRI suit (Ferrell *et al.*, 2002; Murray, 2011; Werpy, 2007).

Prior to undertaking MRI, it is necessary confirm the absence of implants or other ferromagnetic devices in the head and cranial neck. Depending on the localization, microchips can severely affect to image quality. Shoes are usually removed (Murray, 2011).

Once the patient is induced, it is positioned on a padded MRI table outside of the MRI suite by lifting it with a hoist. Various designs of tables have been used for equine MRI, including those made from wood, glass fiber composite with brass screws and MRI compatible stainless steel. Optimal position of the horse-designed MRI table depends on the design of the MRI system; commonly it is localized from the rear of the magnet. However, in some MRI systems the standard patient table can be switched for the equine table. Most MRI systems are designed for human patients; therefore in some instances specific adaptations are necessary, such as disabling the automatic movement of the standard table or overriding some safety interlocks (Kraft and Gavin, 2001; Murray, 2011; Tucker and Farrell, 2001; Werpy, 2007).

For imaging the head, either lateral or dorsal recumbency is possible, and this may be determined by suspected pathology or MRI system characteristics. Correct placement of the horse into the MRI gantry is essential and can be challenging in big or short-necked horses. If the anatomical area to be studied is not placed within the center of the magnet, the imaging FOV may cut off part of the region of interest. This limitation is a big issue when imaging the brain where in some instances the cerebellum and medulla oblongata could be cut off (Tucker and Holmes, 2011). Body coils or the incorporated coil into the MR system housing are commonly the most suitable. However, in foals and miniature horses head coils can also be used, depending on the size of the patient (Lempe *et al.*, 2012; Murray, 2011; Werpy, 2007).

MR-compatible anesthetic equipment (anesthesia machine, ventilator and monitoring devices) is recommended as they are designed not to produce RF interferences. Any clipping must be done prior to entering the MRI room, along with catheters placement. Halters should be removed and non-metallic tracheal tubes and devices for holding the mouth open are mandatory (Kraft and Gavin, 2001).

### B. Technical considerations

Little information regarding technical details and imaging protocols are described in the literature (Ferrell *et al.*, 2002; Kraft and Gavin, 2001). The sequences selected for head examinations in horses usually follow the protocols used in small animals. These include T1W sequences pre- and post-contrast administration and T2W sequences, in brain studies FLAIR and T2*W sequences are commonly used too (Tucker and Sampson, 2007). Three standard anatomic planes (sagittal, transverse and dorsal) are commonly used when imaging any part of the equine head, and are ●●●

INTRODUCTION


**Figure 11.** Positioning of the horse on the MRI table in open low-field (A) and closed high-field (B) MRI systems. Pictures C and D show the positioning of the head within the body RF coil and the integrated body RF coil, respectively. Images B and D are courtesy of Sue J. Dyson (Animal Health Trust, UK) and Anthony Pease (Michigan State University, USA).

most commonly positioned relative to the hard palate or the base of the calvarium (Tucker and Holmes, 2011; Tucker and Sampson, 2007). Additional planes can be obtained for further examination of structures if standard image planes do not offer the optimal visualization of specific regions of interest, such as oblique planes for the optic nerve (Naylor *et al.*, 2010a; Tucker and Holmes, 2011). Acquisition parameters such as FOV, matrix size or slice thickness are not set up for horses, and vary according the institution (Kraft and Gavin, 2001).

### C. Contrast media

Use of gadolinium is not routinely performed in all head MRI examinations, but is more common in brain studies. The intravenous dose of gadolinium has not been scientifically established in horses. The recommended dose in humans and small animals is 0.01 mmol / kg body weight intravenously, which would equate to 100 ml in a 500 kg standard adult horse, significantly increasing the costs. As a consequence, various protocols have been described in the literature based on empirical experiences, including a total bolus of 20 ml, 40 ml or half the dose of small animal protocols (Ferrell *et al.*, 2002; Judy, 2011; Werpy, 2007). ■

Aplicación de
TÉCNICAS DE DIAGNÓSTICO por
IMAGEN AVANZADAS en el estudio
de la CABEZA DEL CABALLO

Application of advanced diagnostic imaging techniques in the study of the equine head

# 2

# HYPOTHESIS AND OBJECTIVES

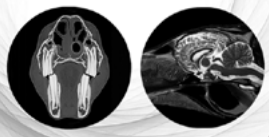



## HYPOTHESIS AND OBJECTIVES

The aim of this PhD thesis was the study of main applications and indications of advanced diagnostic imaging techniques, including computed tomography and magnetic resonance imaging, for assessing equine head disorders in clinical practice.

We hypothesized that both CT and MRI would provide high detailed information regarding the normal anatomy and the lesion features of the equine head. This information would be superior to what it is often obtained from conventional imaging modalities. We also hypothesized that both modalities would be complementary to each other, with CT being better for dental and osseous structures and MRI being better for soft tissues, such as the brain.

Several specific objectives have been addressed for doing so:

- To study the diagnostic usefulness of both high-field and low-field magnetic resonance imaging systems in horses with disorders affecting the head (Paper 1).
- To study the diagnostic usefulness of computed tomography in horses with disorders affecting the head (Paper 2).
- To compare the diagnostic usefulness of magnetic resonance imaging and computed tomography to conventional diagnostic imaging modalities (Papers 1 and 2).
- To develope and to optimize a magnetic resonance angiography protocol for the equine head using low-field and high-field magnetic resonance systems (Paper 3).
- To provide a thorough anatomical description of normal magnetic resonance angiography images from healthy horses (Paper 3).

# Aplicación de TÉCNICAS DE DIAGNÓSTICO por IMAGEN AVANZADAS en el estudio de la CABEZA DEL CABALLO

Application of advanced diagnostic imaging techniques in the study of the equine head

3

**PUBLISHED STUDIES**

PUBLISHED STUDIES

## 3.1. Paper 1


**Title:**

Magnetic resonance imaging characteristics of equine head disorders: 84 cases (2000–2013).

**Authors:**

- Gabriel Manso-Díaz.
  Facultad de Veterinaria.
  Universidad Complutense de Madrid. Spain.
- Sue J. Dyson.
  Centre for Equine Studies.
  Animal Health Trust. UK.
- Ruth Dennis.
  Centre for Small Animal Studies.
  Animal Health Trust. UK.
- José M. García-López.
  Cummings School of Veterinary Medicine.
  Tufts University. USA.
- Marianna Biggi.
  Centre for Equine Studies.
  Animal Health Trust. UK.
- María Isabel García-Real.
  Facultad de Veterinaria.
  Universidad Complutense de Madrid. Spain.
- Fidel San Román.
  Facultad de Veterinaria.
  Universidad Complutense de Madrid. Spain.
- Olivier Taeymans.
  Cummings School of Veterinary Medicine.
  Tufts University. USA.

**Journal:**

Veterinary Radiology & Ultrasound
2014 – doi: 10.1111/vru.12210

| Journal Title | ISSN | Total Cites | Impact Factor | 5-Year Impact Factor |
|---|---|---|---|---|
| VET RADIOL ULTRASOUN | 1058-8183 | 2009 | 1.262 | 1.214 |

# MAGNETIC RESONANCE IMAGING CHARACTERISTICS OF EQUINE HEAD DISORDERS: 84 CASES (2000–2013)

GABRIEL MANSO-DÍAZ, SUE J. DYSON, RUTH DENNIS, JOSÉ M. GARCÍA-LÓPEZ, MARIANNA BIGGI, M. ISABEL GARCÍA-REAL, FIDEL SAN ROMÁN, OLIVIER TAEYMANS

**The equine head is an anatomically complex area, therefore advanced tomographic imaging techniques, such as computed tomography or magnetic resonance imaging (MRI), are often required for diagnosis and treatment planning. The purpose of this multicenter retrospective study was to describe MRI characteristics for a large sample of horses with head disorders. Horses imaged over a period of 13 years were recruited. Eighty-four horses met the inclusion criteria, having neurological ($n = 65$), sinonasal ($n = 14$), and soft tissue ($n = 5$) disorders. Magnetic resonance imaging accurately depicted the anatomy and allowed identification of the primary lesion and associated changes. There were good correlations between MRI findings and intraoperative or postmortem results. Magnetic resonance imaging showed the exact localization of the lesions, their size, and relation to surrounding structures. However, in the neurological group, there were 45 horses with no MRI abnormalities, 29 of which had a history of recurrent seizures, related to cryptogenic epilepsy. Magnetic resonance imaging was otherwise a valuable diagnostic tool, and can be used for studying a broad range of head disorders using either low-field or high-field magnets.** *© 2014 American College of Veterinary Radiology.*

**Key words: brain, horse MRI, sinusitis, skull.**

## Introduction

THE EQUINE HEAD IS ONE OF THE MOST ANATOMICALLY COMPLEX areas of the body, because it contains multiple structures of different tissue density.[1] Diagnosis of conditions affecting the head is frequently challenging, and often requires the use of diagnostic imaging techniques.[1,2] Radiography is mainly useful for osseous, dental, and sinonasal diseases, but interpretation is hampered by superimposition of anatomical structures.[2–6] Ultrasonography is useful for evaluation of superficially located soft tissues of the head, orbit, and temporomandibular joints.[7–10] The limited field of view and inability of the sound beam to penetrate through the osseous structures of the skull and gas within the airways are limitations. Scintigraphy can be useful to identify dental abnormalities and lesions within the temporomandibular joint, tympanic bullae, stylohyoid bone, or skull fractures.[7,11,12] This modality has a high sensitivity for detecting abnormalities, but suffers from a low specificity. The use of advanced cross-sectional imaging techniques, such as computed tomography (CT) and magnetic resonance imaging (MRI), allows us to obtain tomographic images of the head, avoiding superimposition of normal anatomical structures.[13] MRI of the normal equine head has been extensively documented.[14–18] An array of isolated conditions has also been described, but only few retrospective studies including a wide variety of conditions have been performed.[19–21] This is in sharp contrast with the multitude of available reports describing equine head disorders with CT.[22–33]

The aims of this multicenter retrospective study were to describe the MRI features of equine head disorders examined over 13 years, and to compare the MRI findings with intraoperative or postmortem results where possible.

## Materials and Methods

### *Case Selection*

A retrospective review of the medical records from the Animal Health Trust (UK), Complutense University of Madrid (Spain), and Tufts University (USA) was performed from 2000 to 2013. Inclusion criteria were all horses

From the Department of Animal Medicine and Surgery, School of Veterinary Medicine, Universidad Complutense de Madrid, Avda. Puerta de Hierro s/n, 28040-Madrid, Spain (Manso-Díaz, García-Real, San Román); Centre for Equine Studies (Dyson, Biggi) and Centre for Small Animal Studies (Dennis), Animal Health Trust, Kentford, Newmarket, Suffolk, CB8 7UU, UK; Department of Clinical Sciences, Cummings School of Veterinary Medicine, Tufts University, 200 Westboro Road, North Grafton, MA 01536, USA (García-López, Taeymans).

Gabriel Manso-Díaz was supported by MECD FPU fellowship (Re. AP2010–0498).
This study was in part presented at the Annual Meeting of the EAVDI, August 27 to September 1, 2013 in Cascais, Portugal.

Address correspondence and reprint requests to Gabriel Manso-Díaz, at the above address. E-mail: gmanso@ucm.es

Received February 5, 2014; accepted for publication May 20, 2014.
doi: 10.1111/vru.12210

that were presented for a suspected cranioencephalic disease and that had undergone MRI of the head.

*Image Analysis*

Image review was performed retrospectively with a DICOM image viewing software (Osirix Image processing Software, Geneva, Switzerland). Two observers, one board-certified veterinary radiologist (O.T.) and one PhD student (G.M.), simultaneously reviewed the images in a randomized order. Interpretation was reached by consensus. Examiners were blinded to the clinical presentation, surgical and other imaging findings, and postmortem diagnosis.

*Data Evaluation*

A database was compiled for each animal, including signalment, presenting complaint, imaging findings, final diagnosis, treatment performed and, when available, cerebrospinal fluid analysis, gross necropsy, and/or histopathologic findings. Interpretation based on MRI findings was compared with clinical, surgical, and postmortem findings, where available.

Included horses were assigned to one of three groups based on clinical information in the medical record: neurological disease (A), sinonasal pathology (B), and soft tissue abnormalities (C). Specific evaluation criteria were used in each group. For group A, lesions were defined as intra-axial, extra-axial, or affecting the optic nerve. Lesion type, number (defined as focal or multifocal), location, and signal characteristics compared with normal gray matter were recorded. The presence of contrast enhancement was recorded and graded subjectively as mild, moderate, or marked. Evidence of perilesional edema, hemorrhage (determined by a combination of low or high signal intensity in T1-weighted (T1W) images, low signal intensity in T2-weighted (T2W) images, and signal void on T2*W GRE images), brain herniation (transtentorial or transforaminal), and mass effect (deviation of the falx cerebri from midline or compression of the lateral ventricle) was recorded. For groups B and C, lesion type, location, and signal characteristics compared with normal muscle were recorded. The presence of contrast enhancement was subjectively graded as mild, moderate, or marked. Presence of mass effect, bone lysis/atrophy, free fluid, and lymphadenopathy was also recorded.

## Results

A total of 84 horses met the inclusion criteria, including 17 Thoroughbreds, 15 Warmbloods, 10 Andalusians, 8 Ponies, 6 Quarter Horses, 7 Cross breeds, 5 Arabs, 5 Irish, 3 Cobs, 2 Appaloosas, 2 Paint Horses, and one each of the following breeds: Clydesdale, Fjord, Lipizzaner, Miniature horse. There were 10 stallions, 48 geldings, and 26 mares. The mean age was 11.6 years (range 4 days to 28 years; median 11 years).

*MRI Techniques*

Sixty-four and 20 horses were evaluated with a high-field (1.5 T [Magnetom Symphony Maestro Class, Siemens, Erlangen, Germany; Signa Echospeed, General Electric, Milwaukee, WI]) or low-field (0.23 T [Panorama, Philips Medical Systems, The Netherlands]) magnet, respectively. Depending on the size of the patient and the MRI unit, a head, body, or integrated body radiofrequency coil was used. All horses were examined under general anesthesia on a dedicated table, and were placed in lateral recumbency in the low-field magnet and in lateral or dorsal recumbency in the high-field magnet. Imaging protocols varied among patients (Table 1). All the studies included spin echo, turbo/fast spin echo T1W images, and turbo/fast spin echo T2W images in transverse planes. Most studies also included sagittal and dorsal plane images, although not always in all sequences. For group A, most of the studies included fluid-attenuated inversion recovery (FLAIR), and T2*W gradient echo (GRE) sequences. Other sequences used in some patients were short tau inversion recovery (STIR), spoiled gradient echo (SPGR), and 2D time-of-flight magnetic resonance angiography (TOF2D-MRA). In 65 cases, T1W postcontrast images (T1WC) were acquired following intravenous administration of gadolinium (0.02 mmol/kg for adult horses and 0.1 mmol/kg in foals). Observers noted that images obtained from the low-field magnet had lower anatomical resolution compared to those obtained with the high-field magnet, however all were considered to be of adequate diagnostic quality.

*Neurological disease (group A).* Group A ($n = 65$) comprised 5 stallions, 40 geldings, and 20 mares; the mean age was 11.6 years (range 4 days to 27 years; median 11 years). This group included intra-axial disease ($n = 8$), extra-axial disease ($n = 7$), and optic nerve pathology ($n = 4$; Fig. 1); the remaining 46 horses had no detectable abnormalities on MRI. Fifty-four and 11 horses were evaluated with a high-field or low-field magnet, respectively. Specifically, inside the group of horses with normal MRI, 41 and 5 horses were evaluated with a high-field or low-field magnet, respectively. Clinical features are summarized in Table 2.

One horse had a well-defined, wedge-shaped area in the frontal cortex, which was hyperintense on T2W images, hypointense on T1W images, suppressed on FLAIR, and did not show contrast enhancement. This was consistent with an old infarct filled with cerebrospinal fluid. One horse had a bilaterally symmetrical lesion within both caudal colliculi, with a rim-like appearance with hyperintense center

TABLE 1. Technical Parameters Used for Head MRI Examinations of Horses in the Sample Population

| Sequence | Field strength (T) | Repetition time (ms) | Echo time (ms) | Inversion time (ms) | Flip angle | Number of acquisitions (NEX) | Slice thickness (mm) | Gap (mm) | Field of view (mm) | Matrix |
|---|---|---|---|---|---|---|---|---|---|---|
| T1W | 0.23 | 590–650 | 16 | - | 90 | 2 | 4.0–5.5 | 4.4–6.0 | 270–512 × 270–512 | 216–256 × 140–256 |
| | 1.5 | 385–723 | 8–16 | - | 70–90 | 1–4 | 3.0–5.5 | 3.3–6.0 | 200–512 × 200–512 | 125–320 × 125–320 |
| T2W | 0.23 | 5000–6000 | 108–112 | - | 90 | 1–3 | 4.0–5.5 | 4.4–6.0 | 270–512 × 270–512 | 216–300 × 172–300 |
| | 1.5 | 3300–7350 | 82.4–120 | - | 90–180 | 1–3 | 3.0–5.5 | 3.3–6.0 | 192–512 × 192–512 | 154–320 × 154–320 |
| FLAIR | 0.23 | 5960–6460 | 80 | 2000 | 90 | 2 | 6.0 | 7.2 | 360–512 × 360–512 | 216–256 × 172–204 |
| | 1.5 | 8000–9000 | 100–112.5 | 2000–2500 | 90–150 | 2 | 3.0–5.0 | 3.6–6.0 | 242–512 × 242–512 | 179–256 × 179–256 |
| T2*W GRE | 0.23 | 500–990 | 40–50 | - | 25 | 1 | 5.0 | 5.5 | 360–512 × 360–512 | 256–360 × 150–230 |
| | 1.5 | 483–1140 | 15–26 | - | 20 | 1–3 | 4.0–5.0 | 4.4–5.5 | 256–512 × 256–512 | 173–256 × 173–256 |
| STIR | 0.23 | 3800–4500 | 100 | 100 | 90 | 3 | 5.0 | 6.0 | 288 × 256 | 256 × 216 |
| | 1.5 | 3420–3640 | 13.6–14.7 | 120 | 90 | 2 | 5.0 | 6.0 | 256–288 × 256–288 | 192–256 × 192–256 |
| SPGR | 0.23 | 24 | 8 | - | 35 | 1 | 3.0 | - | 506–512 × 506–512 | 270–300 × 192–270 |
| | 1.5 | 8.5 | 3.5 | - | 30 | 1 | 3.0–5.0 | - | 512 × 512 | 256 × 256 |
| TOF2D-MRA | 0.23 | 33 | 11 | - | 70 | 2 | 3.0 | - | 266 × 333 | 260 × 202 |

T1W, T1 weighted; T2W, T2 weighted; FLAIR, fluid-attenuated inversion recovery; T2*W GRE, T2*-weighted gradient echo; STIR, short tau inversion recovery; SPGR, spoiled gradient echo; TOF2D-MRA, 2D time-of-flight magnetic resonance angiography.


FIG. 1. Transverse T2-weighted (T2W) (A, left is to the right), transverse postcontrast T1-weighted (T1WC) (B, left is to the right), and dorsal T1WC (C, rostral is to the top) magnetic resonance images of the brain of three different horses. A Low-field magnet was used in (A), and a high-field magnet was used in (B) and (C). In (A), there is an intra-axial hyperintense lesion at the level of the right thalamus (arrows), in (B) there is large and marked contrast-enhancing pituitary mass (arrowheads), and (C) shows a soft tissue marked contrast-enhancing intraconal mass (white asterisks) attached to the left optic nerve (black asterisk) resulting in the left eyeball being more protuberant than the contralateral side. This mass was consistent with a meningioma, which was confirmed at surgery. (1) Temporal muscle, (2) cerebrum, (3) cerebellum, (4) thalamus, (5) pituitary gland, (6) lateral ventricles, (7) temporomandibular joint, (8)lateral pterygoideus muscle, (9) guttural pouch, (10) ethmoid labyrinth.

on both T2W and FLAIR images, consistent with colliculi edema. A third horse had diffuse hyperintensity in T2W and FLAIR images in the gray matter of the cerebellar cortex, right occipital, and left frontal, parietal, and occipital lobes. On T1W images, these regions were isointense compared with normal gray matter. These lesions had mild heterogeneous contrast enhancement. Histopathologic findings were consistent with postanesthetic cortical necrosis, with laminar ischemic necrosis in the gray matter and associated perivascular and pericellular edema, and microcavitation within the white matter. One horse had an intra-axial mass consisting of a well-defined, rounded, fluid-filled structure within the occipital lobe of the cerebrum. This mass was hyperintense in T2W images and hypointense in T1W images, had a rim of mild contrast enhancement, and there was white matter edema surrounding it. Histopathologic diagnosis was consistent with an astrocytoma. One horse had a fluid-filled fourth ventricle and abnormal accumulation of cerebrospinal fluid around the cerebellum, which was decreased in size with loss of branching of the folia.

TABLE 2. Characteristics of Horses Included in Group A

| Neurological disease ($n = 65$) | MRI diagnosis | Clinical history or signs |
|---|---|---|
| Intra-axial ($n = 8$) | Cortical infarct | Seizures |
| | Colliculi edema | Dystocia and apnea at birth, altered consciousness |
| | Brain necrosis | Postanesthetic acute-onset seizures, head pressing and blindness |
| | Intra-axial tumor | Seizures |
| | Cerebellar abiotrophy | Hypermetric gait and head tremor |
| | Encephalitis | Head tilt, nystagmus, abnormal behavior, and ataxia |
| | Diffuse brain edema | Inappropriate responses to stimuli, stupor, recumbency and opisthotonus |
| | Multiple brain malformations | Bilateral severe visual deficits, absence of the menace response and dazzle reflex, and nystagmus |
| Extra-axial ($n = 7$) | Brainstem meningioma | Left facial paralysis, and absence of left menace response. Wide-base stance with proprioceptive deficits |
| | Cholesterol granuloma | Chronic intermittent episodes of depression, reduced mentation, circling, and collapsing with loss of consciousness |
| | Pituitary mass ($n = 3$) | Lethargy and progressive neurological signs including: ataxia, weakness, behavioral changes, and depression |
| | Soft tissue tumor | Behavioral changes, seizures, and left eye exophthalmos. |
| | Sphenopalatine cyst | Bilateral blindness, mydriasis, head tilt, and ataxia |
| Optic nerve ($n = 4$) | Optic neuritis ($n = 2$) | Sudden onset of unilateral prechiasmic blindness after head trauma |
| | Optic nerve atrophy | Sudden onset of bilateral blindness and mydriasis |
| | Meningioma | Left eye exophthalmos with ipsilateral mydriasis and absence of menace response |
| Normal MRI ($n = 46$) | | Seizures ($n = 29$)<br>Narcolepsy ($n = 4$)<br>Abnormal behavior ($n = 4$)<br>Vestibular disease ($n = 3$)<br>Ataxia ($n = 3$)<br>Head shaking ($n = 2$)<br>Blindness ($n = 1$) |

Microscopic examination of the cerebellum confirmed cerebellar abiotrophy with degeneration of the granular cells, disorganization of the molecular and granular layers of the cerebellar cortex, and shrunken Purkinje cells. The horse with encephalitis had multifocal ill-defined hyperintensities within the internal capsule, thalamus, and midbrain in T2W and FLAIR images (Fig. 1A). These lesions were isointense on T1W images; contrast medium was not administered. A Miniature horse with acute post-traumatic opisthotonus and stupor had a diffuse hyperintensity in the gray matter of the cerebral and cerebellar cortices in T2W and FLAIR images, which was isointense to the normal gray matter on T1W images. There was marked transtentorial and transforaminal herniation of the brain. A 1-month-old filly had multiple congenital malformations including reduced size of both optic nerves, right occipital and parietal lobes, right thalamus, and mesencephalon, and dilation of the right lateral ventricle.

One horse had an ovoid soft tissue mass of mixed signal intensity ventral to the brainstem, centered slightly to the left of the midline and causing moderate compression of the brainstem, typical of a brainstem meningioma. One horse had two large ovoid, well-defined masses located within the lateral ventricles. They were hypointense compared with normal gray matter with small hyperintense foci on T2W images, isointense to slightly hypointense on T1W images, and had signal voids on T2*W GRE images. There was mild heterogeneous contrast enhancement. There was severe mass effect including surrounding white matter edema, shift of the falx cerebri, transtentorial herniation, and obstructive hydrocephalus. These features were consistent with a cholesterol granuloma. Three horses had pituitary masses that had heterogeneous increased signal intensity on T2W images, with multiple small signal voids in two horses. Marked contrast enhancement was observed in all the cases. There was mass effect, with variable degrees of dorsal deviation of the thalamus (Fig. 1B). A moderate obstructive hydrocephalus was seen in the largest of the masses. The masses measured (height × width × length) 20 × 18 × 26 mm, 13 × 20 × 18 mm, and 46 × 42 × 41 mm, respectively. An irregular, highly infiltrative, and osteolytic mass that invaded the cribriform plate, olfactory lobe, and the optic nerve was consistent with a neuroendocrine tumor arising from the orbital soft tissues. One horse had a well-defined, multiloculated, and encapsulated expansile mass of large dimensions (87 × 60 × 53 mm) filled with proteinaceous fluid, hyperintense in T1 and T2W images, which did not suppress in FLAIR and STIR images. This mass, consistent with a sphenopalatine cyst, destroyed the sphenoid bone and invaded the skull, compressing both optic nerves, optic chiasm, frontal and parietal lobes. No brain edema was observed, which suggested slow growth of the mass.

Two horses with acute onset of unilateral prechiasmic blindness had unilateral swelling of the optic nerve with mild increased signal intensity on T2W and FLAIR images, with mild contrast enhancement of the affected nerve, consistent with optic nerve neuritis. Cerebrospinal fluid analysis was normal. A third blind horse had flattening of both optic nerves just rostral to the optic chiasm, with mild increased signal intensity in T2W images and no contrast enhancement, reflecting optic nerve atrophy. There was marked ventral compression of the optic nerves secondary to proteinaceous fluid accumulation in both sphenopalatine sinuses, creating atrophy of the sphenoid bone. A horse with exophthalmos had a retrobulbar mass consisting of a well-defined, ovoid, and homogeneous contrast-enhancing intraconal soft tissue mass, which was intimately associated with the optic nerve (Fig. 1C). This mass was hyperintense to muscle in both T1W and T2W images, and measured 42 × 32 × 29 mm. Histopathological diagnosis was a syncytial meningioma.

All horses with no detectable abnormalities on MR images had normal cerebrospinal fluid analysis. All horses with a history of recurrent seizure-like activity had a normal neurological examination during the period of hospitalization.

Additionally, asymmetry of the lateral ventricles was found without any other abnormality in 4/65 horses, and small rounded signal voids on T2*W GRE images within the lateral ventricles in 6/65 horses (Fig. 2A). In 5 of 65 horses, the pineal gland had diffuse low signal intensity in T2*W GRE without changes of the signal intensity in the other sequences (Fig. 2B). In 6/65 horses at the level of the internal capsule, specifically the globus pallidus, there was a symmetric and bilateral ill-defined low signal intensity in T2*W GRE images, which had slight T2W low signal intensity and T1W hyperintensity (Fig. 2C). Three of 65 horses had ill-defined periventricular hyperintensities on T2W and FLAIR images not identifiable on the rest of the sequences, which were considered to represent leukoariosis (Fig. 3).

*Sinonasal disease (group B).* Group B ($n = 14$) comprised two stallions, eight geldings, and four mares; the mean age was 17.1 years (range 2–28 years; median 14 years). This group included dental disease ($n = 4$), nasal tumors ($n = 4$), ethmoid hematomata ($n = 2$), sinus cysts ($n = 2$), nasal mucocele ($n = 1$), and nasal septum deviation ($n = 1$). Half of the horses were evaluated with a high-field or low-field magnet, respectively. Clinical features are summarized in Table 3.

Sinusitis was present in all cases, except the horse with nasal septum deviation and one with disease of the third upper premolar (207). Sinusitis was characterized by thickening of the sinus mucosa with increased signal intensity in T2W images, and marked contrast enhancement on T1W images. Free fluid, hyperintense in T2W images and hypointense on T1W images, was present in the rostral maxillary sinus (6/12), caudal maxillary sinus (7/12), ventral conchal sinus (6/12), conchofrontal sinus (5/12), and sphenopalatine sinus (3/12).

Horses with dental disease included a periapical abscess and pulp necrosis of 207 ($n = 1$), tooth fracture of 209 ($n = 1$), and sinus abscess formation secondary to previous tooth extraction (109 or 209; $n = 2$). The periapical abscess was characterized by widening of the periodontal space with increase in signal intensity of the alveolar bone in T2W and STIR images, and protrusion of the tooth root into the middle nasal meatus. The proximal pulp cavity was enlarged, and had heterogeneous signal intensity. There was fistula formation from the tooth root to the skin. The horse with 209 fracture had widening of the periodontal space and decreased signal intensity in T1 and T2W images of the alveolar bone, consistent with increased bone density, surrounding 208 and 210. These changes were not identified on radiographs. Both horses with a sinus abscess had a well-defined capsule within the ventral conchal sinus, with heterogeneous signal intensity in T2W images (Fig. 4A and B). There was also a mild mass effect resulting in deviation of the dorsal conchal sinus wall and infraorbital canal.

Four different sinonasal masses were identified, which were verified histopathologically as an osteoma, an adenocarcinoma, a lymphoma, and a squamous cell carcinoma, respectively (Fig. 5). The osteoma appeared as an irregularly shaped mass that was hypointense on both T1W and T2W images, containing small foci isointense to muscle on T2W images. This mass within the middle nasal meatus resulted in atrophy of the maxillary bone. The adenocarcinoma was seen as an ill-defined, highly infiltrative mass originating from the ethmoid labyrinth, spreading into the periorbital region and into the olfactory lobe through the cribriform plate. Signal intensity was increased on T2W images, isointense to muscle on T1W images, and had heterogeneous moderate contrast enhancement. Magnetic resonance features of squamous cell carcinoma and lymphoma were similar, consisting of an expansile heterogeneously and moderate contrast-enhancing mass that completely occluded the nasal cavity. Marked destruction of the dorsolateral aspect of the maxilla, mild-to-moderate nasal septum deviation, extension into the paranasal sinuses, and complete obstruction of the rostral aspect of the ipsilateral choana were also present. Small lesions such as lysis and thinning affecting flat bones of the skull, especially the maxillary and nasal bones, which were identified at in postmortem examination, were difficult to identify in MR images. There were variable degrees of mandibular and retropharyngeal lymph node enlargement ($n = 3$).

Ethmoid hematomata, which were verified histopathologically, were seen as well-defined structures arising from

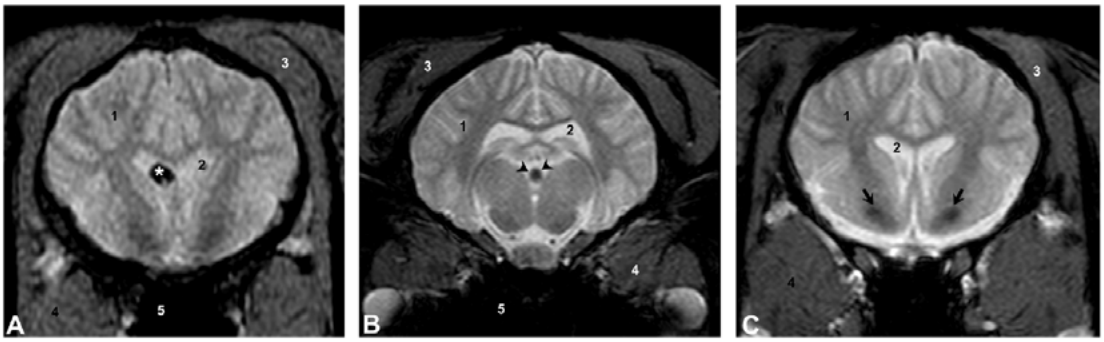


FIG. 2. Transverse T2*-weighted gradient echo magnetic resonance images of the brain of different horses (left is to the right) acquired using a high-field magnet. In (A), there is a focal rounded area of signal void within the right lateral ventricle (asterisk). There is bilateral and symmetrical low signal intensity within the pineal gland (B, arrowheads), and at the level of the globus pallidus (C, arrows). These changes were considered incidental findings, however no histopathological examination was performed. (1) Cerebrum, (2) lateral ventricles, (3) temporal muscle, (4) lateral pterygoideus muscle, (5) guttural pouch.

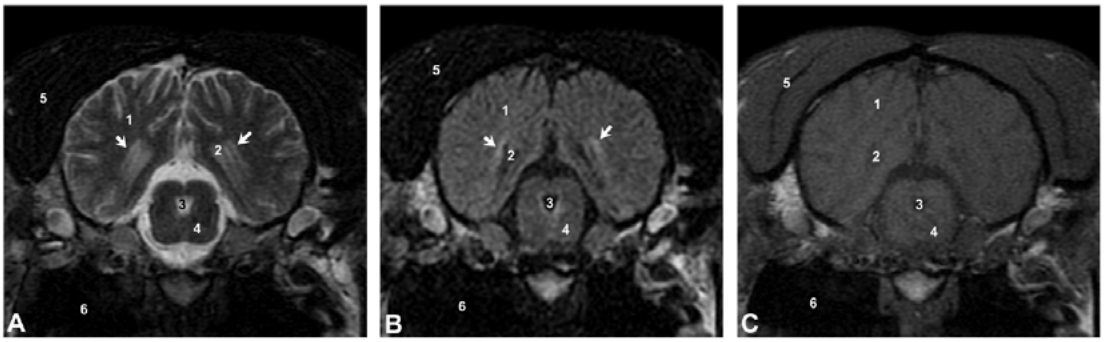


FIG. 3. Transverse T2-weighted (T2W) (A), fluid-attenuated inversion recovery (FLAIR) (B), and T1-weighted (T1W) (C) magnetic resonance images of the brain at the level of the caudal aspect of the lateral ventricles (left is to the right) acquired using a high-field magnet. The arrows depict bilateral periventricular hyperintensities within the white matter in T2W and FLAIR images, which were not visible in T1W images. These changes were considered to represent leukoariosis. (1) Cerebrum, (2) lateral ventricles, (3) mesencephalic aqueduct, (4) mesencephalic tegmentum, (5) temporal muscle, (6) guttural pouch.

the ethmoid labyrinth that extended into the sphenopalatine sinus, with mild heterogeneous increased signal intensity with small areas of signal void on T2W images. On T1W images, these were slightly hyperintense to the surrounding muscles, and no signal voids were seen on T2*W GRE images. No contrast enhancement was observed ($n = 1/1$).

Two horses had well-defined, multiloculated, and encapsulated expansile masses of large dimensions (93 × 59 × 141 mm, and 103 × 77 × 103 mm), consistent with sinus cysts that were surgically resected. These were filled with homogeneous fluid, hyperintense in T2W images and intermediate signal intensity on T1W images (Fig. 4C and D). One cyst was in the dorsal conchal sinus, and the other was in the caudal maxillary sinus, extending into the conchofrontal sinus. A marked mass effect of all surrounding paranasal sinuses, mild deviation of the nasal septum, and atrophy of the nasal and dorsolateral aspect of the maxillary bones were also present.

TABLE 3. Characteristics of Horses Included in Group B

| | MRI diagnosis | Clinical signs |
|---|---|---|
| Sinonasal disease ($n = 14$) | Periapical abscess and pulp necrosis of 207 | Facial fistulous tract |
| | Fracture of 209 | Chronic nasal discharge, facial pain, and loss of weight |
| | Sinus abscess secondary to tooth extraction ($n = 2$) | Unilateral mucopurulent nasal discharge and exophthalmos |
| | Nasal tumor ($n = 4$) | Epistaxis and nasal discharge, with facial deformation in two horses |
| | Ethmoid hematoma ($n = 2$) | Chronic and intermittent epistaxis |
| | Sinus cyst ($n = 2$) | Chronic clear nasal discharge |
| | Nasal mucocele | Chronic nonodorous nasal discharge |
| | Nasal septum deviation | Abnormal inspiratory noise since birth |

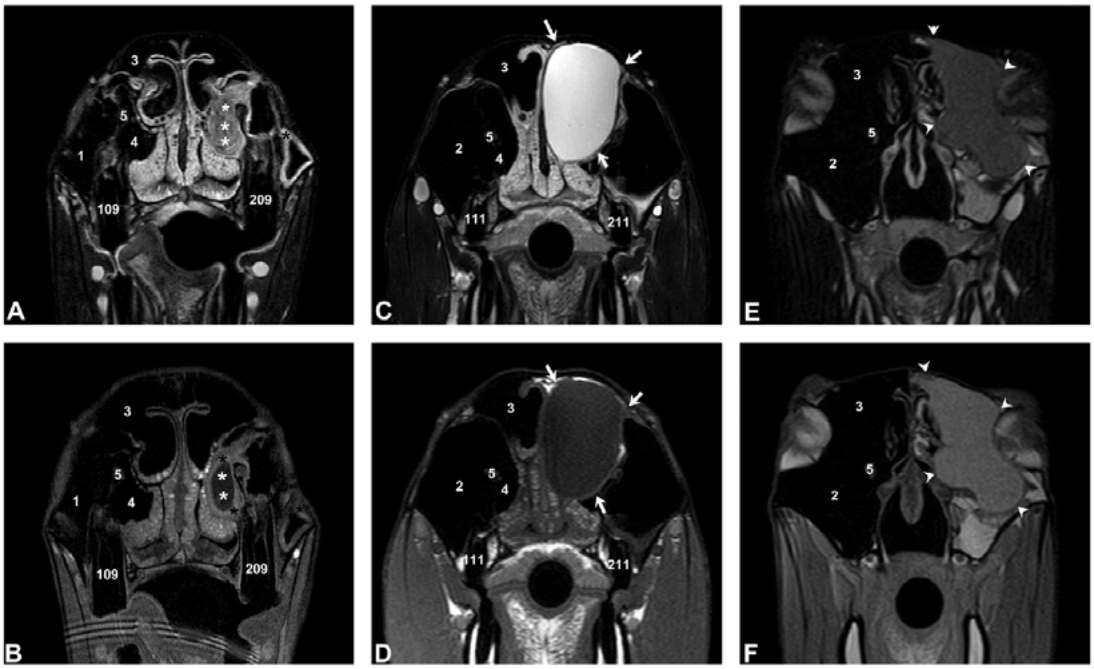


FIG. 4. Transverse T2-weighted (T2W; A, C, and E), T1W postcontrast (T1WC; B), and T1-weighted (T1W; D, F) magnetic resonance images of three different kind of fluid accumulation within the nasal cavities. A High-field magnet was used in (A–D), and a low-field magnet was used in (E) and (F). Horse 1 (A–B) has material of uniform intermediate signal intensity in T2W images within the left ventral conchal sinus that has low signal intensity in T1WC images (white asterisks). There is thickening of the mucosa of the left ventral conchal and rostral maxillary sinuses (black asterisks), with moderate contrast-enhancement. These findings represent an abscess secondary to previous 207 extraction. In horse 2 (C–D), there is an encapsulated expansile mass (arrows) within the left dorsal conchal sinus filled with homogeneous fluid, hyperintense in T2W images and intermediate signal intensity on T1W images, consistent with a sinus cyst. In horse 3 (E–F), the left caudal maxillary and conchofrontal sinuses are filled with intermediate signal intensity material in T1 and T2W images (arrowheads), with higher signal intensity in the T1W compared with T2W image; histopathological diagnosis was mucocele. (1) Rostral maxillary sinus, (2) caudal maxillary sinus, (3) conchofrontal sinus, (4) ventral conchal sinus, (5) infraorbital nerve.

One horse had a diffuse increased opacity of the caudal maxillary and conchofrontal sinuses on radiographs. Magnetic resonance imaging showed that caudal maxillary, conchofrontal, and rostral aspect of sphenopalatine sinuses were filled with material that had intermediate signal intensity on T1W, T2W, and FLAIR images, consistent with protein-rich fluid (Fig. 4E and F). No distinct wall surrounding this structure, and no mass effects were observed. Histopathological diagnosis was nasal mucocele.

A 2-year-old Thoroughbred with inspiratory stridor since birth had thickening and lateral deviation of the rostrodorsal aspect of the nasal septum, resulting in obliteration of the nasal meatus.

*Soft tissue disease (group C).* Group C ($n = 5$) comprised three stallions and two mares; the mean age was 8.4 years (range 3–14 years; median 7 years). This group included a third eyelid mass ($n = 1$), a lingual abscess ($n = 1$), a parotid salivary gland sialocele/mucocele ($n = 1$), a swelling of the guttural pouch ($n = 1$), and a cranial nuchal bursitis ($n = 1$). Three and two horses were evaluated with a high-field or low-field magnet, respectively. Clinical features are summarized in Table 4.

The third eyelid mass was a small (7 × 20 × 2 mm) mildly contrast-enhancing plaque-like mass affecting the third eyelid, which was slightly hyperintense in T2W images and isointense in T1W images. Orbital involvement was not observed. Histopathologic diagnosis was squamous cell carcinoma.

One horse had a well-defined, rounded, and encapsulated mass within the tongue (59 × 11 × 58 mm) in between both hypoglossus muscles. The mass had heterogeneous high signal intensity on T2W images and was isointense on T1W images, with a ring-like enhancement pattern on postcontrast T1W images, consistent with a lingual abscess. Marked mandibular lymphadenopathy was present; no foreign body was observed.

One horse had a fluid-filled (hyperintense in T2W images and hypointense in T1W images) ovoid structure (111 × 71 × 68 mm), located in the retromandibular fossa and intimately associated with the parotid salivary gland

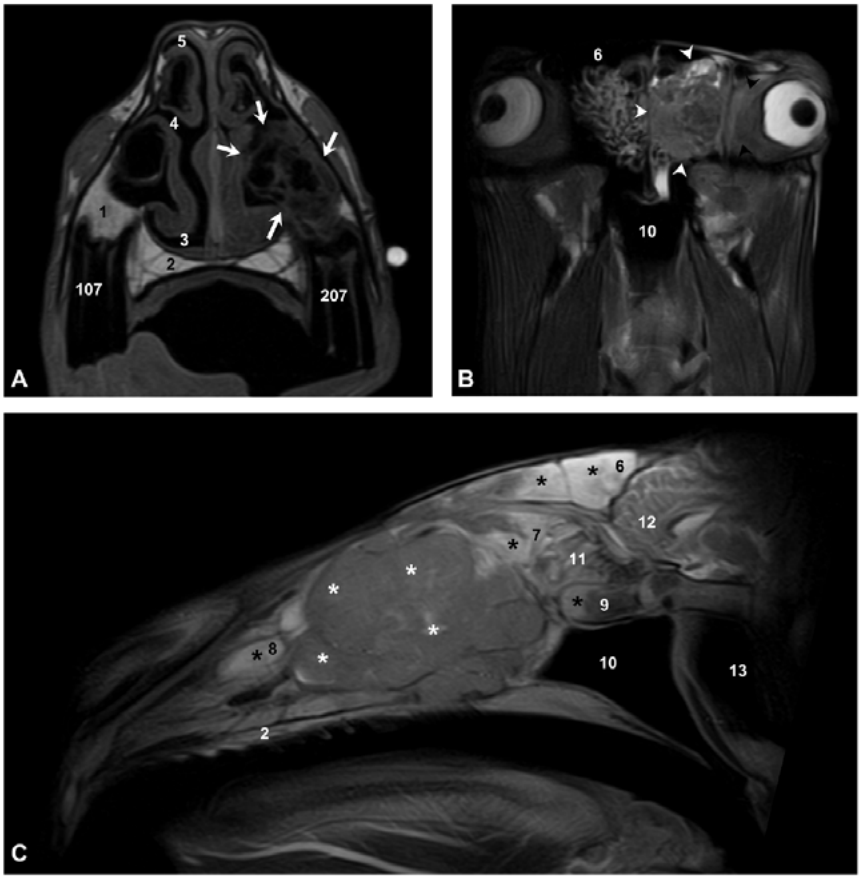


FIG. 5. Transverse T1-weighted (T1W) (A, left is to the right), transverse T2-weighted (T2W) (B, left is to the right), and sagittal T2W (C, rostral is to the left) magnetic resonance images of the nasal cavity of three horses with different types of nasal tumors acquired using a low-field magnet. In (A), there is an irregularly shaped mass with multiple hypointense areas (arrows) within the left middle nasal meatus dorsal to 207, verified by histopathology as an osteoma. In (B), there is a heterogeneous signal intensity mass (white arrowheads) within the left ethmoid labyrinth that invades the left orbit (black arrowheads) and results in protrusion of the left globe. The mass was verified as an adenocarcinoma by histological examination. In (C), there is a large mass (white asterisks) within the nasal cavity, which is hyperintense to muscle and there is high signal intensity consistent with fluid within the conchofrontal, caudal maxillary, sphenopalatine, and ventral conchal sinuses (black asterisks). The mass was confirmed histologically as a lymphoma. (1) Maxillary bone, (2) palatine bone, (3) ventral nasal meatus, (4) middle nasal meatus, (5) dorsal nasal meatus, (6) conchofrontal sinus, (7) caudal maxillary sinus, (8) ventral conchal sinus, (9) sphenopalatine sinus, (10) choana, (11) ethmoid labyrinth, (12) cerebrum, (13) guttural pouch.

TABLE 4. Characteristics of Horses Included in Group C

| | MRI diagnosis | Clinical signs |
|---|---|---|
| Soft tissue disease ($n = 5$) | Third eyelid mass | Orbital swelling |
| | Lingual abscess | Syalorrea, submandibular edema and swelling of the tongue |
| | Parotid gland sialocele | Retromandibular mass |
| | Guttural pouch swelling and internal carotid aneurysm | Mucopurulent nasal discharge |
| | Cranial nuchal bursitis | Nuchal swelling and a fistulous tract |

that was reduced in volume. The fluid content bulged over the lateral compartment of the guttural pouch, in between the maxillary and transverse facial veins. This was consistent with a parotid salivary gland sialocele/mucocele; microscopic diagnosis was parotid mucocele.

A horse with a previous history of unilateral guttural pouch mycosis had thickening of the stylohyoid bone surrounded by soft tissue, marked reduction in size of the medial guttural pouch compartment, retropharyngeal lymphadenopathy, and focal distension of the sigmoid part of the internal carotid artery consistent with an aneurysm.

One horse had a multiloculated, poorly marginated fluid-filled structure, located within the cranial cervical epaxial musculature dorsal to the atlas and connecting with the cranial nuchal bursa, showing marked rim-like contrast enhancement, consistent with cranial nuchal bursitis. At the cerebellomedullary cistern, the structure compressed the ligamentum flavum and spinal cord.

## Discussion

This is the largest equine head MRI series to date and the brain was the most commonly imaged area (65/84 horses, 77%). In the three disease groups, both low-field and high-field magnets were used. Despite observations of inferior anatomical resolution in the low-field images, the authors considered the images to be of adequate diagnostic quality and propose that either system would be suitable for studying the equine head. Abnormal MRI findings were found in 30% (19/65) of the horses with neurological disease in the current study, where a previous MRI study of horses with neurological signs reported a higher prevalence of abnormalities (8/12; 67%). The reason for the higher numbers reported in that study is unclear, but could be related to the smaller number of horses with seizures that were included (1/12; 8.3%).[19] Equine neurological diseases have been well described,[34,35] but not all conditions have been described on MR images. Magnetic resonance imaging features of congenital diseases, such as hydrocephalus[19,36], chiari-like malformation,[37] and cerebellar abiotrophy;[38] traumatic diseases;[39–41] intra-axial diseases such as inflammatory/infectious,[19,40,42–44] or neurodegenerative[19,45] conditions; extra-axial diseases including neoplastic,[19,40,46,47] granulomatous,[48] and infectious[49,50] conditions; and diseases affecting the optic nerve[47,51,52] have been described. To our knowledge, the MRI features of postanesthetic cerebral necrosis have not been reported, although postmortem findings have been documented including diffuse, acute necrosis with edema of the entire cerebral cortex.[53,54] These findings corresponded to the diffuse hyperintensities in T2W and FLAIR images observed within the cortex of the brain of the horse included in this study. Similar MRI findings have been observed in dogs with global brain ischemia following general anesthesia.[55]

From the 65 horses examined for neurological disorders in the current study, 31 had a primary complaint of recurrent seizure-like activity, only two of which had abnormalities on MRI of the brain, an old infarct in one and an intra-axial mass in the other. Intra-axial masses are very uncommon conditions in the equine brain,[35] and other modalities such as CT may fail to show this type of lesion. The remaining horses included a wide range of breeds and ages, and none had any identifiable etiology for seizures. Epilepsy is the most common acquired chronic neurological disorder in humans and dogs, with an estimated prevalence of 0.004–0.01% and 0.5–5.7%, respectively.[56] In people, there are over 40 epileptic syndromes and related conditions.[56] In dogs, however, epilepsy is not usually differentiated into syndromes, and most dogs with recurrent seizures have no identifiable underlying cause, and are by exclusion classified as having idiopathic epilepsy.[56] In these animals, neurological examination, blood tests, MRI, and cerebrospinal fluid analysis demonstrate no significant abnormalities. However, the term idiopathic epilepsy has been used to refer to a suspected genetic predisposition (e.g., Arabian horses aged <1 year).[57] We therefore prefer the term cryptogenic epilepsy. Magnetic resonance imaging was a vital part of the seizure work-up, because it ruled out intracranial causes of the seizures. In a previous study of 57 horses with seizure-like activity, intracranial lesions were not detected by CT.[27] In our study, two horses with seizures had MRI abnormalities and the authors therefore propose that MRI may be a preferred imaging modality for investigation of horses with a history of seizures.

Presumed incidental abnormalities identified in horses of the current study included asymmetry of the lateral ventricles, signal voids on T2*W GRE images within the lateral ventricles, low signal intensity in T2*W GRE throughout the pineal gland and internal capsule (globus pallidus), and leukoaraiosis (Figs. 2 and 3). Asymmetry of lateral ventricles was considered a normal anatomic variation, similar to previous studies in horses[27] and dogs.[58] The ventricular signal voids could represent incidental small nonobstructive cholesterol granulomata. Changes of the pineal gland were the only MRI abnormality in horses with narcolepsy ($n = 2$), seizures ($n = 2$), and abnormal behavior ($n = 1$). Postmortem evaluation of the pineal gland was not performed in any of the cases. Considering the alteration in signal characteristics, we suspect this lesion represents calcification or hemorrhage within the pineal gland. The occurrence of pineal gland calcification has been associated with increasing age in humans.[59] It is speculated to be an indicator of a melatonin deficit, which may be related to sleep disorders. However, a definitive correlation between melatonin production and pineal gland calcification has not yet been established.[59,60] Findings within the internal capsule were symmetrical in all horses, and may represent mineralization or hemorrhage. In a previous equine brain necropsy study, 27% had vascular mineralization near the internal capsule, and more specifically in the globus pallidus and thalamus, with a significant increase with age.[61] Vascular mineralization (siderocalcinosis) in the brain of horses was assumed to be an incidental age-related change of no clinical significance.[62] Leukoaraiosis is a common feature of the human ageing brain of unknown etiology, but the speculated cause is chronic cerebral ischemia.[63,64] It consists of bilateral and either patchy or diffuse areas

of increased signal intensity in T2W and FLAIR images within the cerebral white matter, as seen in several horses in the current study. The underlying histological findings include reduced myelin, axonal loss, and astrocytic gliosis.

Magnetic resonance imaging allowed evaluation of the optic nerves, nasal cavity, paranasal sinuses, and teeth in horses of the current study, as has been previously described.[20] We found subjectively good agreement between MRI findings and intraoperative or pathological results. In all cases, the MRI localization, size, and relation to surrounding structures of the lesions matched surgical and/or gross and histopathological observations. Magnetic resonance imaging was particularly useful for identifying space-occupying lesions (tumors, sinus cysts, or ethmoid hematomata), where the high soft tissue contrast of the images allowed differentiation of tissue types. For example, comparison of the signal intensity observed on different sequences allowed differentiation of cysts, mucocele, or hematomata, and to differentiate between fluid and purulent material in the sinuses. In cases of nasal tumors, MRI helped in assessing the cribriform plate and showing intracranial extension of the tumor. In four horses with dental disease, MRI identified an external fistula and a dental fracture, as well as lesions involving the pulp cavity, roots, and periodontal space. Changes involving the lamina dura and surrounding alveolar bone were observed in all horses, although radiological abnormalities had been identified in only two. These findings indicated that, although CT has been reported to be the gold standard imaging technique for evaluation of dental disease,[22–24] dental changes can also be evaluated using MRI.[21] Previously reported lesions involving the soft tissues of the head on MRI include laryngeal dysplasia,[65] a laryngeal tumor,[66] a pharyngeal tumor,[67] a lingual tumor,[68] an ocular tumor,[69] and a foreign body.[70] Extracranial soft tissue disorders of the head are relatively common, and they usually involve the tongue, salivary glands, lymph nodes, larynx, pharynx, and orbit.[71] In many cases, the diagnosis can be reached by ultrasonography, especially for superficial structures.[9,10,72] Although MRI requires general anesthesia and additional expense, it can complement ultrasonographic information, providing a better global picture of the entire region using multiple planes, providing good differentiation of the soft tissue structures, and establishing an accurate relationship with surrounding structures.[73,74]

The authors acknowledge that either MRI or CT can be used for performing a detailed examination of the equine head and some in conditions both modalities are suitable. Each technique offers advantages over the other for studying certain tissues or structures.[13] Our findings supported the use of MRI for examining the nervous system, sinonasal mucosa, and soft tissues of the head, including muscles, blood vessels, and glands. Nevertheless, limitations were found in horses with small lesions affecting flat bones of the skull that surround the sinuses, especially the maxillary and nasal bones. These bones consist of two layers of compact bone, without an inner medullary cavity resulting in poor signal from these bones.[75] Therefore, accurate evaluation of the flat bones may be difficult and lesions may have been missed. In such horses, CT would have likely allowed a more detailed examination of the osseous structures. The main limitations of MRI demonstrated in this study included the low number of MRI changes in the brain in horses with recurrent seizure-like history. Another limitation of the current study was that techniques for performing MRI evolved during the period of this retrospective study, and therefore imaging protocols were not standardized. Despite a multicenter study performed over 13 years, there were only 84 horses and therefore conclusions related to specific conditions should be interpreted cautiously. This study did not determine whether the results of MRI influenced case management and outcome.

In conclusion, findings from the current study supported the use of low-field or high-field MRI for detailed assessment of the majority of structures of the equine head. Future studies comparing CT and MRI for specific conditions of the equine head would be beneficial.

## REFERENCES

1. Dyce KM, Sack WO, Wensing CJG. The head and ventral neck of the horse. In: Dyce KM, Sack WO, Wensing CJG (eds): Textbook of veterinary anatomy, 4th ed. St Louis: Saunders, 2010;501–531.
2. Wyn-Jones G. Interpreting radiographs 6: the head. Equine Vet J 1985;17:274–278.
3. Gibbs C, Lane JG. Radiographic examination of the facial, nasal and paranasal sinus regions of the horse. II. Radiological findings. Equine Vet J 1987;19:474–482.
4. Head KW, Dixon PM. Equine nasal and paranasal sinus tumours. Part 1: review of the literature and tumour classification. Vet J 1999;157:261–278.
5. Dixon PM, Head KW. Equine nasal and paranasal sinus tumours. Part 2: a contribution of 28 case reports. Vet J 1999;157:279–294.
6. Wyn-Jones G. Interpreting radiographs 6: Radiology of the equine head (Part 2). Equine Vet J 1985;17:417–425.
7. Weller R, Cauvin ERJ, Bowen IM, May SA. Comparison of radiography, scintigraphy and ultrasonography in the diagnosis of a case of temporomandibular joint arthropathy in a horse. Vet Rec 1999;144:377–379.
8. Weller R, Taylor S, Maierl J, Cauvin E, May SA. Ultrasonographic anatomy of the equine temporomandibular joint. Equine Vet J 1999;31:529–532.
9. Chalmers HJ, Cheetham J, Yeager AE, Ducharme NG. Ultrasonography of the equine larynx. Vet Radiol Ultrasound 2006;47:476–481.
10. Valentini S, Tamburro R, Spadari A, Vilar JM, Spinella G. Ultrasonographic evaluation of equine ocular diseases: a retrospective study of 38 eyes. J Eq Vet Sci 2010;30:150–154.
11. Weller R, Livesey L, Maierl J, et al. Comparison of radiography and scintigraphy in the diagnosis of dental disorders in the horse. Equine Vet J 2001;33:49–58.

12. Barakzai SZ, Tremaine WH, Dixon PM. Use of scintigraphy for diagnosis of equine paranasal sinus disorders. Vet Surg 2006;35:94–101.
13. Tucker RL. Magnetic resonance imaging of the equine head and neck region. Equine Vet Educ 2008;20:294–6.
14. Arencibia A, Vázquez JM, Jaber R, et al. Magnetic resonance imaging and cross sectional anatomy of the normal equine sinuses and nasal passages. Vet Radiol Ultrasound 2000;41:313–319.
15. Chaffin MK, Walker MA, McArthur NH, Perris EE, Matthews NS. Magnetic resonance imaging of the brain of normal neonatal foals. Vet Radiol Ultrasound 1997;38:102–111.
16. Arencibia A, Vázquez JM, Ramirez JA, et al. Magnetic resonance imaging of the normal equine brain. Vet Radiol Ultrasound 2001;42:405–409.
17. Vázquez JM, Rivero M, Gil F, et al. Magnetic resonance imaging of two normal equine brains and their associated structures. Vet Rec 2001;148:229–232.
18. Manso-Díaz G, Garcia-Real I, Casteleyn C, San-Roman F, Taeymans O. Time-of-flight magnetic resonance angiography (TOF-MRA) of the normal equine head. Equine Vet J 2013;45:187–192.
19. Ferrell EA, Gavin PR, Tucker RL, Sellon DC, Hines MT. Magnetic resonance for evaluation of neurologic disease in 12 horses. Vet Radiol Ultrasound 2002;43:510–516.
20. Tessier C, Brühschwein A, Lang J, et al. Magnetic resonance imaging features of sinonasal disorders in horses. Vet Radiol Ultrasound 2013;54:54–60.
21. Gerlach K, Ludewig E, Brehm W, Gerhards H, Delling U. Magnetic resonance imaging of pulp in normal and diseased equine cheek teeth. Vet Radiol Ultrasound 2013;54:48–53.
22. Tietje S, Becker M, Böckenhoff G. Computed tomographic evaluation of head diseases in the horse: 15 cases. Equine Vet J 1996;28:98–105.
23. Henninger W, Frame EM, Willmann M, et al. CT features of alveolitis and sinusitis in horses. Vet Radiol Ultrasound 2003;44:269–276.
24. Veraa S, Voorhout G, Klein WR. Computed tomography of the upper cheek teeth in horses with infundibular changes and apical infection. Equine Vet J 2009;41:872–876.
25. Hilton H, Puchalski SM, Aleman M. The computed tomographic appearance of equine temporohyoid osteoarthropathy. Vet Radiol Ultrasound 2009;50:151–156.
26. Lacombre VA, Sogaro-Robinson C, Reed SM. Diagnostic utility of computed tomography imaging in equine intracranial conditions. Equine Vet J 2010;42:393–399.
27. Sogaro-Robinson C, Lacombe V, Reed SM, Balkrishnan R. Factors predictive of abnormal results for computed tomography of the head in horses affected by neurologic disorders: 57 cases (2001–2007). J Am Vet Med Assoc 2009;235:176–183.
28. Veraa S, Dijkman R, Klein WR, van den Belt AJM. Computed tomography in the diagnosis of malignant sinonasal tumours in three horses. Equine Vet Educ 2009;21:284–288.
29. Powder S, Scrivani PV, Bezuidenhout A, Divers TJ, Ducharme NG. Computed tomography of temporal bone fractures and temporal region anatomy in horses. J Vet Intern Med 2010;24:398–406.
30. Huggons NA, Bell RJW, Puchalski SM. Radiography and computed tomography in the diagnosis of nonneoplastic equine mandibular disease. Vet Radiol Ultrasound 2011;52:53–60.
31. Pease AP, Schott HC II, Howey EB, Patterson JS. Computed tomographic findings in the pituitary gland and brain of horses with pituitary pars intermedia dysfunction. J Vet Intern Med 2011;25:1144–1151.
32. Cissell DD, Wisner ER, Textor JA, Mohr FC, Scrivanni PV, Théon AP. Computed tomographic appearance of equine sinonasal neoplasia. Vet Radiol Ultrasound 2012;53:245–251.
33. Textor JA, Puchalski SM, Affolter VK, Macdonald MH, Galuppo LD, Wisner ER. Results of computed tomography in horses with ethmoid hematoma: 16 cases (1993–2005). J Am Vet Med Assoc 2012;240:1338–1344.
34. Mayhew J. Evaluation of large animal neurologic patients. In: Mayhew J (ed): Large animal neurology, 2nd ed. Chichester: Wiley-Blackwell, 2009;3–76.
35. Furr M, Reed SM. Neurologic examination. In: Furr M, Reed SM (eds): Equine neurology, 1st ed. Ames: Blackwell Publishing, 2008;65–77.
36. Oey L, Müller J-MV, Klopmann TV, Jacobsen B, Beineke A, Feige K. Diagnosis of internal and external hydrocephalus in a warmblood foal using magnetic resonance imaging. Tierärztl Prax Ausg 2011;39:41–45.
37. Lempe A, Heine M, Bosch B, Mueller K, Brehm W. Imaging diagnosis and clinical presentation of a Chiari malformation in a thoroughbred foal. Equine Vet Educ 2012;23:618–623.
38. Cavalleri JM, Metzger J, Hellige M, et al. Morphometric magnetic resonance imaging and genetic testing in cerebellar abiotrophy in Arabian horses. BMC Vet Res 2013;9:105–114.
39. Gold R, Kneissl S, Gruber A, Fröhlich W, Leschnik M, Reisinger R. Skull-brain trauma in a trotter filly. Tierärztl Prax Ausg 2010;38:52–56.
40. Tucker R, Garrett K, Reed S, Murray R. The head. In: Murray R (ed): Equine MRI, 1st ed. Ames: Wiley-Blackwell; 2011:467–488.
41. De Zani D, Zani DD, Binanti D, Riccaboni P, Rondena M, Di Giancamillo M. Magnetic resonance features of closed head trauma in 2 foals. Equine Vet Educ 2013;25:493–498.
42. Audigié F, Tapprest J, George C, et al. Magnetic resonance imaging of a brain abscess in a 10-month-old filly. Vet Radiol Ultrasound 2004;45:210–215.
43. Spoormakers TJP, Ensink JM, Goehring LS, et al. Brain abscesses as a metastatic manifestation of strangles: symptomatology and the use of magnetic resonance imaging as a diagnostic aid. Equine Vet J 2003;35:146–151.
44. Gray LC, Magdesian KG, Madigan JE, Sturges BK. Suspected protozoal myeloencephalitis in a two-month-old colt. Vet Rec 2001;149:269–273.
45. Sanders SG, Tucker RL, Bagley RS, Gavin PR. Magnetic resonance imaging features of equine nigropallidal encephalomalacia. Vet Radiol Ultrasound 2001;42:291–296.
46. Dyson PK, Dunn KA, Whitwell K, Dennis R. Ataxia and cranial nerve signs in a pony suffering a brainstem meningioma; clinical, MRI, gross and histopathological findings. Equine Vet Educ 2007;19:173–178.
47. Matiasek K, Cronau M, Schmahl W, Gerhards H. Imaging features and decision making in retrobulbar neuroendocrine tumours in horses-Case report and review of literature. J Vet Med A 2007;54:302–306.
48. Maulet B, Bestbier M, Jose-Cunilleras E, Scrine J, Murray RC. Magnetic resonance imaging of a cholesterol granuloma and hydrocephalus in a horse. Equine Vet Educ 2008;20:74–79.
49. Morresey PR, Garrett KS, Carter D. *Rhodococcus equi* occipital bone osteomyelitis, septic arthritis, and meningitis in a neurological foal. Equine Vet Educ 2010;23:398–402.
50. Johns IC, Finding E, Ciasca T, Erles K, Smith K, Weller R. Intracranial botryomycosis in a mature horse. Equine Vet Educ 2012;26:294–298.
51. Naylor RJ, Dunkel B, Dyson SJ, Paz-Penuelas MP, Dobson J. A retrobulbar meningioma as a cause of unilateral exophthalmos and blindness in a horse. Equine Vet Educ 2010;22:503–510.
52. Barnett KC, Blunden AS, Dyson SJ, Whitwell KE, Carson D, Murray RC. Blindness, optic atrophy and sinusitis in the horse. Vet Ophthalmol 2008;11:20–26.
53. McKay JS, Forest TW, Senior M, et al. Postanaesthetic cerebral necrosis in five horses. Vet Rec 2002;150:70–74.
54. Spadavecchia C, Jaggy A, Fatzer R, Schatzmann U. Postanaesthetic cerebral necrosis in a horse. Equine Vet J 2001;33:621–624.
55. Panarello G, Dewey C, Barone G, Stefanacci J. Magnetic resonance imaging of two suspected cases of global brain ischemia. J Vet Emerg Crit Care 2004;14:269–277.
56. Chandler K. Canine epilepsy: what can we learn from human seizure disorders? Vet J 2006;172:207–217.
57. Lacombe VA, Mayes M, Mosseri S, Reed SM, Fenner WR, Ou HT. Epilepsy in horses: aetiological classification and predictive factors. Equine Vet J 2012;44:646–651.
58. Pivetta M, De Risio L, Newton R, Dennis R. Prevalence of lateral ventricle asymmetry in brain MRI studies of neurologically normal dogs and dogs with idiopathic epilepsy. Vet Radiol Ultrasound 2013;54:516–521.
59. Maslinska D, Laure-Kamionowska M, Deregowski K, Maslinski S. Association of mast cells with calcification in the human pineal gland. Folia Neropathol 2010;48:276–282.
60. Mahlberg R, Kienast T, Hädel S, Heidenreich JO, Schmitz S, Kunz D. Degree of pineal calcification (DOC) is associated with polysomnographic sleep measures in primary insomnia patients. Sleep Med 2009;10:439–445.
61. Capucchio MT, Márquez M, Pregel P, et al. Parenchymal and vascular lesions in ageing equine brains: histological and immunohistochemical studies. J Comp Pathol 2010;142:61–73.

62. Martínez J, Montgomery DL, Uzal FA. Vascular mineralization in the brain of horses. J Vet Diagn Invest 2012;24:612–617.

63. Helenius J, Soinne L, Salonen O, Kaste M, Tatlisumak T. Leukoaraiosis, ischemic stroke, and normal white matter on diffusion-weighted MRI. Stroke 2002;33:45–50.

64. Altaf N, Morgan P, Moody A, MacSweeney S, Gladman J, Auer D. Brain white matter hyperintensities are associated with carotid intraplaque hemorrhage. Radiology 2008;248:202–209.

65. Garrett KS, Woodie JB, Embertson RM, Pease AP. Diagnosis of laryngeal dysplasia in five horses using magnetic resonance imaging and ultrasonography. Equine Vet J 2009;41:766–771.

66. Koenig J, Silveira A, Chalmers HJ, Buenviaje G, Lillie BN. Laryngeal neuroendocrine tumour in a horse. Equine Vet Educ 2012;24:12–16.

67. Jakesova V, Konar M, Gerber V, Brachelente C, Howard J, Tessier C. Magnetic resonance imaging features of an extranodal T cell rich B cell lymphoma in the pharyngeal mucosa in a horse. Equine Vet Educ 2008;20:289–293.

68. Schneider A, Tessier C, Gorgas D, Kircher PR, Mamani J, Miclard J. Magnetic resonance imaging features of a benign peripheral nerve sheath tumour with "ancient" changes in the tongue of a horse. Equine Vet Educ 2010;22:346–351.

69. Bischofberger AS, Konar M, Posthaus H, Pekarkova M, Grzybowski M, Brehm W. Ocular angiosarcoma in a pony—MRI and histopathological appearance. Equine Vet Educ 2008;20:340–347.

70. Santos MP, Gutierrez-Nibeyro SD, Stewart AA, Hyde RM, Rodgerson DH. Identification of a periorbital wooden foreign body as the cause of chronic ocular discharge in a horse. Aust Vet J 2012;90:84–87.

71. Dixon PM. Swellings of the head region in the horse. In Pract 1991;13:257–263.

72. Rathmanner M, Rijkenhuizen ABM. Ultrasonography of the upper cervical region (EUCR) in the horse. Pferdeheilkunde 2012;28:575–582.

73. Dobromylskyj M, Dennis R, Ladlow J, Adams VJ. The use of magnetic resonance imaging in the management of pharyngeal penetration injuries in dogs. J Small Anim Pract 2008;49:74–79.

74. Dennis R. Use of magnetic resonance imaging for the investigation of orbital disease in small animals. J Small Anim Pract 2000;41:145–155.

75. Liebich H-G, König HE. Axial skeleton. In: König HE, Liebich H-G (eds): Veterinary anatomy of domestic mammals, 3rd ed. Stuttgart: Manson Publishing, 2010;49–112.

## 3.2. Paper 2

Equine Veterinary Education

**Title:**
The role of head computed tomography in equine practice.

**Authors:**

- Gabriel Manso-Díaz.
  Facultad de Veterinaria.
  Universidad Complutense de Madrid. Spain.
- José M. García-López.
  Cummings School of Veterinary Medicine.
  Tufts University. USA.
- Louise Maranda.
  Medical School.
  University of Massachusetts. USA.
- Olivier Taeymans.
  Cummings School of Veterinary Medicine.
  Tufts University. USA.

**Journal:**
Equine Veterinary Education
2015 – 27 (3):136-14

| Journal Title | ISSN | Total Cites | Impact Factor | 5-Year Impact Factor |
|---|---|---|---|---|
| EQUINE VET EDUC | 0957-7734 | 739 | 0.773 | 0.775 |

Equine Veterinary Education

136

EQUINE VETERINARY EDUCATION
*Equine vet. Educ.* (2015) **27** (3) 136-145
doi: 10.1111/eve.12275

*Original Article*

# The role of head computed tomography in equine practice

***G. Manso-Díaz*, J. M. García-López†, L. Maranda‡ and O. Taeymans†***

*Department of Animal Medicine and Surgery, School of Veterinary Medicine, Universidad Complutense de Madrid, Madrid, Spain; †Department of Clinical Sciences, Cummings School of Veterinary Medicine, Tufts University, Massachusetts, USA; and ‡Department of Quantitative Health Sciences, University of Massachusetts Medical School, Massachusetts, USA.*
**Corresponding author email: gmanso@ucm.es*

**Keywords:** horse; skull; CT; dental; sinus

## Summary

**This retrospective study describes the computed tomography (CT) findings in 59 horses presented with diseases of the head over 8 years that underwent CT examination of this region, including dental or sinonasal diseases (*Group A*) (n = 42), osseous and/or articular diseases (*Group B*) (n = 11) and soft tissue diseases (*Group C*) (n = 6). For *Group A*, radiographic and CT findings comparison was possible. Computed tomography had higher sensitivity (100%) and specificity (96.7%) than radiography in diagnosing dental disease. Compared to CT, radiographic identification of sinus involvement was less sensitive, particularly for ventral conchal and sphenopalatine sinuses and presented an overall sensitivity of 43.5 and 16.7%, respectively. In *Group B* CT allowed identification of a higher number of bone fragments and fractures in the maxillary, lacrimal, sphenoidal, temporal and zygomatic bones not identified radiographically. Accurate identification of CT changes in the temporomandibular joint and temporohyoid articulation was also possible. *Group C* included both intra- and extra-cranial disease, retrobulbar masses being the most representative pathology (n = 3). In this group, CT was considered the gold standard for detection of periorbital diseases. We conclude that CT is an imaging technique with high diagnostic value for evaluating the equine head, yielding additional information over multiple radiographic views, which may alter the outcome of the case. Additionally, this paper reports several conditions not previously described using CT.**

## Introduction

The equine head is a complex anatomic area (Smallwood *et al*. 2002). Diseases involving the head are frequently encountered in horses and require imaging studies for further work-up (Tucker and Farrell 2001). Historically, radiography has been the primary imaging technique for assessing the skull, nasal cavity, dental structures and paranasal sinuses (Wyn-Jones 1985a,b; Tremaine and Dixon 2001a). However, the anatomic complexity and superimposition of the osseous, dental and soft tissue structures complicate radiographic interpretation (Tucker and Farrell 2001). Cross-sectional imaging modalities, such as computed tomography (CT) and magnetic resonance imaging (MRI), are therefore particularly useful for this area (Kraft and Gavin 2001; Solano and Brawer 2004). Several studies report the use of CT for a wide array of diseases, both intra- and extra-cranially (Tietje *et al*. 1996; Henninger *et al*. 2003; Hilton *et al*. 2009; Sogaro-Robinson *et al*. 2009; Lacombe *et al*. 2010; Pownder *et al*. 2010; Huggons *et al*. 2011; Cissell *et al*. 2012; Textor *et al*. 2012). However, most studies were restricted to certain pathologies and/or had a limited number of cases.

The purpose of the present study was to describe the CT features of the most common equine head disorders of a large number of cases and compare them with radiographs when available.

## Materials and methods

### *Case selection*

A retrospective search of the medical records database from 2004 to 2012 at a referral centre was performed. Inclusion criteria were a final diagnosis of head disease and a CT scan of the head for the same reason.

Three groups were established. Horses included in the first group (*Group A*) presented for dental or sinonasal disease. The second group (*Group B*) included horses that were presented for osseous or articular disease and horses in the third group (*Group C*) for soft tissue, orbital or cerebral pathologies.

### *Radiographic examination*

All horses from *Group A* and most from *Group B* had a radiographic examination consisting of a lateral, dorsoventral and one or both oblique projections (dorsolateral-ventrolateral or ventrolateral-dorsolateral depending on the location of the disease). Radiographs were acquired either with 14 x 17" computed radiography cassettes (Kodak CR 850 System)[1], or using a 14 x 17" direct radiography flat panel (Eklin Mark 5 System)[2].

### *Computed tomography examination*

For CT studies, horses were examined under general anaesthesia in dorsal recumbency on a custom-built CT table. A single slice CT scanner (PQ5000)[3] was used for 31 cases and a 16 slice CT scanner (Toshiba Aquilion 16)[4] used for the remainder of the horses.

The scanning protocol for the first scanner consisted of nonhelical contiguous 5–8 mm transverse slices using a bone algorithm, with a second acquisition of additional thinner slices (3 mm) through the abnormal region. The scanning protocol for the second scanner consisted of helical 0.5 mm slice acquisition. Images were reconstructed as contiguous 5 mm slice thickness in 3 orthogonal planes (transverse, dorsal and sagittal), using both soft tissue and bone reconstruction algorithms, displayed using standard bone and soft tissue window levels and widths. Thinner slices (1 mm) were also reconstructed through the abnormal region using the initial

**TABLE 1: Number of horses with dental disease and number of affected teeth identified clinically and by each imaging modality**

| | No. horses with dental disease | No. horses with number of teeth involved | | | Affected teeth | | |
|---|---|---|---|---|---|---|---|
| | | 1 | 2 | 3 | Premolars | Molars | Total |
| Clinical | 32 | 24 | 8 | 0 | 18 | 22 | 40 |
| Radiography | 29 | 14 | 14 | 1 | 24 | 21 | 45 |
| Computed tomography | 32 | 19 | 13 | 0 | 21 | 24 | 45 |

acquisition data. The same scan area was repeated after i.v. injection of iohexol (Omnipaque)[5] (1 ml/kg bwt) in 7 cases. Fistulography was performed in 2 additional cases from *Group A* and a dacryocystography in another case from *Group B*.

Parameters used for CT scans were 120 kV, 200 mA and 1 s tube rotation time, or 120 kV, 250 mA and 0.75 s for the first and second scanner, respectively.

### *Image analysis*

Image review was performed using DICOM viewing software[6]. Two observers, one board certified radiologist and one PhD student, simultaneously reviewed the images including radiographs when available, in a randomised order. Interpretation was reached by consensus. Examiners were blinded to the clinical presentation, surgical findings and final diagnosis.

### *Data evaluation*

Interpretation based on combined radiographic (in *Groups A* and *B*) and CT findings were compared with clinical, surgical and pathological findings, where available.

Specific evaluation criteria were used in each group. The following characteristics were evaluated separately on radiographs and CT in *Group A*: presence or absence of dental disease including periapical tooth root infection (consisting of disruption of the lamina dura denta, widening of the periodontal space, root resorption and sclerosis of the surrounding alveolar bone) and tooth fractures, side and number of teeth affected. Presence of bony abnormalities, cementomas and draining tracts were also noted. All paranasal sinuses were separately classified as normal, containing fluid lines, or having an overall increase in opacity. When a mass was observed, its shape, size, density and border definition were described. The characteristics described only for CT were presence of gas within the pulp cavity and presence of gas within the infundibulum. The presence or absence of cortical destruction, sclerosis and periosteal proliferation was recorded as dorsal/ventral, palatal/lingual, or buccal in location. Respiratory mucosa was measured at the thickest point in each paranasal sinus and arbitrarily defined as normal when measuring less than 5 mm in thickness (Henninger *et al*. 2003).

In *Group B*, osseous abnormalities including periosteal reaction, lytic changes, presence or absence of fractures and draining tracts were recorded. Articular abnormalities were recorded separately. Tympanic bulla content, shape and wall thickness changes were also noted.

Evaluation criteria in *Group C* included origin of a mass, presence or absence of mass effect, mass size, shape, density, attenuation value and border definition. Local tissue invasion, lymphadenopathy and presence of osseous changes were also recorded. Recorded cerebral abnormalities were defined as intra- or extra-axial. Lesion type, number (defined as focal or multifocal) and location were recorded according to brain region. The presence of contrast enhancement, brain herniation (transtentorial or foramen magnum) and mass effect (deviation of the falx cerebri from midline or compression of the lateral ventricle) were also recorded.

### *Statistical analysis*

Contingency tables were constructed to classify horses from *Group A* according to their radiography and CT results. For dental disease, estimates of sensitivity (Se), specificity (Sp) and positive and negative predictive values (PPV and NPV) were calculated for each technique using clinical and surgical findings as a gold standard. For sinus involvement, these same estimates were calculated for radiographic findings, using CT results as the gold standard. Confidence intervals were associated to each of the estimates, using 95% as a confidence level. Where calculated values were within the 90–100% range, the exact method was used (Blyth 1986).

## Results

A total of 59 horses met the inclusion criteria; 42 in *Group A*, 11 in *Group B* and 6 in *Group C*. Represented breeds were 14 Warmbloods, 14 Thoroughbreds, 12 Quarter Horses, 5 Peruvian Paso, 2 Ponies, 3 Clydesdales, 2 Arabians, 2 Morgan and one each of the following breeds: Andalusian, Appaloosa, Friesian, Haflinger and Lusitan. There were 2 stallions, 31 geldings and 26 mares. The mean age was 11.4 years (range 22 days–25 years).

### *Dental and sinonasal disease* (Group A)

This group of 42 horses consisted of 32 dental disease, 6 sinus cysts, one osteoma, 2 progressive ethmoid haematomas and one choanal stenosis. Diagnosis was confirmed surgically in all the horses, except in one horse that was treated conservatively and the osteoma and choanal stenosis that was confirmed *post mortem*. All horses had a preoperative CT (including all previously mentioned image reconstructions) and radiographs. Three horses also had a repeat CT for recurrent problems. Fistulogram through the draining tract in the facial region was performed in 2 horses.

Number of horses with periapical tooth root infection and number of affected teeth identified by each imaging modality, compared with clinical findings are included in **Table 1**.

Based on clinical examination and surgical findings, 40 teeth were found to be clinically affected and 33 were treated surgically.

In 25 of the 32 horses (78%) radiographs identified at least one of the clinically affected teeth, while in 7 of the 32 horses (22%) none of the clinically affected teeth were identified. Sensitivity, specificity, positive and negative predictive values for diagnosing dental disease using radiography and CT are

**TABLE 2: Sensitivity, specificity and positive and negative predictive values for diagnosing clinically confirmed dental disease in 32 horses of *Group A*, using radiography and computed tomography**

| | Sensitivity (%) | Specificity (%) | PPV (%) | NPV (%) |
|---|---|---|---|---|
| Radiography | 72.5 (66.2–78.8) | 89.5 (85.1–93.8) | 64.4 (57.7–71.2) | 92.5 (88.8–96.2) |
| Computed tomography | 100 (98.5–100) | 96.7 (94.2–99.2) | 88.9 (84.4–93.3) | 100.00 (98.5–100) |

PPV = positive predictive values, NPV = negative predictive values.

summarised in **Table 2**. Computed tomography showed the highest sensitivity and specificity for correctly identifying dental disease.

Computed tomography identified all clinically affected teeth. However, in 5 of the 32 horses (16%), CT showed more abnormal teeth than clinically suspected. Computed tomography and radiographs agreed in the identification of the same teeth in only 16 of the 32 horses (50%). Computed tomography showed tooth fractures in 11 cases, while only 4 of these cases were identified radiographically.

Computed tomography allowed identification of a greater number of dental abnormalities in all horses. In 24 of the 42 horses (57%), the infundibulum showed hypoattenuation in at least one tooth. This hypoattenuation was, however, observed in affected teeth in only 8 cases (18%).

There were 6 sinus cysts, 2 of which appeared multilobulated, while the rest had a rounded shape. Two of the 6 cases (33%) were diagnosed radiographically as a well delineated soft tissue mass. The remaining 4 were missed on radiographs as a result of a diffuse increased soft tissue opacity filling the caudal maxillary and conchofrontal sinuses. On CT they appeared as a well defined structure in 5 cases, while in one case the cyst was silhouetting with fluid present within the sinuses (**Fig 1**). In 2 cases, a faint mineralised capsule was present which was not seen on radiographs. A concurrent mass effect consisted of nasal septum deviation in 3 cases, decrease of the cortical thickness of the maxillary bone in 2 cases and exophthalmos in one horse. Increase of the periodontal space and mild disruption of the *lamina dura* of the tooth ventral to the cyst were observed in 2 cases. Common location of the cyst was the caudal maxillary sinus, with invasion to the conchofrontal and ventral conchal sinuses observed in 2 cases. Invasion to the conchofrontal, ventral conchal and sphenopalatine sinuses was seen in another case. The average CT attenuation of the cyst content was 22 HU. Secondary sinusitis/fluid accumulation of variable amounts was present in all horses (**Fig 1**). This fluid was homogeneous and had an average CT attenuation value of 10 HU.

Agreement between CT and radiographs of sinus involvement was seen when respiratory mucosa was thicker than 10 mm in combination with fluid levels, or when total obstruction of the sinus occurred. Compared to CT, radiographic abnormalities were observed in 19 of 28 horses (68%) and 18 of 24 horses (75%) for the rostral and caudal maxillary sinuses, respectively. Involvement of the conchofrontal sinus was identified radiographically in 15 of 23 horses (65%), while evidence of ventral conchal and sphenopalatine involvement was seen in only 10 of 23 horses (43%) and 3 of 18 horses (17%), respectively (**Fig 2**). Sensitivity, specificity, positive and negative predictive values for identifying sinus involvement confirmed by CT using radiography are summarised in **Table 3**.

Radiographic changes were infrequently seen when respiratory mucosa thickening without fluid accumulation was the only finding on CT. Seven of 28 horses (25%) and 6 of 24 horses (25%) had mucosa thickening without radiographic abnormalities in the rostral maxillary sinus and caudal maxillary sinus, respectively.

Neither of the 2 horses with a progressive ethmoid haematoma had radiographic or endoscopic changes. Computed tomography findings consisted of a heterogeneous and well defined multiloculated structure located at the ethmoid turbinates and both sphenopalatine sinuses, with an average CT attenuation value of 110 HU (**Fig 3**). In both cases, the sphenopalatine sinus septum was deviated and no free fluid was observed in the sinuses. Mild distortion of the ethmoid turbinates was seen in one case.

A single osteoma was seen as a well-defined mineral-dense mass superimposed over the caudal maxillary sinus on the radiographs. Computed tomography findings consisted of a well-delineated, heterogeneous and hyperattenuating mass in the caudal maxillary sinus, compressing the dorsal conchal sinus and displacing the infraorbital nerve canal medially. No dental changes were seen associated with this mass.

Computed tomography features of the choanal stenosis consisted of bilateral and symmetrical narrowing of the choana in a 22-day-old foal; the remaining aperture for airflow was 1.2 $cm^2$. Radiographs failed to show a narrowing of the caudal nasal cavity.

### *Osseous and articular disease (Group B)*

Eleven horses were included in this group: 3 fractures, 2 osteomyelitis, 4 temporohyoid osteoarthropathy, one *otitis media* and one nasofrontal suture exostosis. Eight horses had a radiographic examination. One horse had also a CT dacryocystogram. The dacryocystogram was evaluated for patency of the lumen only.

Fracture cases included one maxillary, one mandibular and one case of multiple craniofacial fractures. There was agreement between radiographs and CT on the location of the mandibular fractures, although in one horse CT allowed identification of further extension of a bilateral comminuted fracture of the vertical rami of the mandibles. Radiographically, it was possible to identify fractures in the frontal and hyoid bones. Only CT allowed identification of fractures in the maxillary, lacrimal, sphenoidal, temporal and zygomatic bones. Identification of a greater number of bone fragments was also possible with CT in all the horses. In the case of multiple craniofacial fractures, CT allowed visualisation of fluid within the tympanic bulla.

Osteomyelitis was observed in 2 cases using CT and radiographs, one in the mandible and the second in the temporal, mandibular, parietal, sphenoidal, frontal and zygomatic bones. In one horse, we identified more extensive

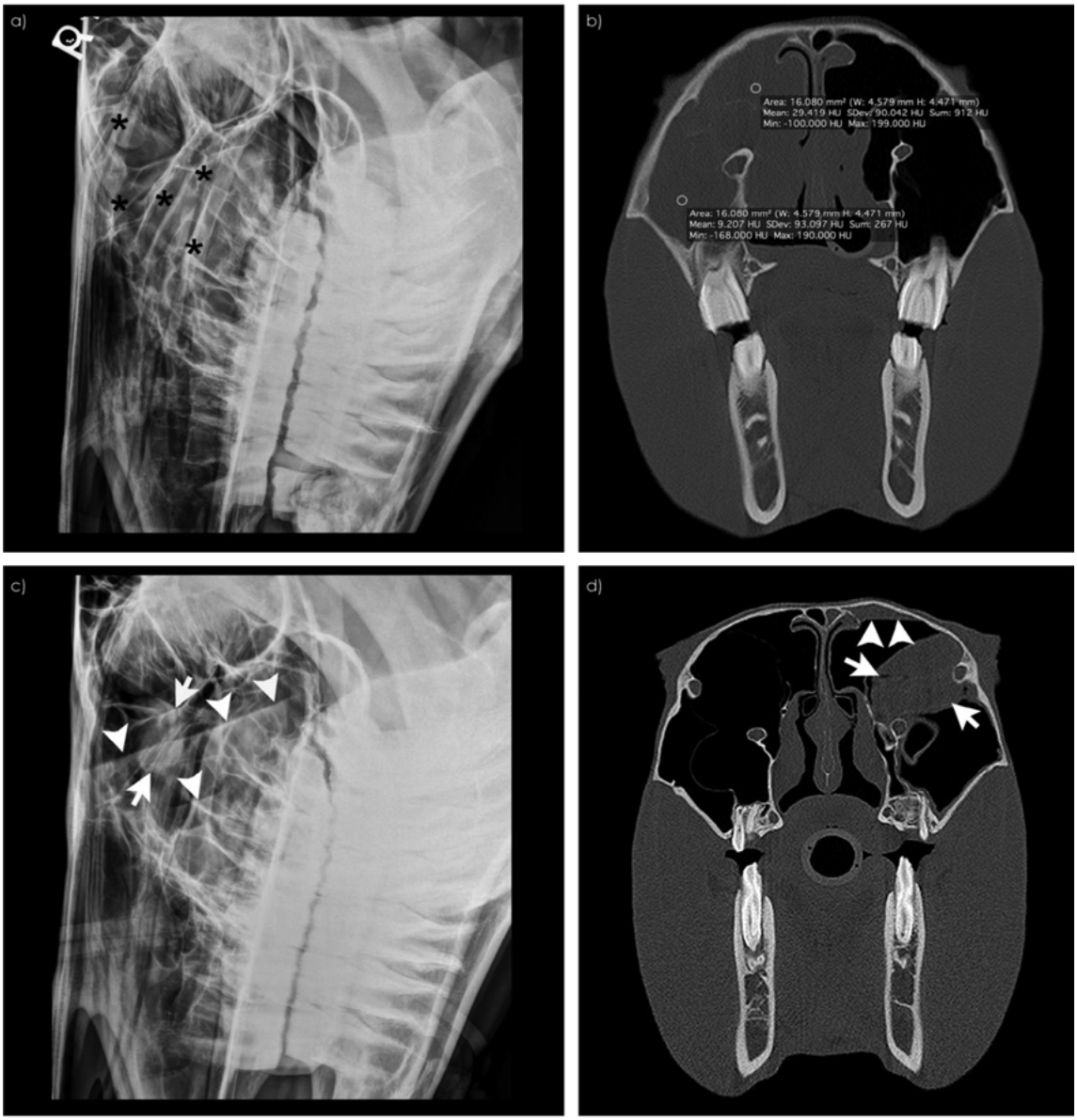


***Fig 1: Lateral radiographs (a and c) (rostral to the left) and transverse CT images (b and d) (right is to the left) of the paranasal sinuses from a Quarter Horse (a and b) and Warmblood (c and d). The first horse has a cyst within the right caudal maxillary and conchofrontal sinuses surrounded by a large amount of fluid. Radiography shows a diffuse increased soft tissue opacity (asterisks), while CT differentiates between the cyst and surrounding fluid based on HU measurements. The second horse shows a small cyst (arrows) within the left ventral conchal sinus, surrounded by a small amount of fluid (arrowheads) within the caudal maxillary and conchofrontal sinuses.***

bone involvement using CT and also found temporomandibular and calvarium infiltration not identified on radiographs. In this case, fluid accumulation within the tympanic bulla and tissue thickening of the external ear canal were also observed. Final diagnosis of this case was botryomycosis.

Since radiographs were only available in one of the 4 horses presented for temporohyoid osteoarthropathy, comparison between CT and radiographic findings was not possible. Computed tomography abnormalities included periosteal reaction along the ceratohyoid (n = 2), stylohyoid (n = 4) and petrous temporal (n = 4) bones, fracture of the

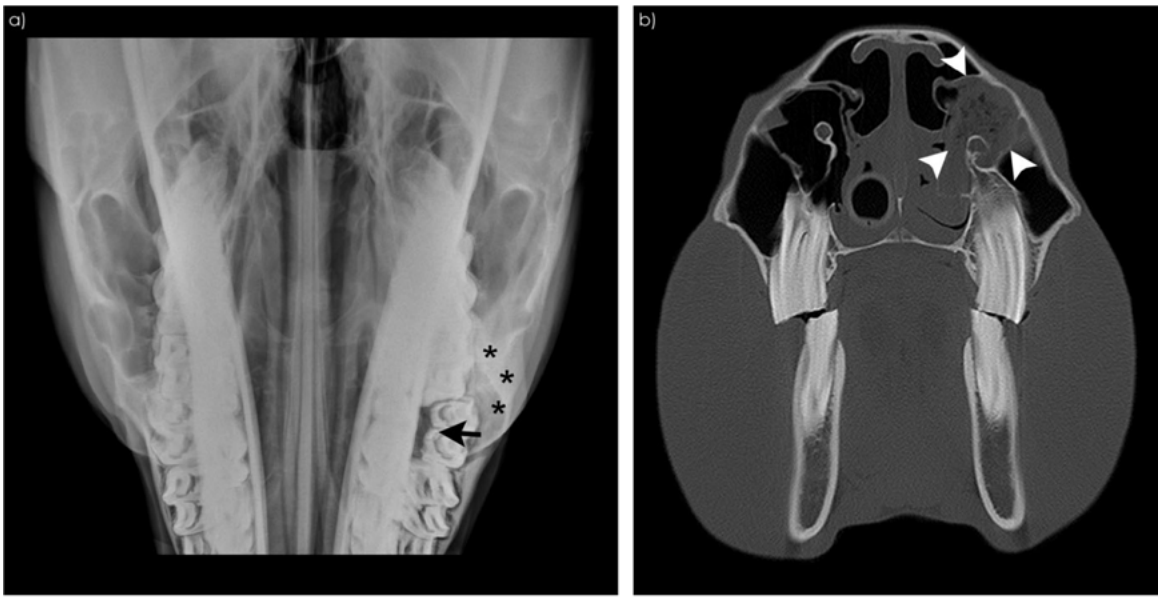


***Fig 2: Dorsoventral radiograph of the nasal cavity and paranasal sinuses (a) and transverse CT image at the level of M2 (the 10's) in a Quarter Horse (right is to the left). Radiography shows that the left PM4 (tooth 208 in the Triadan system) is fractured (arrow) and there is an increase of opacity within the left rostral maxillary sinus (asterisks). Computed tomography showed an abscess with granular appearance within the left conchal (arrowheads) and left rostral maxillary sinuses secondary to a fractured PM4 (208) (not shown).***

**TABLE 3: Radiographic sensitivity, specificity, positive and negative predictive values for identifying sinus involvement confirmed by CT in horses of *Group A***

| | Sensitivity (%) | Specificity (%) | PPV (%) | NPV (%) |
|---|---|---|---|---|
| Rostral maxillary | 67.9 (57.9–77.8) | 92.9 (87.4–98.4) | 82.6 (74.5–90.7) | 85.3 (77.7–92.8) |
| Caudal maxillary | 75 (65.7–84.3) | 95 (90.3–99.7) | 85.7 (78.2–93.2) | 90.5 (84.2–96.8) |
| Conchofrontal | 65.2 (55.0–75.4) | 96.7 (92.9–100) | 88.2 (81.4–95.1) | 88.1 (81.1–94.9) |
| Sphenopalatine | 16.7 (8.7–24.6) | 100 (96.5–100) | 100 (96.5–100) | 81.5 (73.2–89.8) |
| Ventral conchal | 43.5 (32.9–54.1) | 100 (96.5–100) | 90.9 (84.8–97.1) | 82.2 (74.0–90.4) |

PPV = positive predictive values, NPV = negative predictive values.

stylohyoid (n = 1) and petrous temporal (n = 1) bones, fluid accumulation within the tympanic bulla (n = 2) and luxation of the temporohyoid articulation (n = 2) (**Fig 4**). In all cases the condition was unilateral. Incidentally, a hyperattenuating, rounded and well-defined soft tissue mass lateral to the temporomandibular joint (TMJ) was found in one horse. Histological diagnosis was melanoma.

There was one case of *otitis media* and externa. Computed tomography findings included the presence of fluid accumulation within the tympanic bulla and tissue thickening of the external ear canal.

Computed tomography allowed identification of abnormalities in the TMJ in 2 cases. Computed tomography findings in the first one included permeative lysis of the mandibular articular surface with periarticular new bone formation and associated soft tissue swelling. Histological diagnosis was osteomyelitis and infectious arthritis. The second horse was the botryomycosis case previously described, showing marked osteolysis of both articular surfaces. Radiographic findings in the first case consisted of mild periarticular new bone formation, while the botryomycosis case presented a large bony mass at the level of the zygomatic arch.

Computed tomography findings for the nasofrontal suture exostosis included endosteal and periosteal elevation adjacent to widened and irregular sutures between the frontal, maxillary, nasal and lacrimal bones. Computed tomography dacryocystography showed a focal narrowing of the nasolacrimal duct due to the new bone formation in the area of the affected sutures, resulting in partial obstruction of both nasolacrimal ducts.

### *Soft tissue disease* (Group C)

Six horses were included in this group; 3 retrobulbar masses, one acute subdural haematoma, one nuchal ligament bursitis and one parotid mucocele. Radiographs were not performed in any of the horses included in this group.

Retrobulbar masses appeared as a well-defined, rounded and homogeneous structure in the retrobulbar space with an average CT attenuation value of 47 HU. Mass effect and

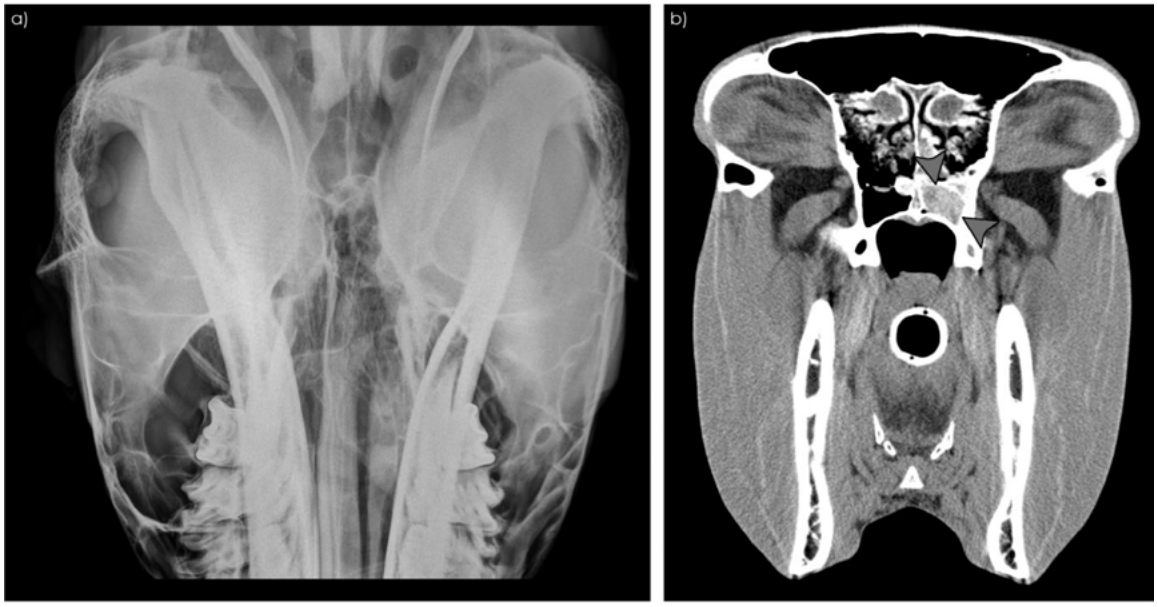


*Fig 3: Dorsoventral radiograph of the caudal nasal cavity and paranasal sinuses (a) and transverse CT image at the level of the ethmoid turbinates in a horse with epistaxis (right is to the left). Computed tomography shows a small ethmoid haematoma and small fluid accumulation within the left sphenopalatine sinus (arrowheads). No radiographic changes are observed.*

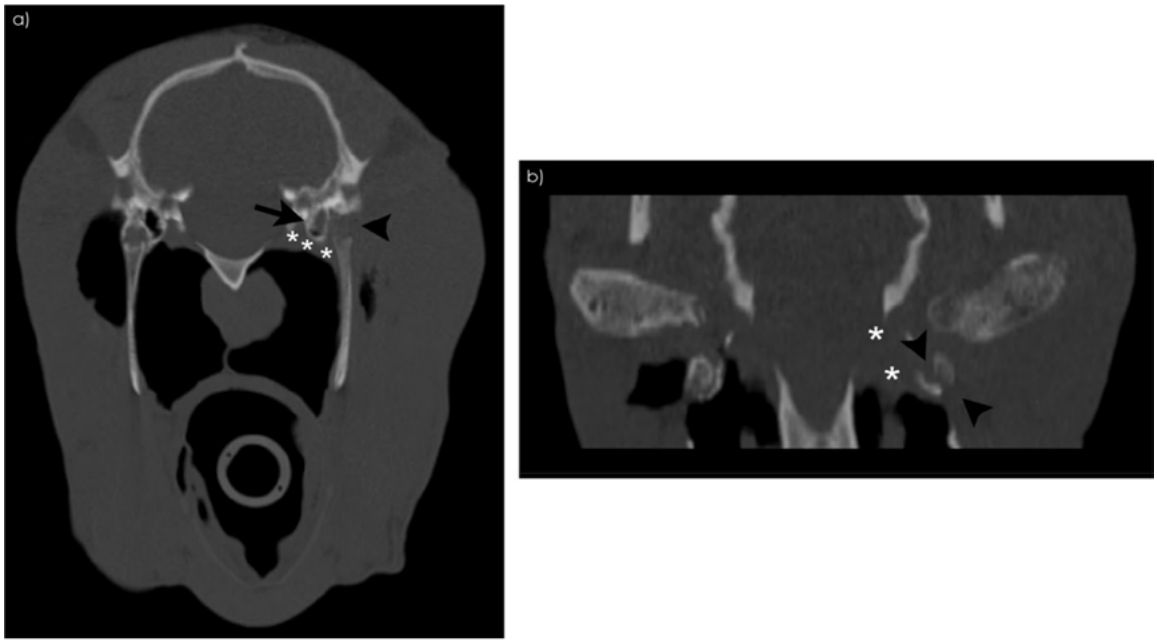


*Fig 4: Transverse CT image (a) and dorsal reconstruction (b) at the level of the temporohyoid articulation (right is to the left). Left temporohyoid articulation is subluxated with lateral displacement of the stylohyoid bone (arrowheads). Soft tissue swelling is observed surrounding the temporohyoid articulation (asterisks),and the left tympanic bulla is fluid-filled (arrow).*


***Fig 5: Transverse CT images of the brain of a foal pre- (a) and post contrast injection (b) (right is to the left). A noncontrast enhancing curvilinear hyperattenuating band is observed between the brain and osseous structures on the right side (asterisks), corresponding to a subdural haematoma. There is swelling of the subcutaneous soft tissues on the left side of the head (arrowheads).***

exophthalmos was observed in all cases. One case had a ring-shaped contrast enhancement confirmed to be an abscess. Squamous cell carcinoma was the final diagnosis in the other 2 cases. One had intracranial invasion with lysis of the presphenoid and temporal bones.

Computed tomography findings for acute subdural haematoma consisted of a curvilinear hyperattenuating area between the brain and osseous structures, with an average CT attenuation value of 75 HU and no contrast enhancement (**Fig 5**). There was also swelling of the subcutaneous soft tissues on the left side of the head.

Abnormalities for the case of nuchal bursitis included dystrophic mineralisation dorsal to the atlas and atlanto-occipital junction and marked distension of the cranial nuchal bursa. It appeared as a large fluid pocket (9 HU) extending from the foramen magnum up to the cranial portion of the second cervical vertebra. A focal mineralisation was also detected within the nuchal ligament dorsal to the distended bursa.

The parotid mucocele consisted of a rounded and well-defined fluid pocket lateral to the parotid gland, with an average density of 14 HU. The remaining parotid gland volume appeared reduced.

## Discussion

Computed tomography is commonly used to obtain images of the head in horses with a wide array of conditions. The aim of the present study was to describe the CT features of the most common equine head disorders and compare them with other imaging modalities when available.

The most prevalent condition was dental disease. Radiographic (Wyn-Jones 1985a; Gibbs and Lane 1987; Townsend *et al*. 2011) and CT (Henninger *et al*. 2003; Veraa *et al*. 2009) features of this condition have previously been described. Radiography is currently still the most commonly employed diagnostic imaging modality for investigating dental disorders (Townsend *et al*. 2011). However, this technique is not a very reliable method for the diagnosis of dental disease in the horse, especially in cases of periapical infection. Previous studies estimated the sensitivity for the diagnosis of periapical infection between 50 (Gibbs and Lane 1987) and 57% (Tremaine and Dixon 2001a). The slightly higher sensitivity using radiography observed in this study could be explained by the use of digital radiography or may merely reflect a difference of population. A comparative study between radiography and scintigraphy showed the latter had a high sensitivity but low specificity (Weller *et al*. 2001). However, no studies comparing radiography and CT are available. Using both modalities, we agreed in identification of affected teeth in 16 of 32 cases (50%) and disagreed on the identification of all clinically relevant teeth in 7 cases (22%). With CT we were able to identify all clinically affected teeth, but in 5 horses the use of CT resulted in identifying abnormalities in more teeth than clinically detectable. The importance of this finding remains questionable and further investigation on the long-term clinical outcome of these teeth is necessary. One of these horses was rescanned for nasal discharge one year later and showed severe changes in one tooth previously described as abnormal by CT. However, mild changes in teeth, such as nondetectable *lamina dura*, have been observed using CT in horses without dental clinical signs (Bühler *et al*. 2014). Availability of standing CT units would make it more feasible to follow-up these subtle findings, avoiding general anaesthesia, which is one of the main limitations of this modality. This would increase the understanding of whether these findings progress over time.

More dental abnormalities, such as disruption of the lamina dura and tooth fractures, were found with CT (**Fig 6**); CT being, for example, superior at detection of pulp and infundibular abnormalities. Detailed examination of the internal structure of the tooth is important in deciding on its treatment. The use of thin slices (1 mm) and multiplanar reconstructions assisted with the identification of mild changes. Infundibular abnormalities, such as hypoattenuation in the infundibulum, must be studied carefully in each case. This can represent air or necrotic cementum. A recent study reported the relationship between infundibular caries and the frequency of CT changes within the infundibulum, but a direct relationship between the 2 processes has not been established (Veraa *et al*. 2009). In another study, infundibular changes occurred as a single CT feature not associated significantly with CT signs of apical

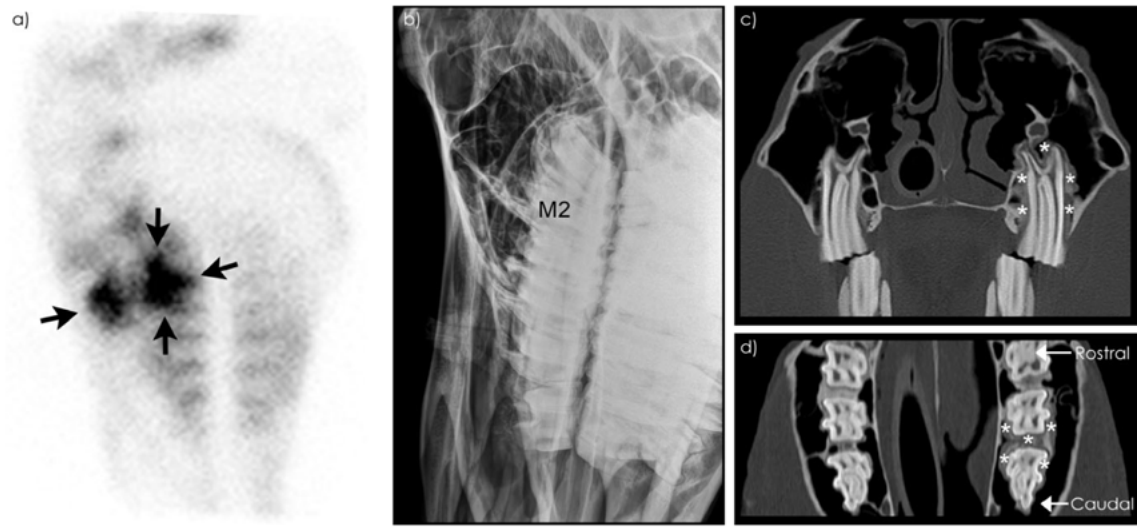


***Fig 6: Left lateral static nuclear medicine image acquired during bone phase (a) (rostral to the left), right dorsal to left ventral oblique radiograph (b) (rostral to the left), transverse (c) (right to the left) and dorsal reconstruction (d) (right to the left) CT images centred at M2 (10's in the Triadan system) from a Warmblood that presented with marked radiopharmaceutical uptake associated with the left maxillary molar region (arrows). Radiographs are normal but CT images show that the bone, lamina dura and mucosa surrounding the roots of left M2 and M3 (210 and 211) roots are thickened and irregular (asterisks).***

infection (Bühler *et al*. 2014). In our study, 24 horses showed infundibular hypoattenuation in at least one tooth, but only in 8 were these changes identified in the clinically affected tooth. Although its clinical significance is unclear, the possibility of dental caries cannot be ruled out. Complementary examinations such as oral endoscopy may yield helpful information for the differentiation between pathological and nonpathological teeth in these cases (Ramzan 2009).

Sinonasal cysts are expansile, mucus-filled cavities within the paranasal sinuses that possess a wall with a mucus-secreting epithelial lining (Tremaine *et al*. 1999). This condition has previously been reported and represents approximately 13% of all paranasal sinus diseases in a study of 277 cases (Tremaine and Dixon 2001a). In the present study, 14% of horses in *Group A* were diagnosed with a sinus cyst. Computed tomography features of this condition consisted of a well-defined, rounded or multiloculated structured that occasionally presented wall mineralisation. Nonmineralised cysts may be difficult to detect when surrounded by large amounts of fluid on CT and impossible to recognise radiographically. In such cases it can be helpful to compare CT attenuation values of the sinus and cyst content. A rim-like contrast enhancement has been observed in post contrast MRI images in horses with sinus cysts (Tessier *et al*. 2013); therefore, a similar change could be expected with CT. In instances of large cysts, mass effect, bone deformation, exophthalmos and nasal septum deviation can be present (Tremaine and Dixon 2001a; Annear *et al*. 2008). Due to the space-occupying nature of the cysts, dental distortion can also be observed (Tucker and Farrell 2001). The typical location of this condition is the caudal maxillary sinus, but other locations include the frontal sinus and ethmoid labyrinth (Tremaine and Dixon 2001a).

Although endoscopy was described as the ancillary diagnostic technique of choice for progressive ethmoid haematomas (Tremaine and Dixon 2001a), CT provided important information, such as the exact location or the extent, when radiographic and endoscopic findings were not conclusive. Other indications for performing CT in progressive ethmoid haematoma cases include sinus involvement or multifocal disease (Textor *et al*. 2012). The sphenopalatine sinus was affected bilaterally in both cases included in this study. Both presented deviation of the sinus septum secondary to a mass effect. In both cases, high CT attenuation values were recorded (100–110 HU) in accordance with a previous study (Textor *et al*. 2012).

Paranasal sinus disease is usually the consequence of obstruction of the drainage ostia as a consequence of inflammatory processes initiated by primary bacterial infections, bacterial or fungal infection secondary to other disease processes such as dental disease and space-occupying expansile lesions and trauma (Tremaine and Dixon 2001b). Changes within individual sinus compartments can be identified with high detail using CT, especially in cases of ventral conchal and sphenopalatine sinus involvement where radiography was shown to be less accurate. Tomographic nature of CT images allows evaluation of each sinus separately, avoiding superimposition of surrounding structures. Moreover, thanks to the higher contrast resolution, it is possible to discriminate between tissues, making it possible to assess the respiratory mucosa. Thickening of the respiratory epithelium without concurrent changes would not be detected on radiographic images.

All CT examinations were obtained in dorsal recumbency. By consequence, when the frontomaxillary aperture is open, fluid from the caudal maxillary sinus can enter the conchofrontal sinus. Presence of fluid in the conchofrontal sinus without concurrent mucosal thickening may therefore not represent primary pathology of that sinus when the head is in this position.

Neoplasia of the nasal cavity and paranasal sinuses is an uncommon condition which represented 8% of the cases from a study of 277 horses with sinonasal disorders (Tremaine and Dixon 2001a). Our study only included one case of an osteoma. Computed tomography appearance of a paranasal osteoma has not been previously described in horses.

The high value of CT as a preoperative planning tool was demonstrated in all cases that underwent surgery. This was particularly evident in cases of sinonasal diseases, including dental disorders, sinus masses and fistulas. New generation multislice scanners obtain thinner slices, but mainly allow multiplanar isovolumetric reconstructions of the acquired volumetric data, increasing diagnostic confidence and determining the exact location of lesions. Impact of any lesions on adjacent structures such as the infraorbital canal and involvement of obscure compartments such as the ventral conchal sinus were also evident. The use of gantry lasers makes it possible to preoperatively localise the lesion with high precision. Dental and sinus anatomy vary with age, breed and as a normal anatomical variation between individuals (Dixon and du Toit 2010). For this reason, empirical estimates of landmarks are often incorrect (Gerard 2012). All the information provided by CT assisted the optimisation of the surgical approach and presumably allowed decreased surgical morbidity.

Skull fractures are difficult to assess radiographically because of the complex morphology of the bones and superimposition of numerous structures (Bar-Am *et al*. 2008). In a comparative study between radiography and CT in dogs and cats with maxillofacial trauma, it was demonstrated that CT was superior to radiography for identification of anatomic structures and traumatic injuries (Bar-Am *et al*. 2008). In our study, CT allowed us to identify a greater number of bone fragments and showed fractures at the maxillary, lacrimal, sphenoidal, temporal and zygomatic bones not visible radiographically. Although there was high agreement between both imaging techniques for visualising mandibular body fractures, CT may be necessary to assess the full extent of the fracture.

Computed tomography provided a comprehensive evaluation of the temporal bone, hyoid apparatus and temporohyoid articulation. Observed CT changes were similar to previous reports (Hilton *et al*. 2009; Pownder *et al*. 2010). Luxation of the temporohyoid articulation was observed in 2 of our cases. This condition was associated with focal soft tissue swelling in both cases and fluid within the tympanic bulla in one of the cases. This finding has not been previously reported in horses and a traumatic origin was suspected.

Several studies have described the diagnostic utility of CT for assessing intracranial structures (Arencibia *et al*. 2000; Cunilleras 2007; Sogaro-Robinson *et al*. 2009; Lacombe *et al*. 2010; Pease *et al*. 2011). However, apart from case reports, utility of CT for evaluation of ophthalmological conditions has not widely been described in horses (Tietje *et al*. 1996; Ramirez and Tucker 2004; van den Top *et al*. 2007; Elce *et al*. 2011). In our cases, CT identified retrobulbar masses, such as abscesses and tumours, intracranial invasion of a tumour and obstruction of the nasolacrimal duct.

In conclusion, the equine head is a clinically important area with complex anatomy susceptible to a large number of different conditions. A consistent description of all cases that underwent CT scan of the head in a period of 8 years was performed and some conditions were described for the first time using this modality, including osteoma, choanal stenosis, stylohyoid subluxation, temporal botryomycosis, subdural haematoma, parotid mucocele and nuchal ligament bursitis. Precise diagnosis was reached using CT in all horses, particularly in cases of dental and sinonasal disorders, and CT should therefore be preferred over radiography in these conditions. Moreover, dental changes of questionable clinical significance were detected with CT. Long-term follow-up of these lesions could be the subject of further studies.

## Authors' declaration of interests

No conflicts of interest have been declared.

## Acknowledgements

The authors would like to thank Linda Kinney for CT image acquisitions and reconstructions as well as for her assistance with data collection. Gabriel Manso-Díaz was supported by MECD FPU fellowship (Re. AP2010-0498).

## Manufacturers' addresses

[1]Carestream Health, Rochester, New York, USA.
[2]Eklin Medical Systems Inc, Santa Clara, California, USA.
[3]Picker International, Highland Heights, Ohio, USA.
[4]Toshiba American Medical Systems Inc., Tustin, California, USA.
[5]Nycomed Inc., Princeton, New Jersey, USA.
[6]Osirix Image processing Software, Geneva, Switzerland.

## References

Annear, M.J., Gemensky-Metzler, A.J., Elce, Y.A. and Stone, S.G. (2008) Exophthalmus secondary to a sinonasal cyst in a horse. *J. Am. Vet. Med. Ass.* **233**, 285-288.

Arencibia, A., Vázquez, J.M., Rivero, M., Latorre, R., Sandoval, J.A., Vilar, J.M. and Ramírez, J.A. (2000) Computed tomography of normal cranioencephalic structures in two horses. *Anat. Histol. Embryol.* **29**, 295-299.

Bar-Am, Y., Pollard, R.E., Kass, P.H. and Verstraete, F.J.M. (2008) The diagnostic yield of conventional radiographs and computed tomography in dogs and cats with maxillofacial trauma. *Vet. Surg.* **37**, 294-299.

Blyth, C.R. (1986) Approximate binomial confidence limits. *J. Am. Stat. Ass.* **81**, 843-855.

Bühler, M., Fürst, A., Lewis, F.I., Kummer, M. and Ohlerth, S. (2014) Computed tomographic features of apical infection of equine maxillary cheek teeth: A retrospective study of 49 horses. *Equine Vet. J.* **46**, 468-473.

Cissell, D.D., Wisner, E.R., Textor, J.A., Mohr, F.C., Scrivanni, P.V. and Théon, A.P. (2012) Computed tomographic appearance of equine sinonasal neoplasia. *Vet. Radiol. Ultrasound* **53**, 245-251.

Cunilleras, E.J. (2007) Advanced diagnostic imaging options in horses with neurological disease that localizes to the head. *Equine Vet. Educ.* **19**, 179-181.

Dixon, P.M. and du Toit, N. (2010) Dental anatomy. In: *Equine Dentistry*, 3th edn., Eds: J. Easley, P.M. Dixon and J. Schumacher, Saunders Ltd, Edinburgh. pp 51-76.

Elce, Y.A., Wilkie, D.A., Santschi, E.M. and Green, E.M. (2011) Metastasis or delayed local extension of ocular squamous cell carcinoma in four horses. *Equine Vet. J.* **23**, 496-499.

Gerard, M. (2012) Sinus anatomy and imaging: tools for decision-making. *ACVS Veterinary Symposium – American College of Veterinary Surgeons*, Maryland, USA. pp. 110-113.

Gibbs, C. and Lane, J.G. (1987) Radiographic examination of the facial, nasal and paranasal sinus regions of the horse. II. Radiological findings. *Equine Vet. J.* **19**, 474-482.

Henninger, W., Frame, E.M., Willmann, M., Simhofer, H., Malleczek, D., Kneissl, S.M. and Mayrhofer, E. (2003) CT features of alveolitis and sinusitis in horses. *Vet. Radiol. Ultrasound* **44**, 269-276.

Hilton, H., Puchalski, S.M. and Aleman, M. (2009) The computed tomographic appearance of equine temporohyoid osteoarthropathy. *Vet. Radiol. Ultrasound* **50**, 151-156.

Huggons, N.A., Bell, R.J.W. and Puchalski, S.M. (2011) Radiography and computed tomography in the diagnosis of nonneoplastic equine mandibular disease. *Vet. Radiol. Ultrasound* **52**, 53-60.

Kraft, S.L. and Gavin, P.R. (2001) Physical principles and technical considerations for equine computed tomography and magnetic resonance imaging. *Vet. Clin. N. Am.: Equine Pract.* **17**, 115-130.

Lacombe, V.A., Sogaro-Robinson, C. and Reed, S.M. (2010) Diagnostic utility of computed tomography imaging in equine intracranial conditions. *Equine Vet. J.* **42**, 393-399.

Pease, A.P., Schott, H.C., II, Howey, E.B. and Patterson, J.S. (2011) Computed tomographic findings in the pituitary gland and brain of horses with pituitary pars intermedia dysfunction. *J. Vet. Intern. Med.* **25**, 1144-1151.

Powndер, S., Scrivani, P.V., Bezuidenhout, A., Divers, T.J. and Ducharme, N.G. (2010) Computed tomography of temporal bone fractures and temporal region anatomy in horses. *J. Vet. Intern. Med.* **24**, 398-406.

Ramirez, S. and Tucker, R.L. (2004) Ophthalmic imaging. *Vet. Clin. N. Am.: Equine Pract.* **20**, 441-457.

Ramzan, P.H.L. (2009) Oral endoscopy as an aid to diagnosis of equine cheek tooth infections in the absence of gross oral pathological changes: 17 cases. *Equine Vet. J.* **41**, 101-106.

Smallwood, J.E., Wood, B.C., Taylor, W.E. and Tate, L.P. (2002) Anatomic reference for computed tomography of the head of the foal. *Vet. Radiol. Ultrasound* **43**, 99-117.

Sogaro-Robinson, C., Lacombe, V., Reed, S.M. and Balkrishnan, R. (2009) Factors predictive of abnormal results for computed tomography of the head in horses affected by neurologic disorders: 57 cases (2001–2007). *J. Am. Vet. Med. Ass.* **235**, 176-183.

Solano, M. and Brawer, R.S. (2004) CT of the equine head: technical considerations, anatomical guide, and selected diseases. *Clin. Tech. Equine Pract.* **3**, 374-388.

Tessier, C., Brühschwein, A., Lang, J., Konar, M., Wilke, M., Brehm, W. and Kircher, P.R. (2013) Magnetic resonance imaging features of sinonasal disorders in horses. *Vet. Radiol. Ultrasound* **54**, 54-60.

Textor, J.A., Puchalski, S.M., Affolter, V.K., Macdonald, M.H., Galuppo, L.D. and Wisner, E.R. (2012) Results of computed tomography in horses with ethmoid hematoma: 16 cases (1993–2005). *J. Am. Vet. Med. Ass.* **240**, 1338-1344.

Tietje, S., Becker, M. and Böckenhoff, G. (1996) Computed tomographic evaluation of head diseases in the horse: 15 cases. *Equine Vet. J.* **28**, 98-105.

Townsend, N.B., Hawkes, C.S., Rex, R., Boden, L.A. and Barakzai, S.Z. (2011) Investigation of the sensitivity and specificity of radiological signs for diagnosis of periapical infection of equine cheek teeth. *Equine Vet. J.* **43**, 170-178.

Tremaine, W.H., Clarke, C.J. and Dixon, P.M. (1999) Histopathological findings in equine sinonasal disorders. *Equine Vet. J.* **31**, 296-303.

Tremaine, W.H. and Dixon, P.M. (2001a) A long-term study of 277 cases of equine sinonasal disease. Part 1: details of horses, historical, clinical and ancillary diagnostic findings. *Equine Vet. J.* **33**, 274-282.

Tremaine, W.H. and Dixon, P.M. (2001b) A long-term study of 277 cases of equine sinonasal disease. Part 2: treatments and results of treatments. *Equine Vet. J.* **33**, 283-289.

Tucker, R.L. and Farrell, E. (2001) Computed tomography and magnetic resonance imaging of the equine head. *Vet. Clin. N. Am.: Equine Pract.* **17**, 131-144.

van den Top, J.G.B., Schaafsma, I.A., Boswinkel, M. and Klein, W.R. (2007) A retrobulbar abscess as an uncommon cause of exophthalmos in a horse. *Equine Vet. Educ.* **19**, 579-583.

Veraa, S., Voorhout, G. and Klein, W.R. (2009) Computed tomography of the upper cheek teeth in horses with infundibular changes and apical infection. *Equine Vet. J.* **41**, 872-876.

Weller, R., Livesey, L., Maierl, J., Nuss, K., Bowen, I.M., Cauvin, E., Weaver, M., Schumacher, J. and May, S.A. (2001) Comparison of radiography and scintigraphy in the diagnosis of dental disorders in the horse. *Equine Vet. J.* **33**, 49-58.

Wyn-Jones, G. (1985a) Interpreting radiographs 6: radiology of the equine head (Part 2). *Equine Vet. J.* **17**, 417-425.

Wyn-Jones, G. (1985b) Interpreting radiographs 6: the head. *Equine Vet. J.* **17**, 274-278.

## 3.3. Paper 3

Equine Veterinary Journal

**Title:**

Time-of-flight magnetic resonance angiography (TOF-MRA) of the normal equine head.

**Authors:**

- Gabriel Manso-Díaz.
  Facultad de Veterinaria.
  Universidad Complutense de Madrid. Spain.
- María Isabel García-Real.
  Facultad de Veterinaria.
  Universidad Complutense de Madrid. Spain.
- Christophe Casteleyn.
  Faculty of Veterinary Medicine.
  University of Ghent. Belgium.
- Fidel San Román.
  Facultad de Veterinaria.
  Universidad Complutense de Madrid. Spain.
- Olivier Taeymans.
  Cummings School of Veterinary Medicine.
  Tufts University. USA.

**Journal:**

Equine Veterinary Journal
2013 – 45(2):187-192

| Journal Title | ISSN | Total Cites | Impact Factor | 5-Year Impact Factor |
|---|---|---|---|---|
| EQUINE VET J | 0425-1644 | 6124 | 2.369 | 2.267 |

Equine Veterinary Journal

Equine Veterinary Journal ISSN 0425-1644
DOI: 10.1111/j.2042-3306.2012.00621.x



# Time-of-flight magnetic resonance angiography (TOF-MRA) of the normal equine head

G. MANSO-DÍAZ*, M. I. GARCÍA-REAL, C. CASTELEYN†, F. SAN-ROMÁN and O. TAEYMANS‡

Department of Animal Medicine and Surgery, School of Veterinary Medicine, Universidad Complutense de Madrid, Spain
†Department of Morphology, Faculty of Veterinary Medicine, Ghent University, Belgium
‡Department of Clinical Sciences, Cummings School of Veterinary Medicine, Tufts University, Massachusetts, USA.

*Correspondence email: gmanso@vet.ucm.es; Received: 22.02.12; Accepted: 20.06.12

## Summary

**Reasons for performing study:** Noncontrast magnetic resonance angiography (MRA) is widely used in human and small animal medicine. However, this technique has not yet been described in the horse, and compared to other angiographic techniques MRA could be more cost efficient and potentially safer.
**Objectives:** The aim of this study was to provide a comprehensive anatomical reference of the normal equine head vasculature using a noncontrast MRA technique, on both low- and high-field MRI.
**Methods:** Five healthy adult horses were examined, 4 with a low-field magnet (0.23T) and the remaining one with a high-field magnet (1.5T). The magnetic resonance angiography sequence used was TOF (time-of-flight) 2D-MRA and CT images of a vascular corrosion cast were subsequently used as anatomical references.
**Results:** The MRA imaging protocol provided good visualisation of all major intra- and extracranial vessels down to a size of approximately 2 mm in diameter on both low- and high-field systems. This resulted in identification of vessels to the order of 3rd–4th branches of ramification. The visibility of the arteries was higher than of the veins, which showed lower signal intensity. Overall, MRA obtained with the high-field protocol provided better visualisation of the arteries, showing all the small arterial branches with a superior resolution.
**Conclusions:** The use of a specific vascular sequence such as TOF 2D-MRA allows good visualisation of the equine head vasculature and eliminates the need for contrast media for MRA.
**Potential relevance:** Magnetic resonance angiography allows for visualisation of the vasculature of the equine head. Vessel morphology, symmetry and size can be evaluated and this may possibly play a role in preoperative planning or characterisation of diseases of the head, such as neoplasia or guttural pouch mycosis.

**Keywords:** horse; head; anatomy; magnetic resonance angiography; magnetic resonance imaging; aneurysm

## Introduction

Imaging of the equine cranial vascular system has been previously described using conventional x-ray angiography [1,2]. However, this method requires surgical arterial exposure with potential risks for the horse [1]. Conventional angiography is gradually being replaced by other advanced imaging modalities, such as computed tomography angiography (CTA) and magnetic resonance angiography (MRA) [3,4]. Magnetic resonance imaging is a well established diagnostic technique in human medicine and is increasingly reported in veterinary medicine [5–15]. In general, MRA can be performed according to 3 different techniques: time-of-flight (TOF-MRA), phase contrast (PC-MRA) and contrast enhanced (CE-MRA) [4,16,17]. The latter requires i.v. injection of gadolinium which increases the signal intensity of flowing blood [3,4,16,17]. On the one hand, TOF-MRA uses signal intensity changes related to differences in saturation between flowing and stationary tissues, whereas PC-MRA relies on phase changes occurring in moving protons which are present in the blood, both making the use of contrast agents for MR angiography obsolete [3,4,16,17]. Both techniques, CTA and CE-MRA, require the use of contrast media for the visualisation of the blood vessels, making them more expensive [17]. Adverse effects associated with the administration of i.v. diatrizoate and intra-arterial ionic iodinated contrast medium have been previously described in horses undergoing a CT examination [18,19]. Anaphylactic reactions to gadolinium-based contrast agent have been described in man and dogs but are unknown in horses [20]. Recommended doses of different contrast media have not yet been described in horses, since they are usually extrapolated from canine or human, which make their use in horses unpredictable. Therefore, noncontrast MRA could be more cost efficient and potentially safer.

The purpose of this study was to provide a comprehensive anatomical reference of the normal equine head vasculature using TOF-MRA in both low- and high-field systems.

## Materials and methods

### MRA examination

Five healthy adult horses (2 Thoroughbreds, 1 Andalusian and 2 mixed breed) were examined. Bodyweights ranged from 450 to 590 kg (mean 498 kg) and ages from 5 to 22 years (mean 15 years). A pilot study was performed in a single horse using TOF 2D-MRA, TOF 3D-MRA and PC-MRA sequences with a 0.23T open magnet (Panorama)[a]. Subjective evaluation of the latter noncontrast sequences showed that TOF 2D-MRA was the technique that provided the best resolution and surrounding tissue attenuation, and was less flow direction-dependent than PC-MRA.

TOF 2D-MRA was performed using a 0.23T open magnet (Panorama)[a] in 4 horses and a 1.5T magnet (Magnetom Symphony Maestro Class)[b] in one horse. Approval was obtained by the ethical committee from Tufts University and Universidad Complutense de Madrid for using high- and low-field MRI on live horses. Following clinical evaluation (physical examination, haematological and biochemical analysis), all horses underwent general anaesthesia and were placed in right lateral and dorsal recumbency for the low- and high-field examinations, respectively. Low-field imaging protocol included a sagittal turbo spin-echo T1-weighted sequence used to depict anatomical landmarks, followed by contiguous transverse TOF 2D-MRA sequences, being repeated 5 times until the entire head was covered. The high-field imaging protocol included a sagittal spin-echo T1-weighted sequence, used to depict anatomical landmarks, followed by 3 contiguous transverse TOF 2D-MRA sequences. Parameters used for each angiographic sequence are included in Table 1.

### Vascular corrosion cast

Computed tomography images of a vascular corrosion cast were subsequently used as anatomical references (Fig S1). Three ponies were first administered 10 ml heparin (Heparin Leo)[c] (5000 I.E./ml) and

**TABLE 1: Parameters used for each angiographic sequence**

| Parameters | TOF 2D-MRA (0.23T) | TOF 2D-MRA (1.5T) |
|---|---|---|
| Generic sequence name | GRE | GRE |
| Repetition time (ms) | 33 | 26 |
| Echo time (ms) | 11 | 7.26 |
| Flip angle | 70 | 70 |
| Slice thickness (mm) | 3 | 2.5 |
| No. slices | 50 | 128 |
| Field of view (mm) | 266 × 333 | 327 × 350 |
| Matrix | 360 × 202 | 256 × 205 |
| Number of acquisitions (NEX) | 2 | 1 |
| Venous saturation band | No | Yes |

subsequently subjected to euthanasia with 30 ml T61[d] via the jugular vein. After decapitation, the cranial blood vessels were flushed with 3 l saline solution via both common carotid arteries. Subsequently, approximately 600 ml Batson's No.17 solution[e], diluted with pure methyl methacrylate[f] and supplemented with bismuth oxide powder[g] to enhance radio-opacity, was injected. After polymerisation of the casting medium, the soft tissues were macerated in warm water (55°C) supplemented with Biotex[h] washing powder. After bleaching the remaining skulls and cast blood vessels with 10% $H_2O_2$[i] were subsequently rinsed with water.

To gain more insight into the 3-dimensional organisation and topography of the blood vessels, the most successful cast was scanned with a 16 slice CT (Mx8000)[a]. Tube current was set at 120 kVp and slices were acquired with a slice thickness of 1.3 mm and interval of 0.6 mm.

## Image analysis

Data were processed using maximum-intensity projection (MIP) and a soft tissue algorithm. MRI and CT images were analysed using a DICOM image viewer[l], with sagittal T1w MR images being used to indicate the level from which each MIP reconstruction was obtained. Arterial and venous vessels were identified and labelled in the post processed MRI images using the slice-by-slice technique, compared with images illustrated in anatomical textbooks and CT images of the vascular corrosion cast (Fig S1). Anatomical terms used in this article are in accordance with *Nomina Anatomica Veterinaria* [21].

## Results

The MRA imaging protocol provided good visualisation of all major intra- and extracranial vessels down to a size of approximately 2 mm in diameter on both low- and high-field systems. Both arterial and venous systems were visualised with the low-field protocol, whereas the high-field protocol included venous saturation and therefore only allowed visualisation of the arterial system. In the low-field protocol, arteries showed higher signal intensity than the veins, as a result of higher blood flow velocity.

The average total examination time per horse, excluding patient positioning, was 40 and 60 min for high- and low-field protocols, respectively. Acquisition time for each transverse TOF sequence was approximately 8–10 min for both protocols.

The common carotid artery and its bifurcation into the external and internal carotid arteries were clearly outlined. The internal carotid artery could be followed up to its junction with the Circle of Willis. The following first order branches of the external carotid artery were identified in all horses (Fig 1): the mandibular gland branch, linguofacial trunk with the ascending palatine, lingual and facial arteries, masseteric branch, caudal auricular artery, superficial temporal artery and maxillary artery. The latter could be followed up to their main branches being second order branches of the external carotid artery (Fig 2): the inferior alveolar artery, pterygoid branches, rostral tympanic artery, deep rostral temporal artery, external ophthalmic artery (and its continuation into the external ethmoid artery), buccal artery, infraorbital artery and descending palatine artery. Proceeding from the facial artery the following second order branches of

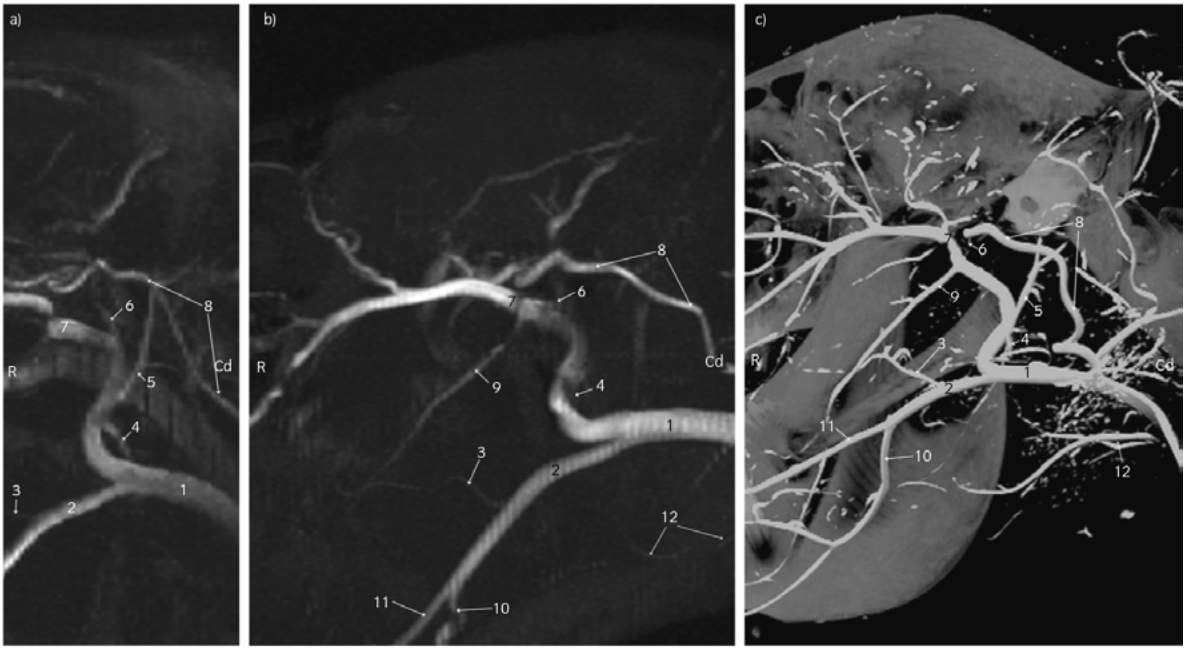


Fig 1: MIP sagittal reconstruction of the main branches of the external carotid artery with the low-field (a) and high-field (b) protocols, compared with the CT scanned cast (c). 1 - external carotid artery, 2 - linguofacial trunk, 3 - ascending palatine artery, 4 - masseteric branch, 5 - caudal auricular artery, 6 - superficial temporal artery, 7 - maxillary artery, 8 - internal carotid artery, 9 - inferior alveolar artery, 10 - facial artery, 11 - lingual artery, 12 - cranial laryngeal artery.

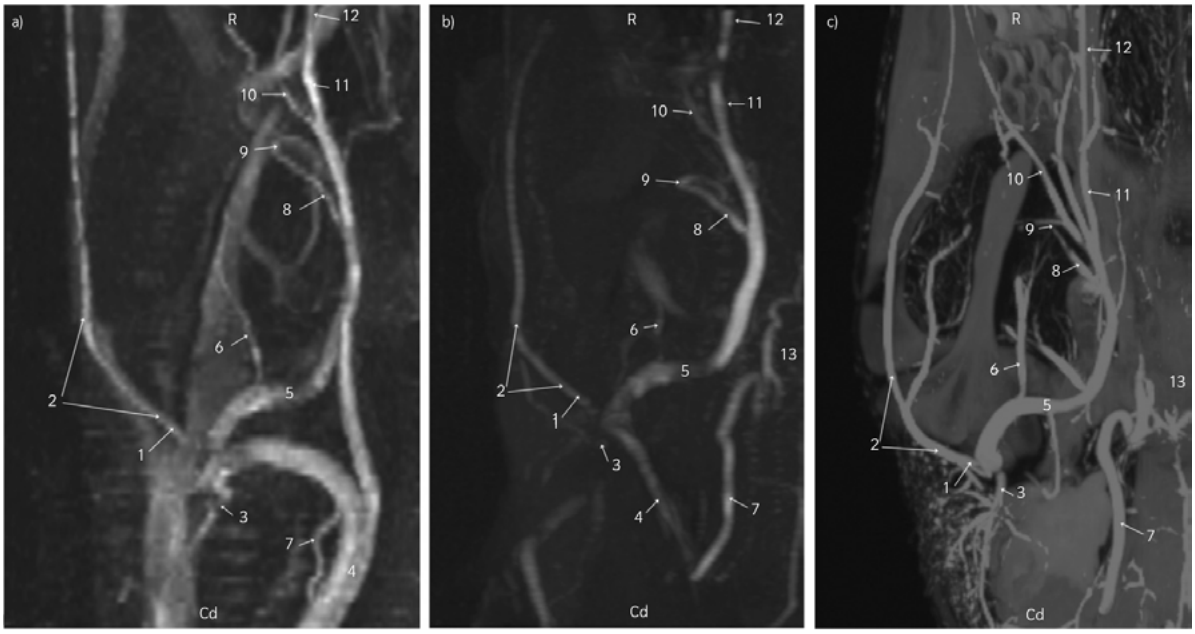


Fig 2: MIP dorsal reconstruction of the main branches of the maxillary artery with the low-field (a) and high-field (b) protocols, compared with the CT scanned cast (c). 1 - superficial temporal artery, 2 - transverse facial artery, 3 - masseteric branch, 4 - external carotid artery, 5 - maxillary artery, 6 - inferior alveolar artery, 7 - internal carotid artery, 8 - external ophthalmic artery, 9 - external ethmoid artery, 10 - infraorbital artery, 11 - descending palatine artery, 12 - greater palatine artery, 13 - Circle of Willis.

the external carotid artery could be seen (Fig 3): the sublingual artery, inferior and superior labial arteries, lateral and dorsal nasal arteries and angular artery of the eye. The following third order branches of the external carotid artery were identified: the transverse facial artery from the superficial temporal artery, malar artery and dental branches proceeding from the infraorbital artery, greater lesser palatine arteries from the descending palatine artery and anastomotic branch to the infraorbital artery branching off the lateral nasal artery. The only fourth

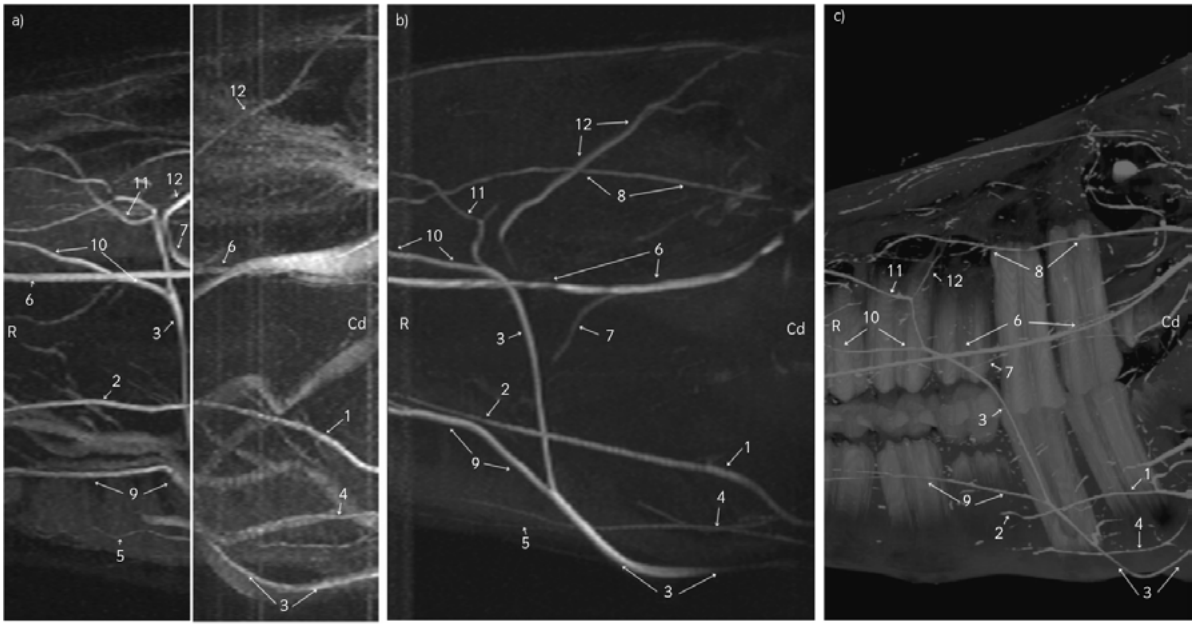


Fig 3: MIP sagittal reconstruction of the main branches of the linguofacial trunk with the low-field (a) and high-field (b) protocols, compared with the CT scanned cast (c). 1 - lingual artery, 2 - deep lingual artery, 3 - facial artery, 4 - sublingual artery, 5 - inferior alveolar artery, 6 - greater palatine artery, 7 - infraorbital artery, 8 - transverse facial artery, 9 - inferior labial artery, 10 - superior labial artery, 11 - lateral nasal artery, 12 - angular artery of the eye.

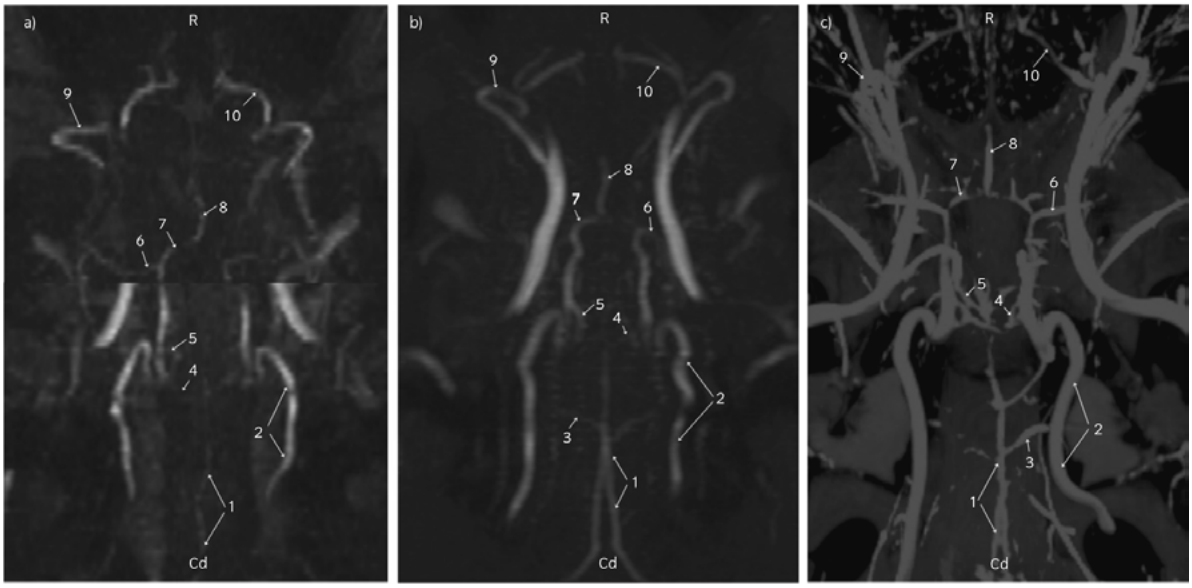


Fig 4: MIP dorsal reconstruction of the Circle of Willis with the low-field (a) and high-field (b) protocols, compared with the CT scanned cast (c). 1 - basilar artery, 2 - internal carotid artery, 3 - caudal cerebellar artery, 4 - posterior communicating artery, 5 - caudal cerebral artery, 6 - middle cerebral artery, 7 - rostral cerebral artery, 8 - corpus callosum artery, 9 - external ophthalmic artery, 10 - external ethmoid artery.

order branch identified was the incisive artery, branching off the greater palatine artery.

Proceeding from the basilar artery, the caudal cerebellar artery was identified. Rostral cerebellar, caudal cerebral, medial cerebral and rostral cerebral, internal ethmoid arteries were identified forming the Circle of Willis (Fig 4).

Overall, MRA obtained with the high-field protocol provided a better visualisation of the arteries, showing all the small arterial branches with a superior resolution. This protocol allowed visualisation of smaller arterial branches, identifying the following third order arterial branches from the external carotid artery: rostral auricular artery from the superficial temporal artery, mental artery from the inferior alveolar artery, supraorbital artery proceeding from the external ophthalmic artery and angular artery of the mouth branching off the inferior labial artery (Fig S2). The cranial laryngeal artery was also identified (Fig 1), which is a third order branch from the common carotid artery. Small arterial branches were seen at the nasal mucosa. At the level of the brain (Fig S3), this protocol allowed better visualisation of smaller arterial branches, such as the corpus callosum artery branching off the rostral cerebral artery.

With the low-field protocol, the linguofacial vein and its first order branches, i.e. lingual and facial veins, were clearly outlined (Fig S4). The second order branches branching off the facial vein were identified (Fig S5): the dorsal and lateral nasal veins, superior and inferior labial veins and deep facial vein. The lingual vein gives off the following second order branches (Fig S4): the sublingual vein and deep lingual vein. Linguofacial veins third order branches that come from the deep facial vein are the deep facial venous sinus, ventral external ophthalmic vein, infraorbital vein and deep palatine vein. Fourth order branches were the sphenopalatine vein and malar vein.

The first order branches from the maxillary vein identified were the following (Fig 5): the cranial thyroid vein, occipital vein, caudal auricular vein, ventral masseteric vein, superficial temporal vein, pterygoid plexus, inferior alveolar vein, sublingual branch and buccal vein. Second order branches identified were the transverse facial vein and buccal venous sinus.

The following venous sinuses were visible (Fig S6): the dorsal sagittal sinus, straight sinus, ventral sagittal sinus, major cerebral vein, confluence of sinuses, transverse sinus, dorsal petrosal sinus, basal cerebral vein, temporal sinus, cavernous sinus, intercavernous sinuses, ventral petrosal sinus and basilar sinus.

## Discussion

The advantage of MRA over conventional angiography is that it is less invasive, more rapid and does not use ionising radiation [3,22]. Compared with CTA, MRA allows multiplanar imaging, having the ability to acquire images in nonaxial imaging planes, providing better visualisation of vascular segments not optimally seen using other diagnostic techniques [4,16]. Noncontrast MRA has the additional advantage of precluding the need for large volumes of expensive and potentially toxic contrast agents [4,17,23]. In our study the TOF-MRA technique was chosen, after a prior pilot study, as it is the noncontrast MRA modality that provides the best imaging resolution and surrounding tissue subtraction and is less flow direction-dependent than PC-MRA. The use of TOF 2D-MRA has been previously reported in human medicine for evaluating the head, neck and lower extremities [4,24]. In veterinary medicine, this technique allows the visualisation of the intracranial vasculature in dogs [11].

The advantages of the high-field over the low-field protocol used in our study were the higher number of slices obtained per sequence and the shorter acquisition time for each TOF sequence. In addition, the visibility of the vessels was higher in the high-field, which resulted in a better identification of the smaller arterial branches.

The mammalian vascular system has a high number of normal anatomical variations and this was also seen in both arteries and veins of the horses used in this study [25]. In the present study, these variations were more commonly noted in the venous system, as evidenced by the pattern of distribution of the facial vein. Despite this variability in branching pattern, the thickness and morphology of the vessels were constant in all horses. The presence of vascular anatomical variations is clinically important in specific conditions such as guttural pouch mycosis [26–28]. These variations that often affect the internal carotid artery can result in surgical treatment failure [26–28]. Although conventional angiography can show the anomalous course of the arteries [1,29], MRA allows comparison of the contralateral vessel while avoiding the superimposition of surrounding tissues [3]. Post processing tools, such as

MIP reconstruction, allow multiplanar views of the area of interest to be created, providing better assessment of the vasculature [3]. Besides identification of anatomical variations, this technique is also more accurate than conventional angiography in assessing vessel anomalies, such as arteriovenous fistulas, aneurysms, thrombosis and cerebral vascular accidents, all being potential clinical indications in horses [3,5,7,8,11]. An illustration of an arterial aneurysm in a horse secondary to a guttural pouch mycosis is shown in Figure 6, demonstrating the direct clinical application of this angiographic technique. Orbital vascular malformations have been previously described in horses but conventional angiography failed to show contrast within the malformation [15,30]. Instead, MRA helped by multiplanar reconstructions, allows visualisation of the complex distribution of small arteries and veins in this location. Finally, MRA could also play an important role in preoperative planning of mass removals, as this technique allows visualisation of tumour feeding vessels.

## Authors' declaration of interests

No competing interests have been declared.

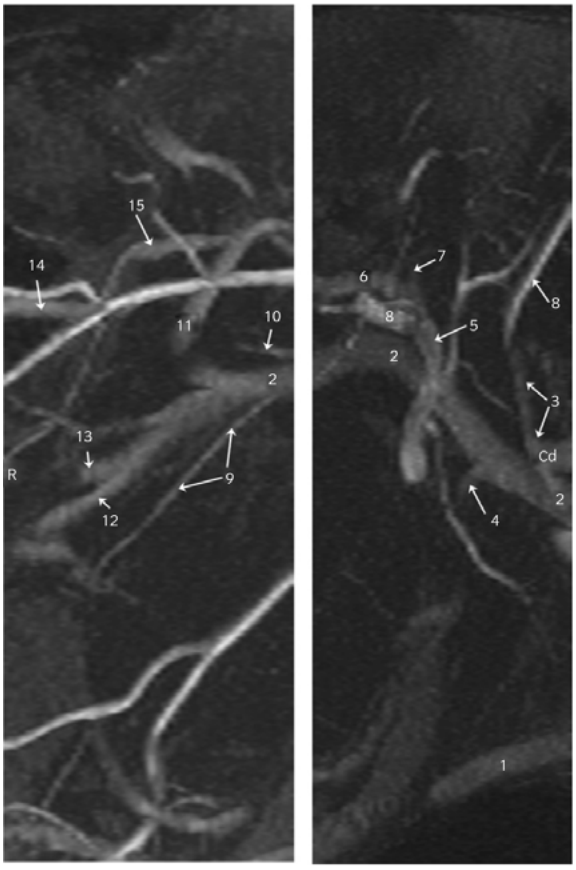


Fig 5: Low-field MIP sagittal reconstruction of the main branches of the maxillary vein. 1 - linguofacial vein, 2 - maxillary vein, 3 - caudal auricular vein, 4 - ventral masseteric vein, 5 - superficial temporal vein, 6 - transverse facial vein, 7 - rostral auricular vein, 8 - emissary vein of the retroarticular foramen, 9 - inferior alveolar vein, 10 - pterygoid vein, 11 - deep temporal vein, 12 - sublingual branch, 13 - buccal vein, 14 - ventral external ophthalmic vein, 15 - emissary vein of the orbital fissure.

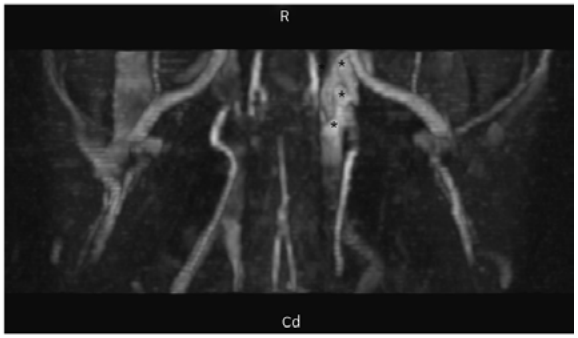


Fig 6: MIP dorsal reconstruction obtained with the low-field protocol at the level of the entrance of the internal carotid artery into the Circle of Willis of a horse with reported guttural pouch mycosis. An aneurysm (asterisks) can be visualised within the sigmoidal part of the left internal carotid artery.

## Source of funding

None.

## Acknowledgements

The authors would like to thank Dr José García-López for his assistance and support, Professor Dr Jimmy Saunders for performing the CT scan of the cast, Drs Isabel Santiago and Jaime Goyoaga for their assistance with MRI acquisitions and Dr Marjan Doom for her assistance during vascular cast preparation.

## Manufacturers' addresses

[a]Philips Medical Systems, AE Eindhoven, The Netherlands.
[b]Siemens, Erlangen, Germany.
[c]Leo Pharma, Amsterdam, The Netherlands.
[d]Intervet, Mechelen, Belgium.
[e]Polysciences, Warrington, Pennsylvania, USA.
[f]Merck, Darmstadt, Germany.
[g]Reade, Rhode Island, USA.
[h]Sara Lee Household & Bodycare Belgium, Grimbergen, Belgium.
[i]Univar Benelux, Brussels, Belgium.
[j]Osirix Image processing Software, Geneva, Switzerland.

## References

1. Colles, C.M. and Cook, W.R. (1983) Carotid and cerebral angiography in the horse. *Vet. Rec.* **113**, 483-489.
2. Cook, W.R. (1973) The auditory tube diverticulum (guttural pouch) in the horse: its radiographic examination. *J. Am. Vet. Radiol. Soc.* **14**, 51-71.
3. Foltin, I., Bruhschwein, A., Rieden, K. and Matis, U. (2008) Magnetic resonance angiography: a comparison of techniques and applications in dogs and humans. *Tierärztl. Prax.* **1**, 75-88.
4. Foo, T.K.F., Polzin, J.A. and Thomasson, D.M. (2005) MR angiography physics: an update. *Magn. Reson. Imaging Clin. N. Am.* **13**, 1-22.
5. Schwarz, T., Rossi, F., Wray, J.D., Ablad, B., Beal, M.W., Kinns, J., Seiler, G.S., Dennis, R., McConnell, J.F. and Costello, M. (2009) Computed tomographic and magnetic resonance imaging features of canine segmental caudal vena cava aplasia. *J. Small Anim. Pract.* **50**, 341-349.
6. Tidwell, A.S., Ross, L. and Kleine, L. (1997) Computed tomography and magnetic resonance imaging of cavernous sinus enlargement in a dog with unilateral exophthalmos. *Vet. Radiol. Ultrasound* **38**, 363-370.
7. Seguin, B., Tobias, K.M., Gavin, P.R. and Tucker, R.L. (1999) Use of magnetic resonance angiography for diagnosis of portosystemic shunts in dogs. *Vet. Radiol. Ultrasound* **40**, 251-258.
8. Drost, W.T., Bahr, R.J., Henry, G.A. and Campbell, G.A. (1999) Aortoiliac thrombus secondary to a mineralized arteriosclerotic lesion. *Vet. Radiol. Ultrasound* **40**, 262-266.

9. Rodriguez, D., Rylander, H., Vigen, K.K. and Adams, W.M. (2009) Influence of field strength on intracranial vessel conspicuity in canine magnetic resonance angiography. *Vet. Radiol. Ultrasound* **50**, 477-482.
10. Contreras, S., Arencibia, A., Gil, F., De Miguel, A., Ramírez, G. and Vázquez, J.M. (2010) Black and bright-blood sequences magnetic resonance angiography and gross sections of the canine thorax: an anatomical study. *Vet. J.* **185**, 231-234.
11. Martin-Vaquero, P., da Costa, R.C., Echandi, R.L., Tosti, C.L., Knopp, M.V. and Sammet, S. (2011) Time-of-flight magnetic resonance angiography of the canine brain at 3.0 Tesla and 7.0 Tesla. *Am. J. Vet. Res.* **72**, 350-356.
12. Mai, W. and Weisse, C. (2011) Contrast-enhanced portal magnetic resonance angiography in dogs with suspected congenital portal vascular anomalies. *Vet. Radiol. Ultrasound* **52**, 284-288.
13. Mai, W., Weisse, C. and Sleeper, M.M. (2010) Cardiac magnetic resonance imaging in normal dogs and two dogs with heart base tumor. *Vet. Radiol. Ultrasound* **51**, 428-435.
14. Bruehschwein, A., Foltin, I., Flatz, K., Zoellner, M. and Matis, U. (2010) Contrast-enhanced magnetic resonance angiography for diagnosis of portosystemic shunts in 10 dogs. *Vet. Radiol. Ultrasound* **51**, 116-121.
15. Sager, M., Assheuer, J., Trümmler, H. and Moormann, K. (2009) Contrast-enhanced magnetic resonance angiography (CE-MRA) of intra- and extra-cranial vessels in dogs. *Vet. J.* **179**, 92-100.
16. Ivancevic, M.K., Geerts, L., Weadock, W.J. and Chenevert, T.L. (2009) Technical principles of MR angiography methods. *Magn. Reson. Imaging Clin. N. Am.* **17**, 1-11.
17. Lohan, D., Saleh, R., Nael, K., Krishnam, M. and Finn, J.P. (2007) Contrast-enhanced MRA versus nonenhanced MRA: pros and cons. *Appl. Radiol.* **12**, 3-15.
18. Pollard, R.E. and Puchalski, S.M. (2011) Reaction to intraarterial ionic iodinated contrast medium administration in anesthetized horses. *Vet. Radiol. Ultrasound* **52**, 441-443.
19. Gunkel, C.I., Valverde, A., Robertson, S.A., Thompson, M.S., Keoughan, C.G. and Ferrell, E.A. (2004) Treatment for a severe reaction to intravenous administration of diatrizoate in an anesthetized horse. *J. Am. Vet. Med. Ass.* **224**, 1143-1146.
20. Girard, N.M. and Leece, E.A. (2010) Suspected anaphylactoid reaction following intravenous administration of a gadolinium-based contrast agent in three dogs undergoing magnetic resonance imaging. *Vet. Anaesth. Analg.* **37**, 352-356.
21. International Committee on Veterinary Gross Anatomical Nomenclature (2005) *Nomina Anatomica Veterinaria*, 5th edn., International Committee on Veterinary Gross Anatomical Nomenclature, Knoxville.
22. Passat, N., Ronse, C., Baruthio, J., Armspach, J.P. and Maillot, C. (2006) Magnetic resonance angiography: from anatomical knowledge modeling to vessel segmentation. *Med. Image Anal.* **10**, 259-274.
23. Babiarz, L.S., Romero, J.M., Murphy, E.K., Brobeck, B., Schaefer, P.W., González, R.G. and Lev, M.H. (2009) Contrast-enhanced MR angiography is not more accurate than unenhanced 2D time-of-flight MR angiography for determining > or = 70% internal carotid artery stenosis. *Am. J. Neuroradiol.* **30**, 761-768.
24. Miyazaki, M. and Lee, V.S. (2008) Nonenhanced MR angiography. *Radiol.* **248**, 20-43.
25. Barone, R. (1996) Organisation générale de l'appareil circulatorie. In: *Anatomie Comparée Des Mammifères Domestiques. Tome 5: Angiologie*, 1st edn., Editions Vigot, Paris. pp 1-5.
26. Miller, C.B., Wilson, D.A., Martin, D.D., Pace, L.W. and Constantinescu, G.M. (1998) Complications of balloon catheterization associated with aberrant cerebral arterial anatomy in a horse with guttural pouch mycosis. *Vet. Surg.* **27**, 450-453.
27. Freeman, D.E., Staller, G.S., Maxson, A.D. and Sweeney, C.R. (1993) Unusual internal carotid artery branching that prevented arterial occlusion with a balloon-tipped catheter in a horse. *Vet. Surg.* **22**, 531-534.
28. Freeman, D.E. and Hardy, J. (2012) Guttural pouch. In: *Equine Surgery*, 4th edn., Eds: J.A. Auer and J.A. Stick, Elsevier Saunders, Saint Louis. pp 623-642.
29. Leveille, R., Hardy, J., Robertson, J.T., Willis, A.M., Beard, W.L., Weisbrode, S.E. and Lepage, O.M. (2000) Transarterial coil embolization of the internal and external carotid and maxillary arteries for prevention of hemorrhage from guttural pouch mycosis in horses. *Vet. Surg.* **29**, 389-397.
30. Trope, G.D., Steel, C.M., Bowers, J.R., Bradbury, L.A., Hodge, P.J. and Maggs, D.J. (2010) Distensible superficial venous orbital malformations involving the lower eyelid in two horses. *J. Am. Vet. Med. Ass.* **237**, 943-948.

## Supporting Information

Additional Supporting Information may be found in the online version of this article:

**Fig S1:** Lateral 3D surface-rendered reconstruction of the CT scanned vascular corrosion cast.
**Fig S2:** MIP sagittal reconstruction showing the angular artery of the mouth with the high-field protocol (A), compared with the CT scanned cast (B). 1 - inferior labial artery, 2 - angular artery of the mouth.
**Fig S3:** MIP sagittal reconstruction of the brain arteries showing the rostral cerebral and the corpus callosum arteries with the high-field protocol (A), compared with the CT scanned cast (B). 1 - basilar artery, 2 - Circle of Willis, 3 - middle cerebral artery, 4 - rostral cerebral artery, 5 - corpus callosum artery.
**Fig S4:** Low-field MIP sagittal reconstruction showing the main branches of the lingual vein. 1 - facial vein, 2 - lingual vein, 3 - deep lingual vein, 4 - sublingual vein, 5 - dorsal lingual vein, 6 - sphenopalatine vein.
**Fig S5:** Low-field MIP sagittal reconstruction of the main branches of the facial vein. 1 - facial vein, 2 - anastomotic branch between the buccal and facial veins, 3 - buccal vein, 4 - buccal venous sinus, 5 - deep facial vein, 6 - venous sinus of the deep facial vein, 7 - transverse facial vein, 8 - superior labial vein, 9 - angular vein of the mouth, 10 - inferior labial vein, 11 - lateral nasal vein.
**Fig S6:** Low-field MIP dorsal reconstruction showing venous sinuses of the dura mater, located ventral (A) and dorsal (B) to the brain. 1 - basilar sinus, 2 - cavernous sinus, 3 - caudal intercavernous sinus, 4 - ventral petrous sinus, 5 - caudal branch of the deep temporal vein, 6 - emissary vein of the orbital fissure, 7 - dorsal cerebral vein, 8 - dorsal sagittal sinus, 9 - confluence of sinuses, 10 - transverse sinus, 11 - temporal sinus, 12 - emissary vein of the retroarticular foramen, 13 - superficial temporal vein, 14 - basal vein of the brain.

# Aplicación de TÉCNICAS DE DIAGNÓSTICO por IMAGEN AVANZADAS en el estudio de la CABEZA DEL CABALLO

Application of advanced diagnostic imaging techniques in the study of the equine head

# 4

# DISCUSSION

## 4.1. Comparison of CT and MRI in the equine head

In the first two papers we studied the clinical applications of both MRI and CT in the equine head by performing two large retrospective studies, in which horses with diseases affecting any region of the head were included. Both modalities provided high quality images allowing accurate diagnoses in all cases. However, depending on the anatomical structure affected, or the type of suspected pathology, one of the imaging modalities can offer more specific information over the other. In the following headings we will discuss the preferability of each technique (MRI and CT) based on our results.

### 4.1.1. Nasal cavity and paranasal sinuses

As mentioned in the introduction, radiographic diagnosis of sinonasal disorders in the horse is challenging due to the anatomical complexity of this region and the inherent lack of soft tissue contrast. Therefore, different pathologies can have similar radiographic features or, in some cases, no radiographic abnormalities can be detected. We observed that radiography has a low to moderate sensitivity for identifying sinusal disease. Depending on the sinus affected, it can however yield a high specificity. The lowest sensitivity using radiographs was seen in the sphenopalatine (16.7%) and the ventral conchal (43.5%) sinuses. Adversely, MRI and CT, can show with high detail the different sinusal compartments thanks to the tomographic characteristics of the images they produce (Arencibia *et al.*, 2000; Brinkschulte *et al.*, 2013; De Zani *et al.*, 2010; Kaminsky and Bienert-Zeit, 2014; Probst *et al.*, 2005; Smallwood *et al.*, 2002). Therefore, identification of individual sinus involvement can be better performed using either MRI or CT. In addition, both modalities are superior in identifying the cause of the disease (e.g. sinusal cysts, progressive ethmoid hematomas, abscesses, neoplasms or sinusitis) (Annear *et al.*, 2008; K. C. Barnett *et al.*, 2008; Bischofberger *et al.*, 2008; Cilliers *et al.*, 2008; Cissell *et al.*, 2012; Fjordbakk *et al.*, 2013; Henninger *et al.*, 2003; Maischberger *et al.*, 2014; Robertson *et al.*, 2002; Tessier *et al.*, 2013; Textor *et al.*, 2012; Veraa *et al.*, 2009a). In our studies, localization, size, and relation to surrounding structures of the lesions seen on CT or MRI matched surgical and/or gross and/or histopathological observations. However, this was not always straight forward, especially with CT. In cases of homogenous soft tissue masses being surrounded by fluid, CT without contrast may show similar attenuation values for both, making differentiation between them complicated. Conversely, MRI images have higher soft tissue contrast, resulting in different signal intensities for each type of soft tissues and fluid. Moreover, MRI showed different signal intensities on different sequences, further allowing differentiation of sinus cysts, mucoceles and abscesses, and allowing differentiation between fluid and purulent material in the sinuses. We appreciated this limitation of CT in a case of a sinusal cyst, which was surrounded by fluid in the corresponding sinus. Only by measuring the HU in both areas, was it possible to determine the different tissue types. Injection of intravenous contrast medium may be recommended in such cases, but measuring HU units within sinus fluid accumulations are therefore considered mandatory.

Both modalities can delineate mild alterations of the mucosal lining of the nasal cavity and paranasal sinuses, which are recognized by thickening of the mucosa and mild contrast enhancement. In MRI, increased T2 signal intensity is commonly observed as well. CT might then be better in cases of subtle lysis of the thin sinusal bony walls, which are typically seen in chronic sinusitis, ethmoid hematomas or tumors (Barker *et al.*, 2013; Cehak *et al.*, 2008). The high bony detail of CT images is particularly useful for assessing the osseous canals that cross the nasal cavity and paranasal sinuses, such as the infraorbital canal and the nasolacrimal duct. The first has high clinical importance as lesions of the infraorbital nerve are commonly associated with headshaking syndrome (Fiske-Jackson *et al.*, 2012; V. L. H. Roberts *et al.*, 2009). However, mild changes within the nerve are difficult to detect by CT, whereas MRI would potentially show them. Similarly to what happen in the infraorbital canal, CT can also delineate the osseous anatomy of the ●●●

nasolacrimal duct. Furthermore, it is possible to assess the patency of its lumen by injection of a contrast medium. Diseases of the nasolacrimal duct commonly consist in an obstruction. Several causes can lead to such obstruction, and these can be identified with CT (Cleary *et al.*, 2011; Manso-Díaz and Taeymans, 2012; Rached *et al.*, 2011). Nonetheless, we successfully described a technique to visualize the nasolacrimal duct in MRI and this modality can therefore be considered as a potential alternative for nasolacrimal duct evaluation (Manso-Díaz *et al.*, 2014).

In conclusion, either MRI or CT should be used when detailed examination of the equine nasal cavity and paranasal sinuses is required. In the majority of conditions CT is commonly preferred due to shorter scan times, better availability, as well as introduction of standing CT techniques in the equine practice (Dakin *et al.*, 2014; Kinns and Pease, 2009). The latter avoids the necessity of general anesthesia, both decreasing risks and costs (Dakin *et al.*, 2014). Another main advantage of shorter scan times with CT results in the possibility of performing both procedures, CT acquisition and surgery, under the same general anesthesia. However, limited protocols using 3D GRE sequences would decrease the anesthesia time and would eliminate the necessity of acquiring sequences in different planes using MRP, and could be considered as a good alternative where CT is not available. Furthermore, CT studies usually generate 10 – 20 times more images, making it impossible to fully interpret a CT study by the time the patient is in surgery.

## 4.1.2. Dental structures

We observed that radiography had a moderate sensitivity (72.5%) and specificity (89.5%) for diagnosis of periapical infections, which is in accordance with previous studies (Townsend *et al.*, 2011). These results show that thorough evaluation of the complex anatomy of the equine teeth and surrounding structures using radiography is insufficient in most cases. Advanced diagnostic imaging modalities are therefore needed when assessing these structures. CT description of both incisors and cheek teeth anatomy and pathology has been previously published (Kopke *et al.*, 2012; Schrock *et al.*, 2013; Windley *et al.*, 2009). This modality is able to distinct with high detail the internal structures of the tooth and its surrounding structures, and is therefore considered the gold standard in detecting lesions of the enamel, infundibulum, pulp cavity, root, lamina dura, periapical bone and periodontal space (Bühler *et al.*, 2014; Henninger *et al.*, 2003; Veraa *et al.*, 2009b; Windley *et al.*, 2009). This was equally reflected in the population samples of our retrospective multi-institutional studies, where we evaluated 32 horses with dental disease using CT, as opposed to only 4 horses with dental disease being studied using MRI. CT not only showed periapical changes, but also identified dental malpositioning (e.g. diastemata formation), dental fractures, and dental fragments or oronasal/orosinus fistula formation following dental removal. Due to its molecular composition, not all dental structures can be visualized with MRI. MRI images do show the pulp cavity, the periodontal space, the lamina dura and the bone marrow of the alveolar bone. Signal voids from enamel, dentin, cement and cortical bone, as well as intraoral air and air within the sinuses are however limiting factors (Gerlach *et al.*, 2013; Gerlach *et al.*, 2007b). Nonetheless, in our MRI study, we were able to identify a horse with periapical infection and pulp necrosis, a horse with a large dental fracture, and two cases of sinus abscesses formation secondary to previous dental extraction. An orosinus fistula was present in both cases, and in one case an osseous fragment was observed in the alveolus. In conclusion, MRI is limited to the diagnosis of only certain dental diseases, such as advanced pulpitis, periapical infections and large fractures. Studies using a 9.7T magnet show that very specific sequences (e.g. ultra short spin echo time and zero spin echo time) are possible to depict both soft and hard (enamel, dentin and cementum) dental tissues in extracted equine and human teeth, but clinical application of this result remains beyond realistic terms (Hövener *et al.*, 2012).

## 4.1.3. Central nervous system

With the exception of pneumocephalus with radiograph, and hydrocephalus in neonates with

●●● ultrasound, neither of the conventional diagnostic imaging modalities can be used for assessing the central nervous system (Archer, 2014; Dunkel *et al.*, 2012). Lesions within the brain are relatively uncommon in the horse, and depending on their localization can be grouped as intraaxial, extraaxial and intraventricular (Divers, 2006; Hecht and Adams, 2010).

The most common lesions in the horse are the extraaxial and intraventricular types. Within the group of extraaxial lesions, traumatic disorders (e.g. hematomas and fractures), abscesses and tumors (e.g. pituitary masses, melanomas or intracranial extension of orbital or nasal tumors) are the most commonly represented. However, any bony lesion of the cranial vault may equally affect the brain (Beccati *et al.*, 2011; Covington *et al.*, 2004; De Zani *et al.*, 2013; P. K. Dyson *et al.*, 2007; Feige *et al.*, 2000; Johns *et al.*, 2012; Maischberger *et al.*, 2014; Matiasek *et al.*, 2007; Morresey *et al.*, 2010; Robertson *et al.*, 2002). Within the intraventricular lesions cholesterol granulomas, aka cholesteatomas, are the most commonly found. Other type of tumors such as ependymomas have also been reported (Dunkel *et al.*, 2012; Finding *et al.*, 2012; Maulet *et al.*, 2008; Vink-Nooteboom *et al.*, 1998). Although MRI has higher soft tissue contrast resolution than CT, both imaging modalities can potentially depict these type of lesions. Injection of intravenous contrast medium is however mandatory for delineating the lesion and assessing its relationship with the surrounding tissues on both modalities. MRI might show associated changes within the brain, such as edema, which are not identifiable with CT; whereas if the lesion involves osseous structures, CT would be able to better delineate it.

Intraaxial lesions are very uncommon in horses. Described disorders using advanced diagnostic imaging techniques include inflammatory/infectious, neoplastic and neurodegenerative diseases (Audigié *et al.*, 2004; Ferrell *et al.*, 2002; Gericota *et al.*, 2010; Gray *et al.*, 2001; Sanders *et al.*, 2001; Spoormakers *et al.*, 2003; Tucker *et al.*, 2011). Within the group of intraaxial lesions, we described disorders that were not previously reported with MRI, such as post-anesthetic cerebral necrosis, cortical infarcts, collicular edema, astrocytoma, and diffuse brain edema. CT would likely fail showing this type of lesions (Lacombe *et al.*, 2010), and MRI should therefore be considered as the gold standard in studying the equine brain.

From the 65 horses examined for neurological disorders in the first paper, 31 had a primary complaint of recurrent seizure-like activity from which only 2 had abnormalities on brain MR images, which included a tumor and an infarct. The remaining horses included a wide range of breeds and ages, and none had any identifiable etiology for seizures. We, therefore, proposed cryptogenic epilepsy as the most likely differential diagnosis in these cases (Lacombe *et al.*, 2014; Lacombe *et al.*, 2012). Although MRI findings were negative in most of these patients, performing this test is still a vital part of the seizure work-up, as it helps ruling out morphological causes for seizures.

Cranial nerve abnormalities are another condition type that can be identified using advanced diagnostic imaging techniques. We only encountered this condition in the MRI study, with the optic nerve being the only diseased structure included. We reported neuronal atrophy, inflammation and neoplasia. Excluding the tumor, the other two lesions would not have been possible to identify with CT. This said, both lesions were secondary to sphenopalatine masses and trauma respectively, making these primary causes (e.g. fracture of the optic canal or the sphenopalatine mass) potentially visible on CT. A recent study compared CT and MRI for anatomical identification of normal cranial nerves in horses, and concluded that MRI allowed for excellent visualization of the cranial nerves, whereas CT allowed for detailed visualization of the osseous canal and foramina (J. J. Dixon *et al.*, 2014a).

We also observed several changes of unknown clinical significance within the brain, which we presumed to represent incidental findings. Post-mortem evaluation of the brain was however not available in any of those cases. The changes consisted of asymmetry of the ventricles, signal voids within the lateral ventricles and low signal ●●●

intensities throughout the pineal gland and internal capsule (globus pallidus) in T2* GRE images, as well as suspected leukoaraiosis. Suspected leukoaraiosis consisted of bilateral ill-defined periventricular hyperintensities on T2W and FLAIR images within the cerebral white matter and looked similar to reports in people. Leukoaraiosis is a common feature of the human ageing brain of unknown etiology, but the speculated cause is chronic cerebral ischemia (Altaf *et al.*, 2008; Helenius *et al.*, 2002). Asymmetry of lateral ventricles was considered a normal anatomic variation, similar to previous studies in horses and dogs (Pivetta *et al.*, 2013; Sogaro-Robinson *et al.*, 2009). Ventricular signal voids may correspond to hyperattenuating areas observed in CT, and could represent incidental small, non-obstructive cholesterol granulomas. Similar changes to what we described on MRI images at the level of the internal capsule have been observed on CT, as bilateral and symmetrical well-defined ovoid hyperattenuating areas. Based on the combined information from previous CT description we hypothesize that these represent areas of mineralization of unknown etiology. Pineal gland changes and leukoaraiosis have not been identified on CT images. Imaging of the equine nervous system still is not performed frequently, and many more studies on this topic will therefore be necessary to increase our knowledge on the clinical significance of those reported changes.

## 4.1.4. Musculoskeletal system

Eleven horses with musculoskeletal abnormalities of the head were evaluated with CT in the second retrospective study, whereas none were evaluated with MRI. The superior bony detail of CT images making it the gold standard for this type of lesions.

The most common musculoskeletal lesions affecting the equine head and assessed with advanced diagnostic imaging techniques are fractures, particularly from the mandible, orbit, cranial vault, skull base, temporal bone, stylohyoid bone and paracondylar process (Barba and Lepage, 2013; Chalmers *et al.*, 2006; De Zani *et al.*, 2013; Ferrell *et al.*, 2002; Gerding *et al.*, 2014; Gold *et al.*, 2010; Kuemmerle *et al.*, 2009; Lim *et al.*, 2013; Lischer *et al.*, 2010; Müller *et al.*, 2011; Pownder *et al.*, 2010). CT is often preferred in horses with head fractures, except when brain injury is suspected. Although MRI is very sensitive for identifying bone marrow lesions, flat bones and petrous temporal bones are shown as signal void on MRI. Subtle lesions affecting these bones are therefore difficult to identify with MRI (Scrivani, 2013). As previously discussed in the introduction, skull fractures are difficult to assess on radiographs because of the complex morphology of the skull bones and overlapping of numerous structures (Bar-Am *et al.*, 2008). Based on our results, CT allowed to identify a greater number of bone fragments and showed fractures of the maxillary, lacrimal, sphenoidal, temporal and zygomatic bones which were not visible radiographically. Although there was good agreement between both imaging techniques for visualizing mandibular body fractures, CT might still be necessary to assess the full extent of the fracture. Less commonly, CT can be used in better assessing osteomyelitis and neoplasia (Carmalt and Linn, 2013; Crijns *et al.*, 2014; Johns *et al.*, 2012; Koch *et al.*, 2012; Loftin *et al.*, 2015; Morresey *et al.*, 2010; Van Thielen *et al.*, 2013).

Both CT and MRI have been previously described in assessing the temporomandibular joint. Their cross-sectional images allow assessing both the medial and the lateral aspects of the joint, as well as the inner structure of the bone as well as the internal articular structures (Rodríguez *et al.*, 2010; 2008). Diseases affecting this joint usually include osteoarthritis and septic arthritis (T. P. Barnett *et al.*, 2014; Nagy and Simhofer, 2006).

In the second study, four horses with temporohyoid osteoathropathy and one horse with otitis media were included. CT provided comprehensive evaluation of the temporal bone and hyoid apparatus, showing similar changes that have been previously reported in all cases (Hilton *et al.*, 2009; Naylor, Perkins *et al.*, 2010b; Pownder *et al.*, 2010; Rand *et al.*, 2012). Luxation of the temporohyoid articulation was however observed in 2 of our cases, a very uncommon con-

dition which, to our knowledge, has not been reported on imaging studies before. A traumatic origin was hypothesized in those cases.

### 4.1.5. Soft tissues

Extracranial soft tissue disorders of the head are relatively common, and they usually involve the tongue, salivary glands, lymph nodes, pharynx, and orbit (P. M. Dixon, 1991; P. M. Dixon *et al.*, 2014b). The use of CT and MRI is less common than for brain conditions, as noted in our first two studies, and is commonly limited to masses that need further pre-operative evaluation after initial ultrasonographic assessment. Compared to ultrasound, CT and MRI provide better coverage of the entire lesion on the images, using multiple imaging planes and larger fields of view, and allow visualization of tissues covered by gas or bone (Bienert-Zeit *et al.*, 2014; Gerlach *et al.*, 2007a; Jakesova *et al.*, 2008; McConnell *et al.*, 2012; Naylor *et al.*, 2010a; Pekarkova *et al.*, 2009; S. Ramirez and Tucker, 2004; Santos *et al.*, 2012; Schneider *et al.*, 2010; van den Top *et al.*, 2007; Wollanke *et al.*, 2006). Although in our cases both techniques allowed identification of the lesions, MRI images provided superior differentiation of the soft tissue structures and were better at establishing accurate relationship with the surrounding structures.

## 4.2. Advances in CT and MRI of the equine head

Clinical use of advanced diagnostic imaging techniques for studying the equine head is increasing substantially over the last few years, which is reflected in the large number of recent publications on this topic. These numbers however remain relatively low compared to the number of publications pertaining to other anatomical regions of the horse, and there still remains a lot of knowledge to be gained on this topic.

Compared to MRI, CT of the equine head is experiencing a revolution due to the introduction of standing CTs in equine practice, which is similar to what happened when standing MRI first appeared (Dakin *et al.*, 2014; Porter and Werpy, 2014). Challenges in equine head CT however remain, such as optimizing protocols for contrast studies.

MRI has a great potential for assessing the equine head, similarly to small animal or human medicine, where several new techniques are being described every year. The main limitation of this technique lies in the low number of MRI scanners available for horses, together with the high costs, the need of general anesthesia and the low brain disease case-load in equine practice (Porter and Werpy, 2014). These factors explain the very low number of such studies in the literature. Recent publications on equine head MRI are focused on describing normal anatomy of specific regions with high-field magnets (J. J. Dixon *et al.*, 2014a; Gutierrez-Crespo *et al.*, 2014; Kaminsky and Bienert-Zeit, 2014). In the third manuscript composing this PhD thesis, we developed and optimized a technique for performing both high-field and low-field MRI angiographic studies of equine heads without the need of injecting a contrast medium. By the same occasion, we performed a thorough description of the normal vascular anatomy using this technique. Accurate evaluation of the equine head vasculature is challenging due to the complex branching pattern and the spatial distribution of the blood vessels. Imaging of the cranial vasculature was previously described using conventional angiography (Cook, 1973; Colles and Cook, 1983). Currently, conventional angiography is gradually being replaced by other advanced imaging modalities, such as computed tomography angiography and magnetic resonance angiography. Both modalities are well established diagnostic techniques in human and small animal medicine; conversely they are barely reported in horses. Although diseases affecting this system are uncommon in this species, costs resulting of the large volume of contrast medium often required in horses seem to be the most likely limitation of its use. Therefore, development of new alternatives, such as the non-contrast MRA technique described in this thesis, will allow performing more vascular studies of the equine head without economic restrictions.

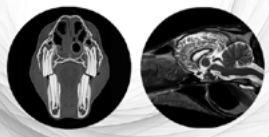



## DISCUSSION

●●● As we mentioned before, there are still several known conditions that are not described with MRI yet. There also remain several findings of unknown clinical significance. Future equine head MRI research is therefore needed in that direction: describing new MRI features of known equine head conditions, determining the significance of MRI findings of the brain and developing new MRI techniques for studying the equine head. ■

# Aplicación de TÉCNICAS DE DIAGNÓSTICO por IMAGEN AVANZADAS en el estudio de la CABEZA DEL CABALLO

Application of advanced diagnostic imaging techniques in the study of the equine head

# 5

# CONCLUSIONS

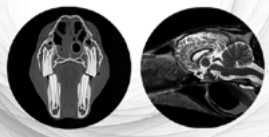



## CONCLUSIONS

**1.** Both high-field and low-field magnetic resonance imaging systems are suitable imaging techniques for assessing the equine head with high detail, but may be inferior to computed tomography for certain conditions.

**2.** Magnetic resonance imaging can be considered the gold standard for studying the central nervous system, including the brain and cranial nerves, as well as the extracranial soft tissues, including the orbit, lymph nodes, blood vessels, muscles, and salivary glands.

**3.** Magnetic resonance imaging is adequate for studying the nasal cavity and paranasal sinuses, and it is particularly useful for differentiating space-occupying lesions, where its high soft tissue contrast resolution allows good differentiation of different tissue types. Diagnostic usefulness of magnetic resonance imaging in cases of dental disease is limited to lesions involving the pulp cavity, the periodontal space, the lamina dura and the bone marrow of the alveolar bone.

**4.** Time-of-flight magnetic resonance angiography is an excellent technique to assess blood vessels of the head and can be performed using both high-field and low-field magnetic resonance imaging systems in equine patients. This rapid sequence provides good visualization of all major intra- and extracranial vessels down to a size of approximately 2 mm in diameter. Visibility of the arterial system is superior than the venous system.

**5.** Time-of-flight magnetic resonance angiography can be incorporated as part of routine imaging protocols in horses affected with soft-tissue space-occupying lesions or vascular abnormalities, without excessive increase in examination time.

**6.** Computed tomography is another suitable imaging technique for assessing the equine head with high detail, but has different indications than magnetic resonance imaging. Both imaging modalities are therefore complementary to each other, and when both modalities are available, preemptive knowledge of the clinically suspected condition is paramount in deciding which modality is most indicated.

**7.** Computed tomography can be considered the gold standard for studying the skull and mandible, the temporomandibular joint, the temporohyoid articulation and the teeth. Computed tomography is adequate for studying the nasal cavity and paranasal sinuses, being particularly useful for identifying subtle nasal and sinusal wall lesions. Computed tomography is undeniably superior to radiology for identifying sinonasal and dental lesions and when available, makes radiology almost obsolete for conditions involving these areas.

**8.** Computed tomography can identify intraventricular and extraaxial brain lesions, however, diagnostic usefulness of computed tomography in cases of intraaxial lesions is limited. Extracranial soft tissue lesions can be identified with computed tomography, but with less detail than with magnetic resonance imaging. ■

# Aplicación de TÉCNICAS DE DIAGNÓSTICO por IMAGEN AVANZADAS en el estudio de la CABEZA DEL CABALLO

Application of advanced diagnostic imaging techniques in the study of the equine head

# 6

# CONCLUSIONES

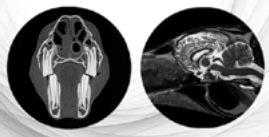



## CONCLUSIONES

**1.** Tanto la resonancia magnética de alto campo como la de bajo campo son técnicas de diagnóstico por imagen adecuadas para la valoración en detalle de la cabeza del caballo.

**2.** La resonancia magnética es la técnica de elección para el estudio del sistema nervioso central, tanto del encéfalo como de los nervios craneales, y de los tejidos blandos extracraneales, como son la órbita, los linfonódulos, los vasos sanguíneos, los músculos y las glándulas salivares.

**3.** La resonancia magnética es una técnica apta para el estudio de la cavidad nasal y los senos paranasales en el caballo. Gracias al gran contraste de tejidos blandos que ofrece esta técnica es posible una buena diferenciación entre los diferentes tipos de tejidos, lo cual resulta particularmente útil para diferenciar el origen de masas ocupantes de espacio en la cavidad nasal y senos paranasales. Sin embargo, el uso de la resonancia magnética en casos de patología dental se limita a lesiones que afectan a la cavidad pulpar, el espacio periodontal, la lámina dura y la médula ósea del hueso alveolar.

**4.** La técnica de angiografía por resonancia magnética es un excelente método para evaluar los vasos sanguíneos de la cabeza equina y se puede aplicar en resonancia magnética tanto de alto como de bajo campo. Esta secuencia permite visualizar los principales vasos sanguíneos intra- y extracraneales con un grosor superior a 2 mm de diámetro aproximadamente. La visualización del sistema arterial es superior a la del sistema venoso.

**5.** La secuencia *time-of-flight* se puede incorporar como parte del protocolo rutinario de resonancia magnética en caballos con masas de tejidos blandos o alteraciones vasculares, sin que implique un aumento excesivo del tiempo de estudio.

**6.** La tomografía computarizada es otra técnica de diagnóstico por imagen apta para la valoración en detalle de la cabeza del caballo, pero presenta diferentes indicaciones a las de la resonancia magnética. Ambas técnicas son, por tanto, complementarias entre sí. Sin embargo, cuando se dispone de ambas es preciso tener en cuenta la sospecha clínica a la hora de decidir qué técnica es la más adecuada.

**7.** La tomografía computarizada es la técnica de elección para el estudio de los huesos del cráneo, la mandíbula, la articulación temporomandibular, la articulación temporohioidea y los dientes. Esta técnica es adecuada para el estudio de la cavidad nasal y los senos paranasales, siendo especialmente útil en la identificación de lesiones sutiles que afectan a las paredes de la cavidad nasal y los senos. La tomografía computarizada es innegablemente superior a la radiología en la identificación de alteración de la cavidad nasal, de los senos paranasales y de los dientes. Por tanto, cuando se dispone de esta técnica la radiología queda postergada a un segundo plano en el diagnóstico de lesiones de esta región.

**8.** La tomografía computarizada puede identificar lesiones del sistema nervioso central a nivel intraventricular y extraaxial, sin embargo, su utilidad en casos de lesiones intraaxiales es muy limitada. Esta técnica también puede utilizarse para la identificación de alteraciones de los tejidos blandos extracraneales, aunque con menor detalle que la resonancia magnética. ■

Aplicación de
TÉCNICAS DE DIAGNÓSTICO por
IMAGEN AVANZADAS en el estudio
de la CABEZA DEL CABALLO

Application of advanced diagnostic imaging techniques in the study of the equine head

# 7

# REFERENCES

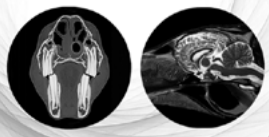



## REFERENCES

Altaf, N., Morgan, P., Moody, A., MacSweeney, S., Gladman, J., & Auer, D. (2008). Brain white matter hyperintensities are associated with carotid intraplaque hemorrhage. *Radiology, 248(1):202-209.*

Annear, M. J., Gemensky-Metzler, A. J., Elce, Y. A., & Stone, S. G. (2008). Exophthalmus secondary to a sinonasal cyst in a horse. *Journal of the American Veterinary Medical Association, 233(2):285-288.*

Archer, D. (2014). Ultrasonography of the head. In J. A. Kidd, K. G. Lu, & M. L. Frazer, Atlas of equine ultrasonography (First edition. pp. 213-223). Oxford: John Wiley & Sons, Ltd.

Archer, D., Blake, C. L., Singer, E. R., Boswell, J. C., Cotton, J. C., Edwards, G. B., & Proudman, C. J. (2003). Scintigraphic appearance of selected diseases of the equine head. *Equine Veterinary Education, 15(6):305-313.*

Archer, D., Blake, C. L., Singer, E. R., Boswell, J. C., Cotton, J. C., Edwards, G. B., & Proudman, C. J. (2010). The normal scintigraphic appearance of the equine head. *Equine Veterinary Education, 15(5):243-249.*

Archer, D., Boswell, J. C., Voute, L. C., & Clegg, P. D. (2007). Skeletal scintigraphy in the horse: current indications and validity as a diagnostic test. *The Veterinary Journal, 173(1):31-44.*

Arencibia, A., Vázquez, J. M., Jaber, R., Gil, F., Ramirez, J., Rivero, M., González, N., Wisner, & Wisner, E. R. (2000). Magnetic resonance imaging and cross sectional anatomy of the normal equine sinuses and nasal passages. *Veterinary Radiology & Ultrasound, 41(4):313-319.*

Audigié, F., Tapprest, J., George, C., Didierlaurent, D., Foucher, N., Faurie, F., Houssin, M., & Denoix, J. M. (2004). Magnetic resonance imaging of a brain abscess in a 10-month-old filly. *Veterinary Radiology & Ultrasound, 45(3):210-215.*

Bar-Am, Y., Pollard, R. E., Kass, P. H., & Verstraete, F. J. M. (2008). The diagnostic yield of conventional radiographs and computed tomography in dogs and cats with maxillofacial trauma. *Veterinary Surgery, 37(3):294-299*.

Barakzai, S. Z. (2005a). How to radiograph the erupted (clinical) crown of equine cheek teeth. Clinical Techniques in *Equine Practice, 4(2):171-174.*

Barakzai, S. Z. (2005b). Use of scintigraphy for the diagnosis of apical infection of equine cheek teeth. *Clinical Techniques in Equine Practice, 4(2):175-180.*

Barakzai, S. Z. (2011). Dental imaging. In J. Easley, P. M. Dixon, & J. Schumacher, Equine Dentistry (Third edition. pp. 199-230). London: Saunders Ltd.

Barakzai, S. Z., & Dixon, P. M. (2003). Effect of sinus trephination on scintigraphy of the equine skull. *Veterinary Record, 152(20):629-630.*

Barakzai, S. Z., Tremaine, H., & Dixon, P. M. (2006). Use of scintigraphy for diagnosis of equine paranasal sinus disorders. *Veterinary Surgery, 35(1):94-101.*

Baratt, R. M. (2013). Advances in equine dental radiology. *The Veterinary Clinics of North America: Equine Practice, 29(2), 367-395.*

Barba, M., & Lepage, O. M. (2013). Diagnostic utility of computed tomography imaging in foals: 10 cases (2008-2010). *Equine Veterinary Education, 25(1):29-38.*

Barbee, D. D., Allen, J. R., & Gavin, P. R. (1987). Computed tomography in horses. *Veterinary Radiology, 28(5):144-151.*

Barker, W. H., Perkins, J. D., & Witte, T. H. (2013). Three horses with bilateral sinonasal progressive haematomas not associated with the ethmoidal labyrinth. *Equine Veterinary Education, 25(10):503-507.*

Barnett, K. C., Blunden, A. S., Dyson, S. J., Whitwell, K. E., Carson, D., & Murray, R. C. (2008). Blindness, optic atrophy and sinusitis in the horse. *Veterinary Ophthalmology, 11(S1):20-26.*

Barnett, T. P., Powell, S. E., Head, M. J., Marr, C. M., Steven, W. N., & Payne, R. J. (2014). Partial mandibular condylectomy and temporal bone resection for chronic, destructive, septic arthritis of the temporomandibular joint in a horse. *Equine Veterinary Education, 26(2):59-63.*

Barrett, M. F., & Easley, J. T. (2013). Acquisition and interpretation of radiographs of the equine skull. *Equine Veterinary Education, 25(12):643-652.*

Beccati, F., Angeli, G., Secco, I., Contini, A., Gialletti, R., & Pepe, M. (2011). Comminuted basilar skull fracture in a colt: Use of computed tomography to aid the diagnosis. *Equine Veterinary Education, 23(7):327-332.*

Behrens, E., Schumacher, J., Morris, E., & Shively, M. (1991). Equine paranasal sinusography. *Veterinary Radiology, 32(3):98-104.*

Bergman, E. H. J., Puchalski, S. M., & Saunders, J. H. (2013). Intracarotid contrast-enhanced computed tomography of the equine head. *Veterinary Radiology & Ultrasound, 54(4):415.*

Bertolini, G., & Prokop, M. (2011). Multidetector-row computed tomography: Technical basics and preliminary clinical appli-

## REFERENCES

●●● cations in small animals. *The Veterinary Journal, 189(1):15-26.*

Bertolini, G., Rolla, E. C., Zotti, A., & Caldin, M. (2006). Three-dimensional multislice helical computed tomography techniques for canine extra-hepatic portosystemic shunt assessment. *Veterinary Radiology & Ultrasound, 47(5):439-443.*

Bienert-Zeit, A., Nordemann, E., Borstel, von, M., Wohlsein, P., Iseringhausen, M., Hellige, M., & Rötting, A. K. (2014). Unilateral exophthalmos in a horse – Diagnosis, management and outcome. *Pferdeheilkunde, 30(1):81-90.*

Bienert-Zeit, A., Reinig, A., Hellige, M., Reichert, C., Hewicker-Trautwein, M., & Feige, K. (2011). Dermoid cyst in the area of the lower jaw in a 7-year-old gelding. *Tierärztliche Praxis Großtiere, 39:397-401.*

Bischofberger, A. S., Konar, M., Posthaus, H., Pekarkova, M., Grzybowski, M., & Brehm, W. (2008). Ocular angiosarcoma in a pony - MRI and histopathological appearance. *Equine Veterinary Education, 20(7):340-347.*

Bolas, N. (2011). Basic MRI principles. In R. C. Murray, Equine MRI (First edition. pp. 3-37). West Sussex: Wiley-Blackwell.

Boswell, J. C., Schramme, M. C., Livesey, L. C., & Butson, R. J. (1999). Use of scintigraphy in the diagnosis of dental disease in four horses. *Equine Veterinary Education, 11(6):294-298.*

Brink, J., Heiken, J., Wang, G., McEnery, K., Schlueter, F., & Vannier, M. (1994). Helical CT: principles and technical considerations. *Radiographics, 14(4):887-893.*

Brinkschulte, M., Bienert-Zeit, A., Lüpke, M., Hellige, M., Staszyk, C., & Ohnesorge, B. (2013). Using semi-automated segmentation of computed tomography datasets for three-dimensional visualization and volume measurements of equine paranasal sinuses. *Veterinary Radiology & Ultrasound, 54(6):582-590.*

Bushberg, J. T., Seibert, J. A., Leidholdt, E. M., & Boone, J. M. (2002a). Computed tomography. In J. T. Bushberg, J. A. Seibert, E. M. Leidholdt, & J. M. Boone, The essential physics of medical imaging (Second edition. pp. 327-372). Philadelphia: Williams & Wilkins.

Bushberg, J. T., Seibert, J. A., Leidholdt, E. M., & Boone, J. M. (2002b). Magnetic resonance imaging. In J. T. Bushberg, J. A. Seibert, E. M. Leidholdt, & J. M. Boone, The essential physics of medical imaging (Second edition. pp. 415-468). Philadelphia: Williams & Wilkins.

Bushberg, J. T., Seibert, J. A., Leidholdt, E. M., & Boone, J. M. (2002c). Nuclear magnetic resonance. In J. T. Bushberg, J. A. Seibert, E. M. Leidholdt, & J. M. Boone, The essential physics of medical imaging (Second edition. pp. 373-414). Philadelphia: Williams & Wilkins.

Butler, J., Colles, C., Dyson, S. J., Kold, S., & Poulos, P. (2008). Clinical Radiology of the Horse (Third Edition.). West Sussex: John Wiley & Sons.

Bühler, M., Fürst, A., Lewis, F. I., Kummer, M., & Ohlerth, S. (2014). Computed tomographic features of apical infection of equine maxillary cheek teeth: A retrospective study of 49 horses. *Equine Veterinary Journal, 46(4):468-473.*

Cao, G., Zhou, X., Xu, H., Pan, K., Chen, W., & Li, R. (2014). Optimizing scan protocol in whole-brain vessel one-stop examination with 640-multislice computed tomography. *Zhonghua Yi Xue Za Zhi, 94(21):1609-1612.*

Carmalt, J. L., & Linn, K. A. (2013). Large segmental mandibulectomy for treatment of an undifferentiated sarcoma in a horse. *Veterinary Surgery, 42(4):433-439.*

Cehak, A., Borstel, von, M., Gehlen, H., Feige, K., & Ohnesorge, B. (2008). Necrosis of the nasal conchae in 12 horses. *Veterinary Record, 163(10):300-302.*

Chalmers, H. J., Cheetham, J., Dykes, N. L., & Ducharme, N. G. (2006). Computed tomographic diagnosis-Stylohyoid fracture with pharyngeal abscess in a horse without temporohyoid disease. *Veterinary Radiology & Ultrasound, 47(2):165-167.*

Cilliers, I., Williams, J. M., Carstens, A., & Duncan, N. M. (2008). Three cases of osteoma and an osseous fibroma of the paranasal sinuses of horses in South Africa. *Journal of the South African Veterinary Association, 79(4):185-193.*

Cissell, D. D., Wisner, E. R., Textor, J. A., Mohr, F. C., Scrivani, P. V., & Théon, A. P. (2012). Computed tomographic appearance of equine sinonasal neoplasia. *Veterinary Radiology & Ultrasound, 53(3):245-251.*

Cleary, O. B., Easley, J. T., Henriksen, M. D. L., & Brooks, D. E. (2011). Purulent dacryocystitis (nasolacrimal duct drainage) secondary to periapical tooth root infection in a donkey. *Equine Veterinary Education, 23(11):553-558.*

Colles, C. M., & Cook, W. R. (1983). Carotid and cerebral angiography in the horse. *Veterinary Record, 113(21):483-489.*

Contreras, S., Arencibia, A., Gil, F., de Miguel, A., Ramirez, G., & Vázquez, J. M. (2010). Black and bright-blood sequences magnetic resonance angiography and gross sections of the canine thorax: an anatomical study. *The Veterinary Journal, 185(2):231-234.* ●●●

## REFERENCES

●●● Cook, W. R. (1970). Skeletal radiology of the equine head. *Veterinary Radiology, 11(1):35–54.*

Cook, W. R. (1973). The auditory tube diverticulum (guttural pouch) in the horse: Its radiographic examination. *Journal of the American Veterinary Radiology Society, 14(1):51–71.*

Covington, A. L., Magdesian, K. G., Madigan, J. E., Maleski, K., Gray, L. C., Smith, P. A., & Wisner, E. R. (2004). Recurrent esophageal obstruction and dysphagia due to a brainstem melanoma in a horse. *Journal of Veterinary Internal Medicine, 18(2):245–247.*

Crawford, C. R., & King, K. F. (1990). Computed tomography scanning with simultaneous patient translation. *Medical Physics, 17(6):967–982.*

Crawley, A., Poublanc, J., Ferrari, P., & Roberts, P. (2003). Basics of diffusion and perfusion MRI. *Applied Radiology, 13–23.*

Crijns, C. P., Vlaminck, L., Verschooten, F., van Bergen, T., De Cock, H. E., Huylebroek, F., Pool, R., & Gielen, I. (2015). Multiple mandibular ossifying fibromas in a yearling Belgian Draught horse filly. *Equine Veterinary Education, 27(1):11-15.*

D'Anjou, M.-A. (2012). Principles of computed tomography and magnetic resonance imaging. In D. E. Thrall, Textbook of veterinary diagnostic radiology (Sixth edition. pp. 50–73). St. Louis: Elsevier.

D'Août, C., Nisolle, J. F., Navez, M., Perrin, R., Launois, T., Brogniez, L., Clegg, P., Hontoir, F., & Vandeweerd, J. M. (2014). Computed tomography and magnetic resonance anatomy of the normal orbit and eye of the horse. *Anat Histol Embryol. doi:10.1111/ahe.12149*

Dakin, S. G., Lam, R., Rees, E., Mumby, C., West, C., & Weller, R. (2014). Technical set-up and radiation exposure for standing computed tomography of the equine head. *Equine Veterinary Education, 26(4):208-215.*

De Clercq, D., van Loon, G., Nollet, H., Delesalle, C., Lefére, L., & Deprez, P. (2003). Percutaneous puncture technique for treating persistent retropharyngeal lymph node infections in seven horses. *Veterinary Record, 152(6):169–172.*

De Zani, D., Borgonovo, S., Biggi, M., Vignati, S., Scandella, M., Lazzaretti, S., Modina, S., & Zani, D. (2010). Topographic comparative study of paranasal sinuses in adult horses by computed tomography, sinuscopy, and sectional anatomy. *Veterinary Research Communications, 34(S1):13–6.*

De Zani, D., Zani, D. D., Binanti, D., Riccaboni, P., Rondena, M., & Di Giancamillo, M. (2013). Magnetic resonance features of closed head trauma in 2 foals. *Equine Veterinary Education, 25(10):493–498.*

Dehghani, S. S., Tadjalli, M., & Seifali, A. (2005). Sialography in horse: technique and normal appearance. *Veterinarski Arhiv, 75(6):531–540.*

Divers, T. J. (2006). Structural and functional diseases of the equine brain. *Clinical Techniques in Equine Practice, 5(1):67–73.*

Dixon, J. J., Lam, R., Weller, R., Smith, M., Manso-Diaz, G., & Piercy, R. J. (2014a). Comparison and clinical application of CT and MRI for evaluation of the equine cranial nerves. *Equine Veterinary Journal, 46(S47):11.*

Dixon, P. M. (1991). Swellings of the head region in the horse. *In Practice, 13(6):257–263.*

Dixon, P. M., & Head, K. W. (1999). Equine nasal and paranasal sinus tumours: part 2: a contribution of 28 case reports. *The Veterinary Journal, 157(3):279–294.*

Dixon, P. M., Loh, N., & Barakzai, S. Z. (2014b). Swellings of the angle of the mandible in 32 horses (1997–2011). *The Veterinary Journal, 199(1):97–102.*

Dixon, P. M., Tremaine, H., Parkin, T. D., Collins, N., Hawkes, C., Townsend, N., Fisher, G., Ealey, R., & Barakzai, S. Z. (2012). Equine paranasal sinus disease: a long-term study of 200 cases (1997-2009): ancillary diagnostic findings and involvement of the various sinus compartments. *Equine Veterinary Journal, 44(3):267–271.*

Driver, A. J. (2003). Basic principles of equine scintigraphy. In S. J. Dyson, R. C. Pilsworth, A. R. Twardock, & M. J. Martinelli, Equine scintigraphy (First edition. pp. 17–24). Newmarket: Equine veterinary journal.

Dunkel, B., Corley, K. T. T., Johnson, A. L., Witte, T. H., Leitch, M., Marr, C. M., & Weller, R. (2012). Pneumocephalus in five horses. *Equine Veterinary Journal, 45(3):367–371.*

Dyson, P. K., Dunn, K. A., Whitwell, K., & Dennis, R. (2007). Ataxia and cranial nerve signs in a pony suffering a brainstem meningioma; clinical, MRI, gross and histopathological findings. *Equine Veterinary Education, 19(4):173–178.*

Easley, J. T., Franklin, R. P., & Adams, A. (2010). Surgical excision of a dentigerous cyst containing two dental structures. *Equine Veterinary Education, 22(6):275–278.*

Ebling, A. J., McKnight, A. L., Seiler, G. S., & Kircher, P. R. (2009). A complementary radiographic projection of the equine temporomandibular joint. *Veterinary Radiology & Ultrasound, 50(4):385–391.*

●●●

## REFERENCES

Feichtenhofer, P., Simhofer, H., Hof, K., & Kneissl, S. (2012). A complementary radiographic projection of the equine maxillary sinus. *Journal of Equine Veterinary Science, 50(4):385-391.*

Feige, K., Eser, M. W., Geissbühler, U., Balestra, E., & Metzler, K. (2000). Clinical symptoms of and diagnostic possibilities for hypophyseal adenoma in horses. *Schweizer Archiv Für Tierheilkunde, 142(2):49-54.*

Ferrell, E. A., Gavin, P. R., Tucker, R. L., Sellon, D. C., & Hines, M. T. (2002). Magnetic resonance for evaluation of neurologic disease in 12 horses. *Veterinary Radiology & Ultrasound, 43(6):510-516.*

Finding, E., Fletcher, N., Avella, C., Volk, H. A., Weller, R., Dunkel, B., & Piercy, R. J. (2012). Standing CT and clinical progression of equine cholesterol granulomata. *Veterinary Record, 170(11):289-290.*

Finnegan, C. M., Townsend, N. B., Barnett, T. P., & Barakzai, S. Z. (2011). Radiographic identification of the equine ventral conchal bulla. *Veterinary Record, 169(26):683-687.*

Fiske-Jackson, A. R., Pollock, P. J., Witte, T. H., Woolford, L., & Perkins, J. D. (2012). Fungal sinusitis resulting in suspected trigeminal neuropathy as a cause of headshaking in five horses. *Equine Veterinary Education, 24(3):126-133.*

Fjordbakk, C. T., Pekarkova, M., Dolvik, N. I., & Teige, J. (2013). Maxillary odontogenic myxoma in young horses: Six cases (2003-2011). *Equine Veterinary Education. doi:10.1111/eve.12096*

Flohr, T. G., Schaller, S., Stierstorfer, K., Bruder, H., Ohnesorge, B. M., & Schoepf, U. J. (2005). Multi-detector row CT systems and image-reconstruction techniques. *Radiology, 235(3):756-773.*

Frame, E. M., Riihimaki, M., Berger, M., Vatne, M., & McEvoy, F. J. (2010). Scintigraphic findings in a case of temporohyoid osteoarthropathy in a horse. *Equine Veterinary Education, 17(1):11-15.*

Geleijns, J. (2014). Computed tomography. In D. R. Dance, S. Christofides, A. D. A. Maidment, I. D. McLean, & K. H. Ng, Diagnostic radiology physics: A handbook for teachers and students (First edition. pp. 257-290). Vienna: International Atomic Energy Agency.

Gerding, J. C., Clode, A. B., Gilger, B. C., & Montgomery, K. (2014). Equine orbital fractures: a review of 18 cases (2006-2013). *Veterinary Ophthalmology, 17(S1):97-106.*

Gericota, B., Aleman, M., Kozikowski, T. A., Pesavento, P. A., Bollen, A. W., Madigan, J. E., & Higgins, R. J. (2010). A grade IV glioblastoma with an oligodendroglial component (GBM-O) in a horse. *Journal of Comparative Pathology, 142(4):332-335.*

Gerlach, K., Cronau, M., McMullen, R. J., & Gerhards, H. (2007a). Magnetic resonance imaging of melanomas in the head region of 3 horses. *Pferdeheilkunde, 23(3):259-262.*

Gerlach, K., Ludewig, E., Brehm, W., Gerhards, H., & Delling, U. (2013). Magnetic resonance imaging of pulp in normal and diseased equine cheek teeth. *Veterinary Radiology & Ultrasound, 54(1):48-53.*

Gerlach, K., Reese, S., & Gerhards, H. (2007b). Using MRI to diagnose tooth related sinusitis in horses (p. 55). Presented at the European Veterinary Diagnostic Imaging Anual Meeting, Porto Carras.

Gibbs, C. (2010). Radiography of the head and soft tissues of the neck. *Equine Veterinary Education, 8(S3):23-29.*

Gibbs, C., & Lane, J. G. (1987). Radiographic examination of the facial, nasal and paranasal sinus regions of the horse. II. Radiological findings. *Equine Veterinary Journal, 19(5):474-482.*

Gold, R., Kneissl, S., Gruber, A., Fröhlich, W., Leschnik, M., & Reisinger, R. (2010). Skull-brain trauma in a trotter filly. *Tierärztliche Praxis Großtiere, 38(G):52-56.*

Gray, L. C., Magdesian, K. G., Madigan, J. E., & Sturges, B. K. (2001). Suspected protozoal myeloencephalitis in a two-month-old colt. *Veterinary Record, 149(9):269-273.*

Greenberg, S. M., Plummer, C. E., Brooks, D. E., Porter, M., Farina, L. L., & Winter, M. D. (2011). Unilateral orbital lacrimal gland abscess in a horse. *Veterinary Ophthalmology, 14(1):55-60.*

Gutierrez-Crespo, B., Kircher, P. R., & Carrera, I. (2014). 3 Tesla magnetic resonance imaging of the occipitoatlantoaxial region in the normal horse. *Veterinary Radiology & Ultrasound, 55(3):278-285.*

Hathcock, J., & Stickle, R. (1993). Principles and concepts of computed tomography. *The Veterinary Clinics of North America: Small Animal Practice, 23(2):399-415.*

Haynes, P. F., Beadle, R. E., McClure, J. R., & Roberts, E. D. (1990). Soft palate cysts as a cause of pharyngeal dysfunction in two horses. *Equine Veterinary Journal, 22(5):369-371.*

Head, K. W., & Dixon, P. M. (1999). Equine nasal and paranasal sinus tumours. Part 1: review of the literature and tumour classification. *The Veterinary Journal, 157(3):261-278.*

Hecht, S., & Adams, W. H. (2010). MRI of brain disease in veterinary patients part 1: Basic principles and congenital

## REFERENCES

brain disorders. *The Veterinary Clinics of North America: Small Animal Practice, 40(1):21-38.*

Helenius, J., Soinne, L., Salonen, O., Kaste, M., & Tatlisumak, T. (2002). Leukoaraiosis, ischemic stroke, and normal white matter on diffusion-weighted MRI. *Stroke, 33(1):45-50.*

Henninger, W., Frame, E. M., Willmann, M., Simhofer, H., Malleczek, D., Kneissl, S. M., & Mayrhofer, E. (2003). CT features of alveolitis and sinusitis in horses. *Veterinary Radiology & Ultrasound, 44(3):269-276.*

Hilbert, B. J., Little, C. B., Klein, K., & Thomas, J. B. (1988). Tumours of the paranasal sinuses in 16 horses. *Australian Veterinary Journal, 65(3):86-88.*

Hilton, H., Puchalski, S. M., & Aleman, M. (2009). The computed tomographic appearance of equine temporohyoid osteoarthropathy. *Veterinary Radiology & Ultrasound, 50(2):151-156.*

Hounsfield, G. N. (1973). Computerized transverse axial scanning (tomography): Part 1. Description of system. *The British Journal of Radiology, 46(552):1016-1022.*

Hövener, J.-B., Zwick, S., Leupold, J., EisenbeiÐ, A.-K., Scheifele, C., Schellenberger, F., Henning, J., Elverfeldt, D. V., & Ludwig, U. (2012). Dental MRI: imaging of soft and solid components without ionizing radiation. *Journal of Magnetic Resonance Imaging, 36(4):841-846.*

Jacobs, M., Ibrahim, T., & Ouwerkerk, R. (2007). AAPM/RSNA physics tutorials for residents: MR imaging: brief overview and emerging applications. *Radiographics, 27(4):1213-1229.*

Jakesova, V., Konar, M., Gerber, V., Brachelente, C., Howard, J., & Tessier, C. (2008). Magnetic resonance imaging features of an extranodal T cell rich B cell lymphoma in the pharyngeal mucosa in a horse. *Equine Veterinary Education, 20(6):289-293.*

Johns, I. C., Finding, E., Ciasca, T., Erles, K., Smith, K., & Weller, R. (2012). Intracranial botryomycosis in a mature horse. *Equine Veterinary Education, 26(6):294-298.*

Judy, C. E. (2011). Contrast agents in equine MRI. In R. C. Murray, Equine MRI (First edition. pp. 63-74). West Sussex: Wiley-Blackwell.

Kaminsky, J., & Bienert-Zeit, A. (2014). 3 Tesla magnetic resonance imaging of the nasal cavities, paranasal sinuses and adjacent anatomical structures in 13 healthy horses. *Pferdeheilkunde, 30(4):1-19.*

Kilcoyne, I., Whitcomb, M. B., Watson, J. L., Spier, S. J., & Vaughan, B. (2015). Septic sialoadenitis in equids: A retrospective study of 18 cases (1998-2010). *Equine Veterinary Journal, 47(1):54-59.*

Kinns, J., & Pease, A. (2009). Computed tomography in the evaluation of the equine head. *Equine Veterinary Education, 21(6):291-294.*

Kinns, J., Malinowski, R., McEvoy, F., Schwarz, T., & Zwingenberger, A. L. (2011). Special software applications. In T. Schwarz & J. H. Saunders, Veterinary computed tomography (First edition. pp. 67-74). West Sussex: Wiley-Blackwell.

Klugh, D. O. (2005). Intraoral radiology in equine dental disease. *Clinical Techniques in Equine Practice, 4(2):162-170.*

Knottenbelt, D. C., Hetzel, U., & Roberts, V. (2007). Primary intraocular primitive neuroectodermal tumor (retinoblastoma) causing unilateral blindness in a gelding. *Veterinary Ophthalmology, 10(6):348-356.*

Koch, E., Ryan, C., Leitch, M., Del Piero, F., & Boyle, A. (2012). Magnetic resonance imaging of a solid, multilobular ameloblastoma in the mandible of a pony. *Equine Veterinary Education, 26(11):599-604.*

Kopke, S., Angrisani, N., & Staszyk, C. (2012). The dental cavities of equine cheek teeth: three-dimensional reconstructions based on high resolution micro-computed tomography. *BMC Veterinary Research, 25(8):173-189.*

König, H. E., & Liebich, H.-G. (2010). Veterinary Anatomy of Domestic Mammals. Manson Publishing Ltd.

Kraft, S. L., & Gavin, P. R. (2001). Physical principles and technical considerations for equine computed tomography and magnetic resonance imaging. The Veterinary Clinics of North *America: Equine Practice, 17(1):115-130.*

Krings, T., Hans, F.-J., Möller-Hartmann, W., Thiex, R., Brunn, A., Scherer, K., Stein, K. P., Meetz, A., Dreeskamp, H., Allery, E., & Thron, A. (2002). Time-of-flight-, phase contrast and contrast enhanced magnetic resonance angiography for pre-interventional determination of aneurysm size, configuration, and neck morphology in an aneurysm model in rabbits. *Neuroscience Letters, 326(1):46-50.*

Kuemmerle, J. M., Kummer, M., Auer, J. A., Nitzl, D., & Fürst, A. E. (2009). Locking compression plate (LCP) osteosynthesis of complicated mandibular fractures in six horses. *Veterinary and Comparative Orthopaedics and Traumatology, 22(1):54-58.*

Lacombe, V. A., Mayes, M., Mosseri, S., Reed, S. M., & Ou, T. H. (2014). Distribution and predictive factors of seizure types in 104 cases. *Equine Veterinary Journal, 46(4):441-445.*

Lacombe, V. A., Mayes, M., Mosseri, S., Reed, S. M., Fenner, W.

## REFERENCES

R., & Ou, H. T. (2012). Epilepsy in horses: aetiological classification and predictive factors. *Equine Veterinary Journal, 44(6):646-651.*

Lacombe, V. A., Sogaro-Robinson, C., & Reed, S. M. (2010). Diagnostic utility of computed tomography imaging in equine intracranial conditions. *Equine Veterinary Journal, 42(5):393-399.*

Lane, J. G., Gibbs, C., Meynink, S. E., & Steele, F. C. (1987a). Radiographic examination of the facial, nasal and paranasal sinus regions of the horse: I. Indications and procedures in 235 cases. *Equine Veterinary Journal, 19(5):466-473.*

Lane, J. G., Longstaffe, J. A., & Gibbs, C. (1987b). Equine paranasal sinus cysts: a report of 15 cases. *Equine Veterinary Journal, 19(6):537-544.*

Latimer, C. A., Wyman, M., Diesem, C., & Burt, J. (1984). Radiographic and gross anatomy of the nasolacrimal duct of the horse. *American Journal of Veterinary Research, 45(3):451-458.*

Leach, M. O. (2014). Magnetic resonance imaging. In D. R. Dance, S. Christofides, A. D. A. Maidment, I. D. McLean, & K. H. Ng, Diagnostic radiology physics: A handbook for teachers and students (First edition. pp. 361-391). Vienna: International Atomic Energy Agency.

Lempe, A., Heine, M., Bosch, B., Mueller, K., & Brehm, W. (2012). Imaging diagnosis and clinical presentation of a Chiari malformation in a Thoroughbred foal. *Equine Veterinary Education, 24(12):618-623.*

Lim, C. L., Saulez, M. N., Viljoen, A., & Carstens, A. (2013). Basilar skull fracture in a Thoroughbred colt: Radiography or computed tomography? *Journal of the South African Veterinary Association, 84(1):1-6.*

Lipson, S. A. (2006). 3D Workstations: basic principles and pitfalls. In S. A. Lipson, MDCT and 3D workstations - A practical guide and teaching file (First edition. pp. 41-63). New York: Springer Science & Business Media.

Lischer, C. J., Walliser, U., Witzmann, P., Eser, M. W., & Ohlerth, S. (2010). Fracture of the paracondylar process in four horses: advantages of CT imaging. *Equine Veterinary Journal, 37(5):483-487.*

Loftin, P., Fowlkes, N., & McCauley, C. (2015). Mandibular squamous cell carcinoma in a 5-year-old Tennessee Walking Horse. *Equine Veterinary Education, 27(1):4-8.*

Macdonald, D. G., Fretz, P. B., Baptiste, K. E., & Hamilton, D. L. (1999). Anatomic, radiographic and physiologic comparisons of the internal carotid and maxillary artery in the horse. *The Veterinary Journal, 158(3):182-189.*

MacDonald, M. H. (1993). Clinical examination of the equine head. The Veterinary Clinics of North America: *Equine Practice, 9(1):25-48.*

Mair, T. S., Love, S., Schumacher, J., Smith, R. K. W., & Frazer, G. (2013). Equine Medicine, Surgery and Reproduction. Elsevier Health Sciences.

Maischberger, E., Jackson, M. A., Kühn, K., Grest, P., de Brot, S., & Wehrli Eser, M. (2014). Ethmoid adenocarcinoma: Severe neurological complications after combined laser ablation and intralesional formalin injection. *Equine Veterinary Education, 26(11):563-567.*

Manso-Díaz, G., García-López, J. M., Herrán, R., Garcia-Real, I., & Taeymans, O. (2014). Magnetic resonance dacryocystography in the horse (p. 52). Presented at the European Veterinary Diagnostic Imaging Anual Meeting, Utrecht.

Manso-Díaz, G., & Taeymans, O. (2012). Imaging diagnosis-Nasofrontal suture exostosis in a horse. *Veterinary Radiology & Ultrasound, 53(5):573-575.*

Mason, B. J. (1975). Empyema of the equine paranasal sinuses. *Journal of the American Veterinary Medical Association, 167(8):727-731.*

Matiasek, K., Cronau, M., Schmahl, W., & Gerhards, H. (2007). Imaging features and decision making in retrobulbar neuroendocrine tumours in horses-Case report and review of literature. *Journal of Veterinary Medicine A, 54(6):302-306.*

Maulet, B., Bestbier, M., Jose-Cunilleras, E., Scrine, J., & Murray, R. C. (2008). Magnetic resonance imaging of a cholesterol granuloma and hydrocephalus in a horse. *Equine Veterinary Education, 20(2):74-79.*

May, S. A., & Wyn-Jones, G. (1987). Contrast radiography in the investigation of sinus tracts and abscess cavities in the horse. *Equine Veterinary Journal, 19(3):218-222.*

McConnell, E. J., Sanz, M. G., Kafka, U. C. M., & Duncan, N. M. (2012). Parotid salivary gland carcinoma in a geriatric horse. *Equine Veterinary Education, 26(11):610-615.*

Montgomery, K., Ortved, K., Devries, J., Hackett, R., Kern, T., Irby, N., & Ducharme, N. G. (2012). Bilateral parotid duct transposition for keratoconjunctivitis sicca in a Connemara stallion. *Veterinary Ophthalmology, 16(4):303-311.*

Morresey, P. R., Garrett, K. S., & Carter, D. (2010). Rhodococcus equi occipital bone osteomyelitis, septic arthritis, and

## REFERENCES

meningitis in a neurological foal. *Equine Veterinary Education, 23(8):398–402.*

Muñoz, J., Iglesias, M., Lloret Chao, E., & Bussy, C. (2014). Ultrasound guided transarterial coil placement in the internal and external carotid artery in horses. *Veterinary Surgery. doi:10.1111/j.1532-950X.2014.12287.x*

Murray, R. C. (2011). Practicalities and image acquisition. In R. C. Murray, Equine MRI (First edition. pp. 39–50). West Sussex: Wiley-Blackwell.

Müller, J.-M. V., Hellige, M., Hoffmann, M. V., Uhlendorf, F., Steinmetz, S., & Feige, K. (2011). Parietal cerebral defect after skull fracture as a cause of posttraumatic epilepsy in an Icelandic horse. *Pferdeheilkunde, 27(3):306–310.*

Nagy, A. D., & Simhofer, H. (2006). Mandibular condylectomy and meniscectomy for the treatment of septic temporomandibular joint arthritis in a horse. *Veterinary Surgery, 35(7):663–668.*

Naylor, R. J., Dunkel, B., Dyson, S. J., Paz-Penuelas, M. P., & Dobson, J. (2010a). A retrobulbar meningioma as a cause of unilateral exophthalmos and blindness in a horse. *Equine Veterinary Education, 22(10):503–510.*

Naylor, R. J., Perkins, J. D., Allen, S., Aldred, J., Draper, E., Patterson-Kane, J., & Piercy, R. J. (2010b). Histopathology and computed tomography of age-associated degeneration of the equine temporohyoid joint. *Equine Veterinary Journal, 42(5):425–430.*

Nykamp, S. G., Scrivani, P. V., & Pease, A. P. (2004). Computed tomography dacryocystography evaluation of the nasolacrimal apparatus. *Veterinary Radiology & Ultrasound, 45(1):23–28.*

Ohlerth, S., & Scharf, G. (2007). Computed tomography in small animals – Basic principles and state of the art applications. *The Veterinary Journal, 173(2):254–271.*

Park, R. D. (1993). Radiographic examination of the equine head. *The Veterinary Clinics of North America: Equine Practice, 9(1):49–74.*

Pascual, A., Lopez-Mut, J., Benlloch, V., Chamarro, R., Soler, J., & Lainez, M. (2007). Perfusion-weighted magnetic resonance imaging in acute intracerebral hemorrhage at baseline and during the 1st and 2nd week: a longitudinal study. *Cerebrovasc Dis, 23(1):6–13.*

Passat, N., Ronse, C., Baruthio, J., Armspach, J.-P., & Maillot, C. (2006). Magnetic resonance angiography: from anatomical knowledge modeling to vessel segmentation. *Medical Image Analysis, 10(2):259–274.*

Pekarkova, M., Kircher, P. R., Konar, M., Lang, J., & Tessier, C. (2009). Magnetic resonance imaging anatomy of the normal equine larynx and pharynx. *Veterinary Radiology & Ultrasound, 50(4):392–397.*

Perkins, J. D., Windley, Z., Dixon, P. M., Smith, M., & Barakzai, S. Z. (2009). Sinoscopic treatment of rostral maxillary and ventral conchal sinusitis in 60 horses. *Veterinary Surgery, 38(5):613–619.*

Pirie, R. S., & Dixon, P. M. (1993). Mandibular tumours in the horse: a review of the literature and 7 case reports. *Equine Veterinary Education, 5(6):287–294.*

Pivetta, M., De Risio, L., Newton, R., & Dennis, R. (2013). Prevalence of lateral ventricle asymmetry in brain MRI studies of neurologically normal dogs and dogs with idiopathic epilepsy. *Veterinary Radiology & Ultrasound, 54(5):516–521.*

Plummer, C. E., & Reese, D. J. (2014). Ultrasonography of the eye and orbit. In J. A. Kidd, K. G. Lu, & M. L. Frazer, Atlas of equine ultrasonography (First edition. pp. 445–453). Oxford: John Wiley & Sons, Ltd.

Pollard, R. E., & Puchalski, S. M. (2011). CT contrast media and applications. In T. Schwarz & J. H. Saunders, Veterinary computed tomography (First edition. pp. 57–65). West Sussex: John Wiley & Sons, Ltd.

Porter, E. G., & Werpy, N. M. (2014). New concepts in standing advanced diagnostic equine imaging. *The Veterinary Clinics of North America: Equine Practice, 30(1):239–268.*

Powell, S. E. (2010). Use of multi-detector computed tomographic angiography in the diagnosis of a parapharyngeal aneurysm in a 6-week-old foal. *Equine Veterinary Journal, 42(3):270–273.*

Pownder, S., Scrivani, P. V., Bezuidenhout, A., Divers, T. J., & Ducharme, N. G. (2010). Computed tomography of temporal bone fractures and temporal region anatomy in horses. *Journal of Veterinary Internal Medicine, 24(2):398–406.*

Probst, A., Henninger, W., & Willmann, M. (2005). Communications of normal nasal and paranasal cavities in computed tomography of horses. *Veterinary Radiology & Ultrasound, 46(1):44–48.*

Puchalski, S. M. (2006). Computed tomographic and ultrasonographic examination of equine dental structures: normal and abnormal findings (pp. 173–180). Presented at the American Association of Equine Practitioners - Focus Meeting,

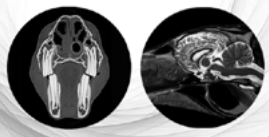



## REFERENCES

●●● Indianapolis.

Pusterla, N., Latson, K. M., Wilson, W. D., & Whitcomb, M. B. (2006). Metallic foreign bodies in the tongues of 16 horses. *Veterinary Record, 159(15):485–488.*

Rached, P. A., Canola, J. C., Schlüter, C., Laus, J. L., Oechtering, G., de Almeida, D. E., & Ludewig, E. (2011). Computed tomographic-dacryocystography (CT-DCG) of the normal canine nasolacrimal drainage system with three-dimensional reconstruction. *Veterinary Ophthalmology, 14(3):174-179.*

Ramirez, O., III, Jorgensen, J. S., & Thrall, D. E. (1998). Imaging basilar skull fractures in the horse: a review. *Veterinary Radiology & Ultrasound, 39(5):391-395.*

Ramirez, S., & Tucker, R. L. (2004). Ophthalmic imaging. *The Veterinary Clinics of North America: Equine Practice, 20(2):441-457.*

Ramzan, P. (2003). The head. In S. J. Dyson, R. C. Pilsworth, A. R. Twardock, & M. J. Martinelli, Equine scintigraphy (First edition. pp. 225–238). Newmarket: Equine veterinary journal.

Ramzan, P., Marr, C. M., Meehan, J., & Thompson, A. (2008). Novel oblique radiographic projection of the temporomandibular articulation of horses. *Veterinary Record, 162(22):714-716*.

Rand, C. L., Hall, T. L., Aleman, M., & Spier, S. J. (2012). Otitis mediaÐinterna and secondary meningitis associated with Corynebacterium pseudotuberculosis infection in a horse. *Equine Veterinary Education, 24(6):271-275.*

Rathmanner, M., & Rijkenhuizen, A. B. M. (2012). Ultrasonography of the upper cervical region (EUCR) in the horse. *Pferdeheilkunde, 28(2):575-582.*

Ravenel, J. G., & McAdams, H. P. (2003). Multiplanar and three-dimensional imaging of the thorax. *Radiologic Clinics of North America, 41(3):475-489.*

Reef, V. B. (1998). Ultrasonographic evaluation of small parts. In V. B. Reef, Equine diagnostic ultrasound (First edition. pp. 480–547). Philadelphia: Saunders.

Reimer, J. M., & Latimer, C. S. (2011). Ultrasound findings in horses with severe eyelid swelling, and recognition of acute dacryoadenitis: 10 cases (2004-2010). *Veterinary Ophthalmology, 14(2):86-92.*

Roberts, V. L. H., McKane, S. A., Williams, A., & Knottenbelt, D. C. (2009). Caudal compression of the infraorbital nerve: a novel surgical technique for treatment of idiopathic headshaking and assessment of its efficacy in 24 horses. *Equine Veterinary Journal, 41(2):165-170.*

Robertson, I. D., Davis, J. L., Gilger, B. C., Spaulding, K. A., & Jones, S. L. (2002). Nasal adenocarcinoma with diffuse metastases involving the orbit, cerebrum, and multiple cranial nerves in a horse. *Journal of the American Veterinary Medical Association, 221(10):1460-1463.*

Rodríguez, M. J., Agut, A., Soler, M., López-Albors, O., Arredondo, J., Querol, M., & Latorre, R. (2010). Magnetic resonance imaging of the equine temporomandibular joint anatomy. *Equine Veterinary Journal, 42(3):200-207.*

Rodríguez, M. J., Latorre, R., López-Albors, O., Soler, M., Aguirre, C., Vázquez, J. M., Querol, M., & Agut, A. (2008). Computed tomographic anatomy of the temporomandibular joint in the young horse. *Equine Veterinary Journal, 40(6):566-571.*

Rodríguez, M. J., Soler, M., Latorre, R., Gil, F., & Agut, A. (2007). Ultrasonographic anatomy of the temporomandibular joint in healthy pure-bred Spanish horses. *Veterinary Radiology & Ultrasound, 48(2):149-154.*

Rubin, G. D. (2003). 3-D imaging with MDCT. *European Journal of Radiology, 45(S1):37-41.*

Sanders, S. G., Tucker, R. L., Bagley, R. S., & Gavin, P. R. (2001). Magnetic resonance imaging features of equine nigropallidal encephalomalacia. *Veterinary Radiology & Ultrasound, 42(4):291-296.*

Santos, M. P., Stewart, A. A., Hyde, R. M., Rodgerson, D. H., & Gutierrez-Nibeyro, S. B. (2012). Identification of a periorbital wooden foreign body as the cause of chronic ocular discharge in a horse. *Australian Veterinary Journal, 90(3):84-87.*

Saunders, J. H., Nelson, A., & Vanderperren, K. (2011). Particularities of equine CT. In T. Schwarz & J. H. Saunders, Veterinary computed tomography (First edition. pp. 421–426). West Sussex: Wiley-Blackwell.

Schaer, B. D. (2007). Ophthalmic emergencies in horses. *The Veterinary Clinics of North America: Equine Practice, 23(1):49-65.*

Schneider, A., Tessier, C., Gorgas, D., Kircher, P. R., Mamani, J., & Miclard, J. (2010). Magnetic resonance imaging features of a benign peripheral nerve sheath tumour with "ancient"changes in the tongue of a horse. *Equine Veterinary Education, 22(7):346-351.*

Schrock, P., Lüpke, M., Seifert, H., & Staszyk, C. (2013). Three-dimensional anatomy of equine incisors: tooth length, enamel cover and age related changes. *BMC Veterinary Research, 9(1):249.* ●●●

## REFERENCES

Scotty, N. C., Cutler, T. J., Brooks, D. E., & Ferrell, E. (2004a). Diagnostic ultrasonography of equine lens and posterior segment abnormalities. *Veterinary Ophthalmology, 7(2):127-139.*

Scotty, N. C., Ford, M., Williams, F., Loiacono, C., Johnson, P. J., Messer, N. T., Turnquist, S. E., & Exxman, S. (2004b). Exophthalmia associated with paranasal sinus osteoma in a Quarter horse mare. *Journal of Veterinary Diagnostic Investigation, 16(2):155-160.*

Scrivani, P. V. (2013). Neuroimaging in horses with traumatic brain injury. *Equine Veterinary Education, 25(10):499-502.*

Seco Diaz, O. (2004). Ultrasound of the equine eye and adnexa and clinical applications. *Clinical Techniques in Equine Practice, 3(3):317-325.*

Smallwood, J. E., Wood, B. C., Taylor, W. E., & Tate, L. P. (2002). Anatomic reference for computed tomography of the head of the foal. *Veterinary Radiology & Ultrasound, 43(2):99-117.*

Smith, L. C. R., Zedler, S. T., Gestier, S., Keane, S. E., Goodwin, W., & van Eps, A. W. (2012). Bilateral dentigerous cysts (heterotopic polyodontia) in a yearling Standardbred colt. *Equine Veterinary Education, 24(11):573-578.*

Smith, L. J., & Perkins, J. D. (2009). Standing surgical removal of a progressive ethmoidal haematoma invading the sphenopalatine sinuses in a horse. *Equine Veterinary Education, 21(11):577-581.*

Sogaro-Robinson, C., Lacombe, V., Reed, S. M., & Balkrishnan, R. (2009). Factors predictive of abnormal results for computed tomography of the head in horses affected by neurologic disorders: 57 cases (2001-2007). *Journal of the American Veterinary Medical Association, 235(2):176-183*.

Solano, M., & Brawer, R. S. (2004). CT of the equine head: technical considerations, anatomical guide, and selected diseases. *Clinical Techniques in Equine Practice, 3(4):374-388.*

Solano, M., & Penninck, D. G. (1996). Ultrasonography of the canine, feline and equine tongue: Normal findings and case history reports. *Veterinary Radiology & Ultrasound, 37(3):206-213.*

Song, H. K. (2014). Physics of magnetic resonance. In D. R. Dance, S. Christofides, A. D. A. Maidment, I. D. McLean, & K. H. Ng, Diagnostic radiology physics: A handbook for teachers and students (First edition. pp. 333-360). Vienna: International Atomic Energy Agency.

Spoormakers, T. J. P., Ensink, J. M., Goehring, L. S., Koeman, J. P., Braake, Ter, F., van der Vlugt-Meijer, R. H., & van den Belt, A. J. M. (2003). Brain abscesses as a metastatic manifestation of strangles: symptomatology and the use of magnetic resonance imaging as a diagnostic aid. *Equine Veterinary Journal, 35(2):146-151.*

Staszyk, C., Bienert, A., Kreutzer, R., Wohlsein, P., & Simhofer, H. (2008). Equine odontoclastic tooth resorption and hypercementosis. *The Veterinary Journal, 178(3):372-379.*

Sutherland-Smith, J., King, R., Faissler, D., Ruthazer, R., & Sato, A. F. (2011). Magnetic resonance imaging apparent diffusion coefficients for histologically confirmed intracranial lesions in dogs. *Veterinary Radiology & Ultrasound, 52(2):142-148.*

Tessier, C., Brühschwein, A., Lang, J., Konar, M., Wilke, M., Brehm, W., & Kircher, P. R. (2013). Magnetic resonance imaging features of sinonasal disorders in horses. *Veterinary Radiology & Ultrasound, 54(1):54-60.*

Textor, J. A., Puchalski, S. M., Affolter, V. K., MacDonald, M. H., Galuppo, L. D., & Wisner, E. R. (2012). Results of computed tomography in horses with ethmoid hematoma: 16 cases (1993-2005). *Journal of the American Veterinary Medical Association, 240(11):1338-1344.*

Tidwell, A. S., & Jones, J. (1999). Advanced imaging concepts: A pictorial glossary of CT and MRI technology. *Clinical Techniques in Small Animal Practice, 14(2):65-111.*

Townsend, N. B., Cotton, J. C., & Barakzai, S. Z. (2009). A tangential radiographic projection for investigation of the equine temporomandibular joint. *Veterinary Surgery, 38(5):601-606.*

Townsend, N. B., Hawkes, C. S., Rex, R., Boden, L. A., & Barakzai, S. Z. (2011). Investigation of the sensitivity and specificity of radiological signs for diagnosis of periapical infection of equine cheek teeth. *Equine Veterinary Journal, 43(2):170-178.*

Tremaine, H. (2013). Progressive ethmoidal haematoma. *Equine Veterinary Education, 25(10):508-510.*

Tremaine, H., & Dixon, P. M. (2001). A long-term study of 277 cases of equine sinonasal disease. Part 1: details of horses, historical, clinical and ancillary diagnostic findings. *Equine Veterinary Journal, 33(3):274-282.*

Tucker, R. L., & Farrell, E. (2001). Computed tomography and magnetic resonance imaging of the equine head. The Veterinary Clinics of North America: *Equine Practice, 17(1):131-144.*

Tucker, R. L., & Holmes, S. P. (2011). The head. In R. C. Murray, Equine MRI (First edition. pp. 249-268). West Sussex: Wiley-Blackwell.

Tucker, R. L., & Sampson, S. N. (2007). Magnetic resonance

## REFERENCES

●●● imaging protocols for the horse. *Clinical Techniques in Equine Practice, 6(1):2-15.*

Tucker, R. L., Garrett, K. S., Reed, S. M., & Murray, R. C. (2011). The head. In R. C. Murray, Equine MRI (First edition. pp. 467-488). West Sussex: Wiley-Blackwell.

van den Top, J. G. B., Schaafsma, I. A., Boswinkel, M., & Klein, W. R. (2007). A retrobulbar abscess as an uncommon cause of exophthalmos in a horse. *Equine Veterinary Education, 19(11):579-583.*

Van Thielen, B., Busoni, V., Chiers, K., de Mey, J., De Munter, M., Grulke, S., & Verwilghen, D. (2013). MRI and CT features of an equine juvenile mandibular ossifying fibroma. *Journal of Equine Veterinary Science, 33(8):658-662.*

Veraa, S., Dijkman, R., Klein, W. R., & van den Belt, A. J. M. (2009a). Computed tomography in the diagnosis of malignant sinonasal tumours in three horses. *Equine Veterinary Education, 21(6):284-288.*

Veraa, S., Voorhout, G., & Klein, W. R. (2009b). Computed tomography of the upper cheek teeth in horses with infundibular changes and apical infection. *Equine Veterinary Journal, 41(9):872-876.*

Vink-Nooteboom, M., Junker, K., van den Ingh, T. S., & Dik, K. J. (1998). Computed tomography of cholesterinic granulomas in the choroid plexus of horses. *Veterinary Radiology & Ultrasound, 39(6):512-516.*

Walker, A. M., Sellon, D. C., Comelisse, C. J., Hines, M. T., Ragle, C. A., Cohen, N., & Schott, H. C., II. (2002). Temporohyoid osteoarthropathy in 33 horses (1993-2000). *Journal of Veterinary Internal Medicine, 16(6):697-703.*

Weller, R., Cauvin, E. R. J., Bowen, I. M., & May, S. A. (1999a). Comparison of radiography, scintigraphy and ultrasonography in the diagnosis of a case of temporomandibular joint arthropathy in a horse. *Veterinary Record, 144(14):377-379.*

Weller, R., Livesey, L., Maierl, J., Nuss, K., Bowen, I. M., Cauvin, E. R. J., Weaver, M., Schumacher, J., & May, S. A. (2001). Comparison of radiography and scintigraphy in the diagnosis of dental disorders in the horse. *Equine Veterinary Journal, 33(1):49-58.*

Weller, R., Taylor, S., Maierl, J., May, S. A., & Cauvin, E. R. J. (1999b). Ultrasonograpic anatomy of the equine temporomandibular joint. *Equine Veterinary Journal, 31(6):529-532.*

Werpy, N. M. (2007). Magnetic resonance imaging of the equine patient: A comparison of high- and low-field systems. *Clinical Techniques in Equine Practice, 6(1):37-45.*

Whatmough, C., & Lamb, C. R. (2006). Computed tomography: principles and applications. *Compendium on Continuing Education Practical Veterinary, 789-800.*

Windley, Z., Tremaine, H., Weller, R., & Perkins, J. D. (2009). Two- and three-dimensional computed tomographic anatomy of the enamel, infundibulae and pulp of 126 equine cheek teeth. Part 2: Findings in teeth with macroscopic occlusal or computed tomographic lesions. *Equine Veterinary Journal, 41(4):441-447.*

Wollanke, B., Gerhards, H., & Cronau, M. (2006). Diagnosis and therapy of periorbital diseases in horses: Indication for computed tomography (CT) or magnetic resonance tomography (MRT). *Pferdeheilkunde, 22(4):431-438.*

Wong, D. M., Gross, W., Madron, M., & Alcott, C. J. (2011). What Is Your Diagnosis? Soft palate cyst in a foal. *Journal of the American Veterinary Medical Association, 238(2):157-158.*

Woodford, N. S., & Lane, J. G. (2006). Long-term retrospective study of 52 horses with sinunasal cysts. *Equine Veterinary Journal, 38(3):198-202.*

Wyn-Jones, G. (1985a). Interpreting radiographs 6: Radiology of the equine head (Part 2). *Equine Veterinary Journal, 17(6):417-425.*

Wyn-Jones, G. (1985b). Interpreting radiographs 6: The head. *Equine Veterinary Journal, 17(4):274-278.* ■